Master's thesis

NTNU
Norwegian University of Science and Technology
Faculty of Natural Sciences
Department of Chemical Engineering

Martine Paulsen

Simulation of H_2S Removal from Biogas Using Aspen Plus

Master's thesis in Chemical Engineering
Supervisor: Hanna Knuutila, Diego Di Domenico Pinto
June 2019

NTNU
Norwegian University of
Science and Technology

Martine Paulsen

Simulation of H_2S Removal from Biogas Using Aspen Plus

Master's thesis in Chemical Engineering
Supervisor: Hanna Knuutila, Diego Di Domenico Pinto
June 2019

Norwegian University of Science and Technology
Faculty of Natural Sciences
Department of Chemical Engineering

NTNU
Norwegian University of
Science and Technology

Preface

This Master Thesis was written during the spring semester of 2019 at the Norwegian University of Science and Technology (NTNU) as a part of the five-year Master's Degree program of Chemical Engineering and Biotechnology. The final report is the result of TKP4900 - Chemical Engineering Master Thesis, in the research area of Environmental Engineering and Reactor Technology.

The assignment was prepared by Professor Hanna Knuutila and Dr. Diego Di Domenico Pinto, who also served as supervisor and co-supervisor respectively during the project period.

Trondheim, June 11, 2019

Martine Paulsen

Acknowledgment

I would like to express my greatest gratitude to my supervisor, Professor Hanna Knuutila and my co-supervisor, Dr. Diego Di Domenico Pinto for all patience and valuable guidance throughout the semester. I would also like to thank PhD Candidate Ricardo Ramos Wanderley who has assisted with questions and guidance during meetings and discussions. Hanna, Diego and Ricardos help and guidance has been absolutely crucial for the implementation of this Master thesis.

In the end, I would like to thank my friends and family for their support and kind words through these five years of study.

M.P.

Abstract

Biogas is a renewable energy source, and can be used as a natural gas substitute. The biogas needs to be purified before it can be upgraded to biomethane. Components that can damage the process equipment, such as hydrogen sulfide (H_2S), must be removed either before or simultaneously with carbon dioxide (CO_2). Several techniques can be used to remove H_2S, and the choice of it depends on different factors such as biogas flow, composition and the desired purity, which is usually set to meet the country regulations or equipment specifications. Both water scrubbing and amine scrubbing are widely used methods, and these methods are investigated further in this thesis. Methyl diethanolamine (MDEA) was used in the amine scrubbing simulations. The main goal was to purify the biogas to a maximum H_2S content of 5 ppm. Aspen Plus was used to perform the simulations in both cases, and a vapour-liquid equilibrium (VLE) validation was performed to assure that Aspen Plus predicted accurate results. All the simulations were performed with rate-based calculations in the absorber and desorber. The validation results showed that the solubility of H_2S in water deviates 4 % from literature data in loading, and 3 % in the total pressure at 45 °C. The solubility of H_2S in aqueous MDEA had an average deviation of 19-32 % in loading and 68-137 % in partial pressure of H_2S. The effect of a gas recycle was also investigated, and showed that the methane loss could be decreased from 3.1 to 0.03 %.

In this thesis, water scrubbing and amine scrubbing absorption performance was compared, primarily in terms of purity target and energy demand. Three different cases of water scrubbing and one for amine scrubbing were mainly simulated. The content of the biogas was specified equally in all cases, and the purified gas was compressed to 8 bar in the amine scrubbing simulation to have the same outlet pressure as in water scrubbing. This was done to get comparable results from the energy analysis. The simulation results showed that it was possible to achieve the purity of maximum 5 ppm H_2S by several techniques.

It was found that the absorption of CO_2 had a higher impact on the absorption of H_2S than expected in the amine scrubbing process. This may be due to the high formation of bicarbonate in the process. The CO_2 content of the biogas may also have been too high to obtain selectively absorption of H_2S. No cost analysis was carried out in this work.

Sammendrag

Biogass er en forbybar energikilde og kan brukes som en substitutt til naturgass. Biogass må renses før den kan oppgraderes til biometan. Komponenter som kan gjøre skade på prosessutstyret, som for eksempel hydrogen sulfid (H_2S), må fjernes enten før eller samtidig med karbondioksid (CO_2). Flere teknikker kan brukes for å fjerne H_2S, og valget avhenger av forskjellige faktorer som mengde biogass, innhold og ønsket renhet, som ofte blir satt slik at de møter landets restriksjoner eller spesifikasjoner på utstyret. Både vannskrubbing og aminskrubbing er mye brukte metoder, og disse metodene er undersøkt nærmere i denne oppgaven. Metyldietanolamin (MDEA) ble brukt som amin i simuleringene for aminskrubbing. Hovedmålet var å rense biogassen til et maksimalt H_2S-innhold på 5 ppm. Aspen Plus ble brukt til å utføre simuleringer i begge tilfellene, og en damp-væske likevekt (VLE) validering ble gjennommført for å for å sikre at Aspen Plus forutsier nøyaktige resultater. Alle simuleringene ble utført med rate-baserte beregninger i henholdsvis absorber og desorber. Valideringen viste at løseligheten av H_2S i vann hadde et avvik på 4 % fra litteraturdata i loadingen og 3 % i totaltrykk ved 45 °C. Løseligheten av H_2S i vandig MDEA hadde et gjennomsnittlig avvik på 19-32 % i loadingen og 68-137 % i partialtrykk av H_2S. Effekten av en gass-resirkulering ble også undersøkt, og viste at metantapet kunne reduseres fra 3,1 til 0,03 %.

I denne oppgaven ble absorpsjonsevnen til vannskrubbbing og aminskrubbing sammenlignet, hovedsaklig basert på renhetskrav og energibehov. Det ble i hovedsak simulert tre forskjellige caser for vannskrubbing og en for aminskrubbing. Innholdet i biogassen ble spesifisert likt i alle casene, og den rensede gassen ble komprimert til 8 bar i aminskrubbing for å ha samme utgangstrykk som i vannskrubbing. Dette ble gjort for å få sammenlignbare resultater til energianalysen. Resultatene fra simuleringene viste at det var mulig å oppnå kravet om et maksimalt H_2S-innhold på 5 ppm ved flere av teknikkene.

Det ble oppdaget at absorpsjonen av CO_2 hadde en høyere innvirkning på absorpsjon av H_2S enn forventet i aminskrubbing systemet. Dette kan skyldes den høye dannelsen av bikarbonat i prosessen. CO_2-innholdet i biogassen kan også ha vært for høyt til å oppnå en selektiv absorbsjon av H_2S. Det ble ikke utført noen kostnadsanalyse i dette arbeidet.

Contents

Preface i
Acknowledgment iii
Abstract v

1 Introduction **1**
1.1 Background and Motivation 3
1.1.1 Renewable Energy 3
1.1.2 Biogas 4
1.1.3 Biogas Purification 5
1.2 Objectives 6
1.3 Outline of the Thesis 7

2 Biogas Purification Absorption Technologies **9**
2.1 Water Scrubbing 9
2.2 Amine Scrubbing 11
2.3 Rate-based and Equilibrium-Stage Simulation Approach 13

3 Simulation Models **15**
3.1 Validation 15
3.1.1 Solubility of H_2S in Water 17
3.1.2 Solubility of CH_4 in Water 19
3.1.3 Solubility of CO_2 in Water 20
3.1.4 Solubility of H_2S in Aqueous MDEA Solutions 22
3.2 Water Scrubbing 27
3.2.1 Simple Flash, C-1 27
3.2.2 Flash with Purge, C-2 29
3.2.3 Air Stripping, C-4 32
3.3 Amine Scrubbing 34
3.3.1 Reactions 34

4 Results and Discussion **39**
4.1 Water Scrubbing 39

4.1.1 Simple Flash, C-1 . . . 39
4.1.2 Flash with Purge, C-2 . . . 41
4.1.3 Air Stripping, C-4 . . . 45
4.1.4 Comparison of the Different Water Scrubbing Techniques . . . 49
4.2 Amine Scrubbing, C-5 and C-6 . . . 50
4.3 Water Scrubbing vs. Amine Scrubbing . . . 59

5 Summary **63**
5.1 Conclusion . . . 63
5.2 Further Work . . . 64

A Additional Information **I**
A.1 Simulations . . . I
A.1.1 Water Scrubbing . . . I
A.1.2 Amine Scrubbing . . . X
A.2 Calculations . . . XII
A.2.1 Energy/kg Impurity Absorbed . . . XII

List of Figures

1.0.1 World Total Primary Energy Supply from 1970 to 2015 as presented by The International Energy Agency [1]. . . . 1
1.0.2 CO_2 emission by source, graph borrowed from Our World in Data [3]. . . . 2
1.1.1 Illustation of the greenhouse effect [6]. . . . 3

2.1.1 Water scrubbing of H_2S for biogas upgrading [9]. . . . 10
2.2.1 Structural formula for the MDEA molecule [24]. . . . 12
2.2.2 Amine based biogas H_2S and CO_2 scrubber [19]. . . . 12
2.3.1 Illustration of the difference between Rate-based and Equilibrium-stage approach [27]. . . . 13

3.1.1 Illustration of the flash used in VLE validation. . . . 16
3.1.2 Validation of the binary $H_2S - H_2O$ system at different temperatures compared to literature data [29]. The graph on the right hand side shows the same result presented on logscale. . . . 18
3.1.3 Validation of the binary $CH_4 - H_2O$ system at different temperatures compared to literature data [30]. . . . 19
3.1.4 Aspen simulation at low partial pressures of CO_2 compared to literature data of Carroll et al. [31]. The right graph presents the data in logscale. . . . 20
3.1.5 Aspen simulation at high partial pressures of CO_2 compared to literature data of Valtz et al. [32]. The right graph presents the data with logscale. . . . 20
3.1.6 Validation at 11.9 wt% MDEA [35]. The graph on the right side presents the same graph with log scale. . . . 22
3.1.7 Validation at 23.7 wt% MDEA [34]. The graph on the right side presents the same graph with log scale. . . . 22
3.1.8 Validation at 50.0 wt% MDEA [35]. The graph on the right side presents the same graph with log scale. . . . 23
3.1.9 Average deviation in partial pressure of H_2S from literature Jou et al. [35] as a function of loading for an MDEA concentration of 11.9 wt %. . . . 25
3.1.10 Average deviation in partial pressure of H_2S from literature Jou et al. [35] as a function of loading for an MDEA concentration of 23.7 wt %. . . . 25

3.1.11 Average deviation in partial pressure of H_2S from literature Jou et al. [35] as a function of loading for an MDEA concentration of 50.0 wt %. 26
3.2.1 Water scrubbing with regeneration of water with a simple flash tank. 28
3.2.2 Water scrubbing with regeneration of water by a flash and a water purge. 29
3.2.3 Process flow diagram of the system including water purge excluding gas recycle, where the split is inserted after the flash tank. 30
3.2.4 Water scrubbing with regeneration of water by a flash. A water purge was implemented as well as a gas recycle. 31
3.2.5 Absorber system including gas recycling. 32
3.2.6 Water scrubbing system with air stripping and gas recycle. 33
3.3.1 Process flow diagram of the amine scrubbing system. 36

4.1.1 Mole fraction of H_2S in the purified biogas as a function of L/G-ratio when water is regenerated through a flash at 90 °C. 39
4.1.2 The split fractions needed to obtain the target of 5 ppm in the gas out of the absorber as a function of L/G-ratio. 41
4.1.3 Removal efficiency as a function of L/G-ratio for an absorber system including a compressor train for compression of biogas, and a gas recycle to minimize the methane loss. 43
4.1.4 Amount of H_2S in the purified gas plotted as a function of L/G-ratio when the biogas is compressed in a compressor train and the gas is recycled. 43
4.1.5 Rich loading plotted as a function of L/G-ratio when a compressor train for the biogas is implemented as well as a gas recycle. 44
4.1.6 Methane loss plotted as a function of the L/G-ratio when the absorber system includes a compressor train to compress the biogas and a gas recycle. 44
4.1.7 Mole fraction of H_2S in the purified gas plotted as a function of L/G-ratio for the air stripping system, excluding gas recycle. 45
4.1.8 Rich loading plotted as a function of L/G-ratio for the air stripping system excluding gas recycle. 46
4.1.9 Methane loss as a function of L/G-ratio for the air stripping system excluding gas recycle. 46
4.1.10 Mole fraction of H_2S in purified gas plotted as a function of the L/G-ratio. 47
4.1.11 Rich loading plotted as a function of L/G-ratio in the system with a gas recycle. . 48
4.1.12 Methane loss at different L/G-ratios for the system including gas recycling. 48
4.2.1 Removal efficiency plotted as a function of absorber height when L/G = 10 and D = 0.3 m. 50

4.2.2 Rich loading of H_2S plotted as a function of height when L/G = 10 m and D = 0.3 m. 51
4.2.3 Removal efficiency as a function of L/G-ratio when H = 20 m and D = 0.35 m . . 51
4.2.4 Rich loading plotted as a function of L/G ratio when H = 20 m D = 0.35 m. The lean loading was fixed and is marked as a dashed, orange line. 52
4.2.5 Amount of H_2S in purified gas plotted as a function of L/G ratio when H = 20 m and D = 0.35 m. 53
4.2.6 Rich loading of CO_2 plotted as a function of L/G-ratio when H = 20 m and D = 0.35 m. 54
4.2.7 Methane loss plotted as a function of L/G-ratio when H = 20 m and D = 0.35 m. . 54
4.2.8 Temperature profiles for the absorber. The left graph presents the liquid temperature profile, and the right graph represents the vapor temperature profile. 55
4.2.9 Concentration profile for H_2S in vapor phase. 56
4.2.10 Concentration profile for CO_2 in liquid phase. 56
4.2.11 Concentration profile for CH_4 in liquid phase. 57

A.1.1 Validation at 16 °C. I
A.1.2 Validation at 35 °C. II
A.1.3 Validation at 45 °C. II
A.1.4 Validation at 55 °C. III
A.1.5 Validation at 65 °C. III
A.1.6 Removal efficiency as a function of L/G-ratio. IV
A.1.7 Mole fraction of H_2S in gas out of the absorber as a function of L/G-ratio. The target of 5 ppm is illustrated by the dashed, orange line. V
A.1.8 Removal efficiency plotted as a function of the absorber height when the L/G-ratio is fixed at 100. V
A.1.9 Rich loading as a function of L/G-ratio. VI
A.1.10 Mole fraction of H_2S and methane loss plotted as a function of L/G-ratio for a flash temperature of 60 °C. VI
A.1.11 Mole fraction of H_2S and methane loss plotted as a function of L/G-ratio for a flash temperature of 80 °C. VII
A.1.12 Removal efficiency plotted as a function of the absorber packed height when L/G is fixed at 10 and the diameter at 0.3 m. X

List of Tables

1.1.1 Typical content in biogas from different sources [11] [9]. 4

3.1.1 Overview of literature data with associated temperature and pressure ranges used in the validation. 15
3.1.2 Average deviations from literature data for the binary $H_2S - H_2O$ system [29]. . . 18
3.1.3 Average deviations from literature data [30]. 19
3.1.4 Average deviations from literature data of Carroll et al. [31] (low partial pressures) and Valtz et al. [32] (high partial pressures). 21
3.1.5 Average deviations from literature data of Rogers et al., (1998) [33] (23.7 wt%), GPA report, (1998) [34] (23.7 wt%) and Jou et al., (1982) [35] (11.9, 23.7 and 50 %). 24
3.2.1 Absorber specifications in the case with regeneration through a simple flash. . . . 28
3.2.2 Absorber specifications in the case with regeneration through a flash including a water purge. 30
3.2.3 Absorber specifications in the case with no regeneration of the lean stream. The gas out of the flash is recycled back to the absorber. 32
3.2.4 Absorber and desorber specifications in the case with air stripping. 33
3.3.1 Reactions from Aspen Plus for the amine scrubbing system using the ELECNRTL_Rate_Based_MDEA_Model template. 34
3.3.2 Absorber and desorber specifications for amine scrubbing. 36
3.3.3 The main cases implemented in Aspen Plus. 37

4.1.1 Comparison of energy demand and type for four different water scrubbing cases. . 40
4.1.2 Effect of a gas recycle to the system containing a water purge. 42
4.1.3 Results from the main cases of the water scrubbing technique. 49
4.2.1 Energy demand and type for the amine scrubbing simulation at L/G = 14 and L/G = 16. 58
4.3.1 Comparison of energy demand for the three most promising cases. 59
4.3.2 Energy demand per kg H_2S and CO_2 removed for the three most promising techniques. 59

4.3.3 Energy demand per kg impurity absorbed from literature for water scrubbing and amine scrubbing [16][41]. 60
4.3.4 Sulfide content in lean disposal streams. 61

A.1.1 Stream overview in the case with regeneration through a simple flash. VII
A.1.2 Stream overview in the case with a flash and a water purge. VIII
A.1.3 Stream overview in the case with an absorber and no lean stream recycle. VIII
A.1.4 Stream overview in the air stripping case. IX
A.1.5 Stream overview for Amine scrubbing at L/G = 14. XI
A.1.6 Stream overview for Amine scrubbing at L/G = 16. XI

List of Symbols

Symbol	Description	Unit
E	Activation energy	kJ/mol
k	temperature-independent constant	-
K_{eq}	Equilibrium constant	-
L	Liquid	kmol/hr
N	Number of stages	-
n	Constant	-
P	Partial pressure	bar
p_A	Partial pressure of A in vapor phase	bar
P_{tot}	Total pressure	bar
R	Ideal gas constant	kJ/mol
T	Temperature	°C
V	Vapor	kmol/hr
y_A	Mole fraction of A in vapor phase	-
α	Loading	mole/mole

Acronyms

AR Assessment Report

DEA Diethanolamine

ELECNRTL Electrolyte NRTL with Redlich–Kwong equation of state

ENRTL Electrolytic NRTL

ENRTL-RK Unsymmetric electrolyte NRTL with Redlich–Kwong equation of state

GPA Gas Processors Association

IEA International Energy Agency

IPCC Intergovernmental Panel on Climate Change

KPa Kilo pascal

kW Kilo watt

MDEA Methyldiethanolamine

MEA Monoethanolamine

NRTL Non-Random-Two-Liquid

NTNU Norwegian University of Science and Technology

ppm Parts per million

ppmv Parts per million volume based

TPES Total Primary Energy Supply

UNIQUAC Universal Quasichemical activity coefficient model

VLE Vapor-liquid equilibrium

Chapter 1

Introduction

One of the biggest challenges we face in modern time is the increasing energy demand along with the pollution this entails. This includes pollution from electricity generation plants as well as public transportation. The energy requirement in the world has increased significantly since 1975 as shown in figure 1.0.1 presenting the World Total Primary Energy Supply (TPES) by fuel. This type of energy originates from natural sources such as crude oil and natural gas, and approximately 75-80 % of the energy is reproduced by fossil fuels.[1]

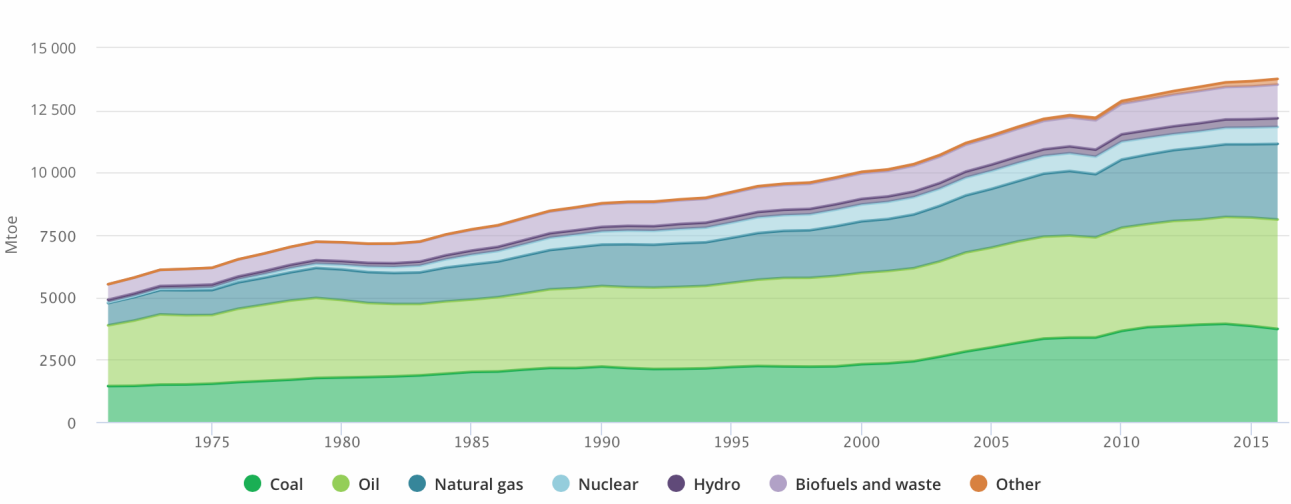

Figure 1.0.1: World Total Primary Energy Supply from 1970 to 2015 as presented by The International Energy Agency [1].

According to the IPCC's Fifth Assessment Report (AR5), about 78% of the total Greenhouse gas emission increase from 1970 to 2010 was due to CO_2 emissions from fossil fuel combustion and industrial processes [2]. This underlines the importance of both CO_2 emission limitation and capture. Figure 1.0.2 presents carbon dioxide emissions by sector, measured in tonnes per year [3]. It is clear that the energy sector is a major contributor to the emission of CO_2, and it is therefore a great potential in making this industry more renewable.

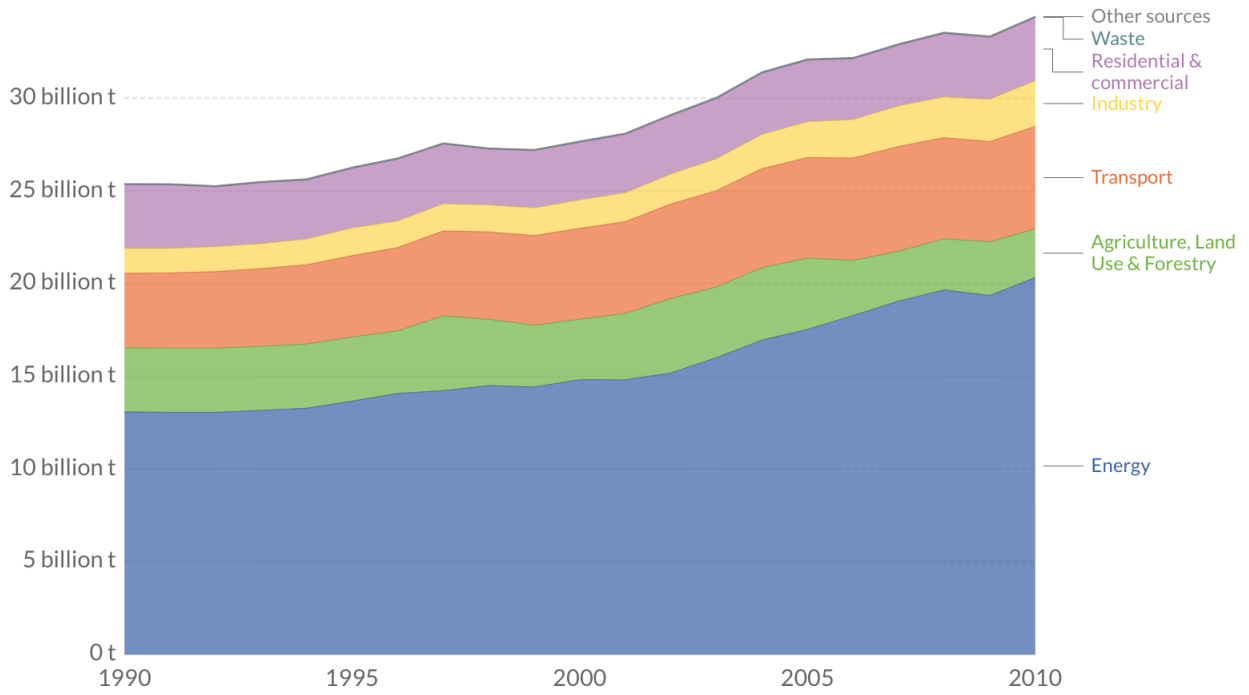

Figure 1.0.2: CO_2 emission by source, graph borrowed from Our World in Data [3].

Both hydropower, wind, solar and biogas are considered renewable energy sources. Hydropower includes capturing of water flowing in rivers and transforming it into electricity. Hydropower provides practically all of the electricity in Norway, and over 40 % of the electricity that is used in developing countries. On a global scale, large-scale hydropower provides 20 % of the electricity. Sunlight and wind are made into electricity through solar panels or windmills. Solar panels collect the solar radiation energy in a special type of heat exchanger and transforms it to internal energy. It is also possible to convert solar energy to chemical energy by using the solar energy to split water into oxygen and hydrogen. Wind energy is generally used to power windmills or pump water, and has been used for a long time. In recent times, wind turbines have been designed for electricity generation with promising results.[4]

Finding new renewable energy sources is becoming increasingly important in our modern society as the development of technology is evolving and the Earth's resources are diminishing. Biogas is becoming increasingly popular, both as an energy source and as a substitute to natural gas. The International Energy Agency states that the electricity sector will provide the most rapidly growth in terms of renewables. They anticipate that renewables will provide approximately 30 % of the power demand in 2023 compared to the 24 % in 2017. This is due to the increasing use of solar, wind, hydropower and bioenergy.[5]

1.1 Background and Motivation

1.1.1 Renewable Energy

The increasing emissions of greenhouse gases due to industrialization and increased consumption of fossil fuels has led to an increased concentration of these gases in the atmosphere. This includes compounds such as carbon dioxide (CO_2), methane (CH_4) and nitrous oxide (N_2O) where CO_2 is the main greenhouse gas related to global warming. These gases contribute to hold heat in the atmosphere, which increases the temperature on earth. This temperature rise can lead to major problems for the life on earth in terms of climate changes, and should therefore be limited. Figure 1.1.1 illustrates schematically how the greenhouse effect takes place.[4]

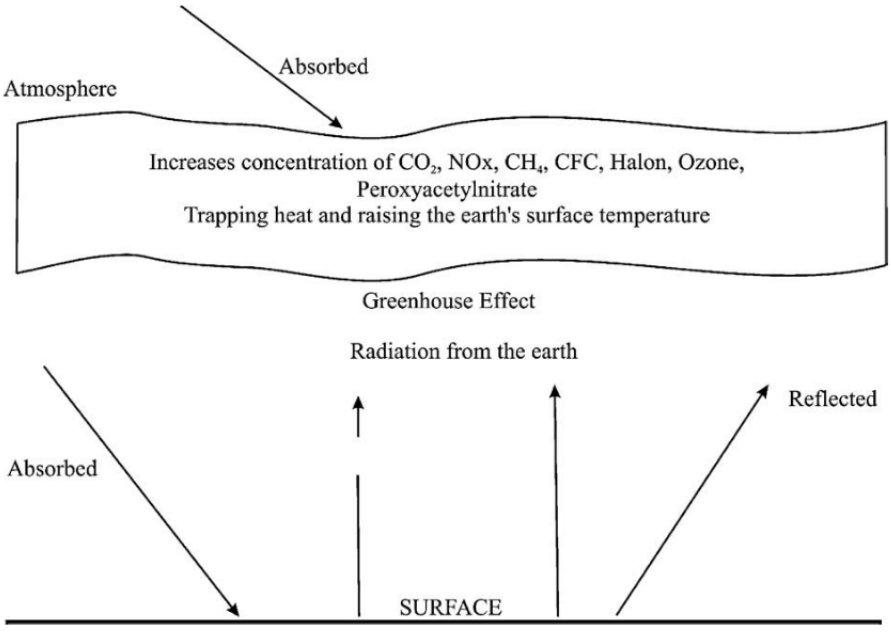

Figure 1.1.1: Illustation of the greenhouse effect [6].

Renewable energy sources have an everlasting energy supply and thus contribute to a sustainable development. They have the ability to release no or almost zero emissions neither from air pollutants or greenhouse gases, making it a cleaner alternative than conventional and fossil energy sources.[4] Renewable energy technologies use primary energy resources that will not be depleted [7]. Optimal use of renewable technologies and resources can minimize the environmental impacts and contribute to produce a minimum of residual waste materials.[6] In 2013 it was estimated that 19.1 % of the global energy consumption originated from renewable sources [8], and this proportion is constantly increasing. An increasing number of companies involved in the oil and gas

industry has also made this type of technology their main focus area the last years, and they are investing large amounts of money to contribute to the renewable future.

1.1.2 Biogas

Biogas is produced from biodegradable organic materials and can therefore originate, for example from the methanation of biomass or organic wastes from sewage sludge, anaerobic digestion, landfills and animal farm manure.[9] The wide variation of sources also gives great variations in the biogas content. The biogas content will also be influenced by factors such as the animal diet composition.[10]

Biogas mainly consists of $\sim$ 60% methane (CH_4) and $\sim$ 40% carbon dioxide (CO_2). It can also contain small amounts of impurities such as hydrogen sulfide (H_2S), water, siloxanes and ammonia (NH_3). Table 1.1.1 presents the typical content in biogas from landfill, anaerobic digestion and municipal waste.[10]

Table 1.1.1: Typical content in biogas from different sources [11] [9].

Component/Biogas source	Landfill	Anaerobic digestion	Municipal waste
CH_4 (vol.%)	40-70	60-70	50-60
CO_2 (vol.%)	30-60	30-40	34-38
N_2 (vol.%)	3-5	0-0.5	0-5
O_2 (vol.%)	0-3	0	0-1
H_2O (vol.%)	100 % (saturated at digester exit temperature)	1-5 % (Water vapor)	100% (saturated at digester exit temperature)
H_2 (vol.%)	0-5	0	
CO (vol.%)	0-3		
H_2S (ppm)	0-20000	0-4000	70-650
Aromatic (mg/m^3)	30-1900		0-200
Ammonia	5 ppm	100 ppm	
Halogenated compounds (mg/m^3)	1-2900	0-5 (Total chlorine as Cl^-)	100-800
Benzene (mg/m^3)	0.6-2.3		
Toluene (mg/m^3)	1.7-5.1		
Siloxanes (ppmv)	0.1-3.5		
Non-methane organics (% dry weight)	0-0.25		
Volatile organics (% dry weight)	0-0.1		

Biogas is considered an attractive energy source because of its elevated CH_4 content. It is often considered a low-grade natural gas with its 55-65% methane content compared to natural gas at about 90-95% methane.[10] Biogas has several applications, and its main uses includes fuel for heat, steam and electricity generation, substitute of natural gas and vehicle fuel [12].

1.1.3 Biogas Purification

Biogas is often purified to biomethane and the process usually includes two steps: trace component removal and biogas upgrading. The second step, where CO_2 is removed, is usually conducted to increase the calorific value to meet requirements in terms of vehicle fuel standards or injection to the natural gas grid. The final product, biomethane, typically consists of 95-97 % CH_4.[12]

In the first step, where small amounts of impurities such as hydrogen sulfide (H_2S), water, siloxanes and ammonia (NH_3) are removed, several technologies are used. Adsorption, absorption, membranes and biological filters are commonly used techniques. The choice of technique is usually based on quality requirements, efficiency and operational conditions.[12] Adsorption is based on the possibility of a gas or liquid to adsorb on the surface of a solid substance. This process should also include regeneration of adsorbent which is often costly.[13] Absorption is quite similar to adsorption, but is based on different solubility of gas components in a liquid solution [9]. Separation by membranes is based on the selective permeability of various components through a semi-permeable membrane [13]. Membranes often have a high removal efficiency and the possibility of removing multiple components simultaneously [12]. Biological filters are especially used in processes to remove odors and to remove H_2S from biogas. For H_2S removal, the method is based on the use of a specific bacteria that is able to oxidize H_2S.[12]

When water reacts with compounds like H_2S and CO_2, it can form acids which can lead to corrosion. Water may also accumulate in pipes and can cause condensation or freezing at elevated pressure. Quality standards for pipelines require a water content of maximum 100 mg/m^3.[12][14] The removal of water is usually performed by physical separation of condensed water or by chemical drying. These methods also make it possible to remove impurities such as foam and dust simultaneously.[12]

Landfill gas and biogas from municipal waste often require removal of siloxanes. Removal of siloxanes is necessary as they can cause severe damage to engines. Siloxanes are oxidized to form silicon oxide during incineration, which can deopsit as microcrystalline quartz that may erode the inside of the motor. The maximum siloxane content limit for purified biogas varies between 0.03

and 0.28 mg/m^3. Removal of siloxanes generally happens through adsorption, physical or chemical absorption or cryogenic separation.[12]

Ammonia can be corrosive when it is dissolved in water, and should therefore be removed from the biogas. This is usually done by an acid wash, adsorption or absorption. Ammonia is also toxic and harmful to human health. Trace components like ammonia may require extra removal steps as a surplus to acid wash, adsorption or absorption, if the removal is not sufficient.[12] Technical specifications for injection of biogas in natural gas grid and use as vehicle fuel in Sweden, Switzerland and Germany requires an NH_3 level lower than 20 mg/Nm^3. In France and Netherlands the limit is as low as 3 mg/Nm^3.[13]

Hydrogen sulfide can cause corrosion on process equipment if it reacts with water. It is also toxic, and can form SO_2 and SO_3 that are even more toxic than H_2S itself [12]. These impurities must therefore be removed to avoid damage on equipment and human health. Technical specifications for injection of biogas into the natural gas grid and use as vehicle fuel require an H_2S level lower than 5 mg/Nm^3 in countries like Germany, France and Austria.[13] There are also regulations on the H_2S content in liquid disposal. Brazilian laws allow a maximum sulfide amount of 2 ppm (mass basis) for disposal in rivers and lakes.[15] For disposal in the ocean, it is the same limit. Hydrogen sulfide (H_2S) is one of the most harmful impurities present in biogas, and this Master Thesis is therefore constructed to investigate the process of H_2S removal from biogas. The purification techniques investigated in this thesis will be further presented in chapter 2.

1.2 Objectives

The main objective of this Master Thesis is to examine different methods for H_2S removal from biogas using Aspen Plus. The objective of this Master Thesis is divided into 3 sub-tasks:

- Perform a literature review on H_2S removal techniques for biogas
- Simulate water scrubbing and amine scrubbing based on MDEA in Aspen Plus.
- Compare the energy requirement of the two technologies to each other and the literature.

1.3 Outline of the Thesis

Chapter 1 has given an introduction to renewable energy sources, including biogas, and the process for cleaning the biogas to biomethane. Chapter 2 gives a description of the techniques for biogas purification used in this Master thesis. The validation of the simulation models used, as well as the simulation models designed, are described in detail in chapter 3, before chapter 4 summarizes the results with subsequent discussion. Finally, chapter 5 includes the conclusion and recommendations for further work.

Chapter 2

Biogas Purification Absorption Technologies

2.1 Water Scrubbing

H_2S has a higher solubility in water than CH_4, which makes it possible to absorb H_2S by using water as the absorption medium [16]. Water scrubbing is known as one of the most effective upgrading technologies, because of the possibility of simultaneous H_2S and CO_2 removal [17]. Biogas upgrading by water scrubbing can achieve high efficiencies (>97 % methane) and low methane losses (<2 %) [18]. However, this technique is less effective for large volumes of biogas [19]. Another disadvantage with water scrubbing is the possibility of microbial growth on the packing material as well as low flexibility in the variation of gas [18]. The process provides its optimal results at high pressures and low temperatures as physical absorption of water increases with decreasing temperature and increasing pressure [20].

Water scrubbing can be implemented in several ways, and the design depends on the amount of polluting compound in the gas. The absorption usually occurs in a gas-liquid-contactor, often packed bed or spray towers.[9] This is to provide a high gas-liquid mass transfer [18]. The biogas is introduced into the bottom of the absorber, while the water is introduced at the top. The raw biogas flows counter currently with the water, and H_2S will dissolve in the water stream. The absorption occurs through physical absorption, which means that there will be no chemical reaction such as in chemical absorption. The absorber can be operated at different pressures, but the most common is somewhere between 8 and 10 bar. The temperature can typically be 20-40 °C. [17][16]

It is possible to implement the upgrading process both with and without regeneration of water, although the latter requires large amounts of pure water. Cozma et al. [17] reports that a water regenerating plant is able to consume nearly 100 times less water than a plant with no water regeneration. Despite of the increased cost and energy demand related to regeneration, this method is usually recommended. The large amount of water required in the case without regeneration, makes this technique best suited for countries with good access to water.[18] The water can be regenerated

by decompression at atmospheric pressure. This will lead to removal of H_2S and CO_2, and usually occurs by air stripping.[16] Regeneration of water happens in a stripper, which is commonly operated at 1 bar [17]. Figure 2.1.1 illustrates biogas purification with water scrubbing of H_2S.

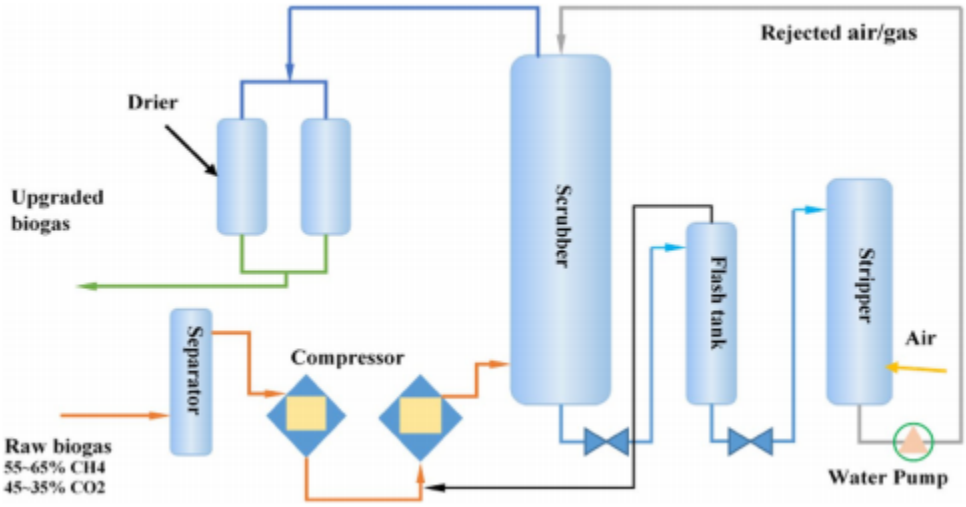

Figure 2.1.1: Water scrubbing of H_2S for biogas upgrading [9].

2.2 Amine Scrubbing

It is possible to remove H_2S by introducing solvents that lead to a chemical reaction. This is possible by using different solvents such as amines, ferric oxides, iron oxides and zinc oxides. Chemical absorption of H_2S with amines has shown good absorption results, and it has also shown to have a good effect on the removal of CO_2. Another advantage with amine scrubbing is the fact that amines can be regenerated. Chemical absorption by amines can be operated cheaply, but expensive investment and required heat for regeneration increase the cost.[19]

Several types of amines can be used in chemical absorption. Organic compounds derived from ammonia such as Monoethanolamine (MEA), Diethanolamine (DEA) and Methyldiethanolamine (MDEA) are commonly used. The general reactions in chemical absorption by amines with regeneration are given below.[19] The H_2S absorption process includes exothermic chemical reactions [21], which means that heat will be released and the temperature will rise.

$$2RNH_2+H_2S \rightarrow (RNH_3)_2S \tag{2.2.1}$$

$$RNH_2+H_2S \rightarrow RNH_3HS \tag{2.2.2}$$

MEA has long been used to remove CO_2 and H_2S from natural gas. MEA has the advantage of high reactivity and low cost. In addition, MEA has a low capacity for absorption of hydrocarbons. At high temperatures, MEA becomes unstable, which can lead to corrosion. It can also form stable carbamates which will give higher energy consumption for the amine regeneration. MEA has a high vapour pressure, and will therefore cause loss of amine by evaporation. DEA has similar properties as MEA, but is more thermally stable and forms less stable carbamates. Compared to MEA, DEA also has higher absorbing capacity. The main disadvantage of using DEA is the need for vacuum distillation in regeneration of spent solutions. MDEA is more costly than MEA and DEA, and has a low rate of reaction with CO_2. This is because MDEA is a tertiary amine, making it more reactive towards H_2S.[22] The reaction between H_2S and aqueous amines is considered infinitely fast as the reaction only involves a proton transfer. In the case of CO_2, the reaction rate with tertiary amines will be lower than for primary and secondary, since CO_2 cannot bind directly to the amine group of tertiary amines. It has previously been researched on the reaction kinetics of CO_2 in aqueous MDEA solutions, where some researchers have concluded that MDEA acts as a catalyst for bicarbonate formation through the hydrolysis of CO_2.[23]

Despite of the increased cost, MDEA is commonly used, especially because of its selectivity towards H_2S. Regeneration of MDEA is also more energy efficient than MEA and DEA because of the low reaction enthalpy. MDEA does not cause corrosion as easily as MEA and DEA because of its high stability. This is a great advantage in terms of equipment maintenance.[22]

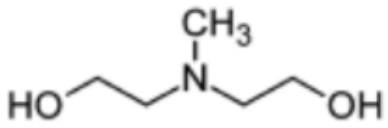

Figure 2.2.1: Structural formula for the MDEA molecule [24].

The biogas scrubber system for removal of H_2S and CO_2 usually consist of an absorption column, a desorption column and a water wash scrubber as shown in figure 2.2.2[19]. The biogas enters the absorption column in the bottom and flows counter currently with the regenerated amine solution. The absorber column is usually operated at atmospheric pressure, and temperatures between 25 and 70 °C.[25][16][13] The amine solution reacts with H_2S and CO_2 before the saturated solution is passed on to the desorption column where the impurities are stripped off. Amines desorb H_2S and CO_2 when heated up to about 120-130 °C and at pressures up to 3 bar.[19][25] The biogas is fed into the water wash scrubber to remove amine traces. The H_2S concentrated gas stream leaving the top of the regeneration unit is often forwarded to be converted to elemental sulfur in the so-called Claus process [26].

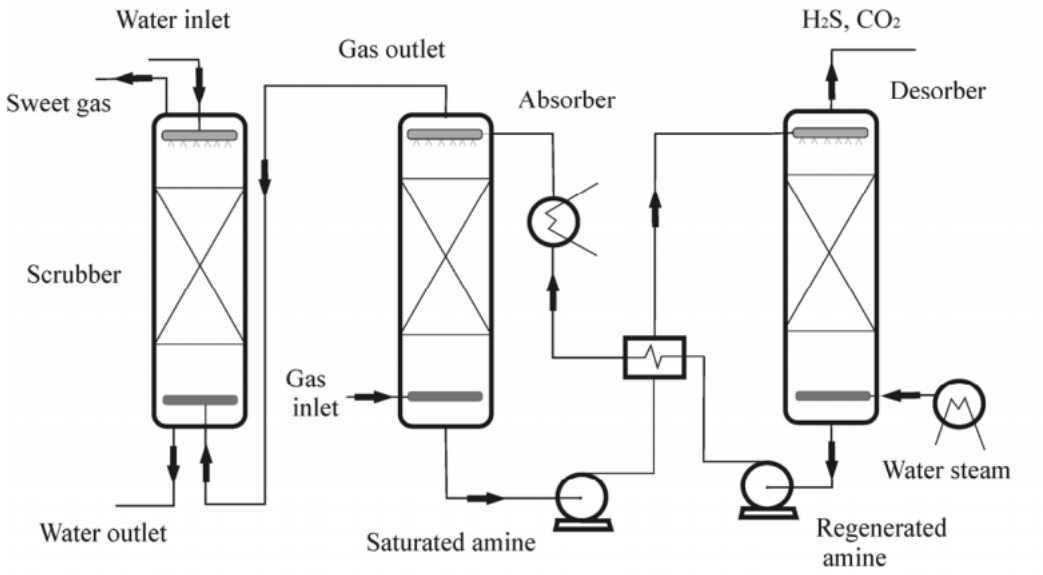

Figure 2.2.2: Amine based biogas H_2S and CO_2 scrubber [19].

2.3 Rate-based and Equilibrium-Stage Simulation Approach

There are two approaches in the simulation of vapor-liquid mass-transfer for absorption processes, rate-based and equilibrium-stage. Both approaches are illustrated in figure 2.3.1.

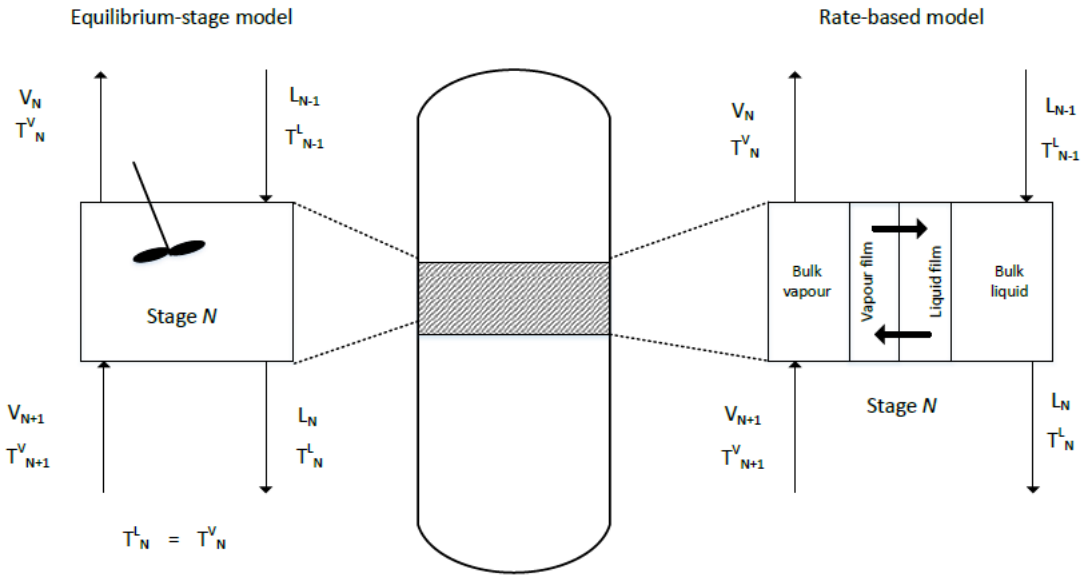

Figure 2.3.1: Illustration of the difference between Rate-based and Equilibrium-stage approach [27].

The equilibrium-stage approach assumes that the vapour and liquid phases are in equilibrium, and that they are perfectly mixed. The vapour and liquid phase temperatures will therefore be the same as they leave the packed section. The rate-based model uses actual rates for mass and heat transfer. The rate-based model does also take into account the chemical reactions for the system. The mass transfer can be described based on the two-film theory.[27] The equilibrium model is simple compared to the rate-based model, and may provide less accurate results. The rate-based model is more accurate, but at the same time it is more difficult to make it converge as the model is more complicated [28].

Chapter 3

Simulation Models

All simulations in this Master Thesis are conducted in Aspen Plus version 10, a part of the Aspen Engineering Suite 10.1 from AspenTech. All simulation models implemented in this Master Thesis are described in this chapter.

3.1 Validation

Before simulation of the different techniques could be implemented, the models had to be validated to make sure that the model predicts reliable results. The vapour-liquid equilibrium (VLE) validation was performed using a sensitivity analysis in Aspen Plus, and comparing data from Aspen Plus with experimental data found in literature. By calculating the deviation between Aspen results and literature data, it is thus possible to assess the model accuracy. The following sections summarize the validations, and an overview of literature data can be found in table 3.1.1.

Table 3.1.1: Overview of literature data with associated temperature and pressure ranges used in the validation.

Literature	System	MDEA concentration	Temperature	Pressure
Antonin Chapoy et al. [29]	$H_2S - H_2O$	-	16-65 °C	4.83-39.62 bar (P_{tot})
Antonin Chapoy et al. [30]	$CH_4 - H_2O$	-	2-40 °C	9.73-179.98 bar (P_{tot})
John J. Carroll, John D. Slupsky, and Alan E. Mather [31]	$CO_2 - H_2O$	-	25-70 °C	0.50-5.00 bar (P_{CO_2})
Alain Valtz et al. [32]	$CO_2 - H_2O$	-	35-45 °C	4.53-79.43 bar (P_{CO_2})
William J Rogers, Jerry A Bullin, and Richard R Davison. [33]	$MDEA - H_2O - H_2S$	23.7 wt%	40-120 °C	6.9E-6-27.30 bar (P_{H_2S})
S. H. Huang and H.-J. Ng. [34] (GPA Report)	$MDEA - H_2O - H_2S$	23.7 wt%	40-120 °C	0.0033 - 0.22 bar (P_{H_2S})
Fang Yuan Jou, Alan E. Mather, and Frederick D. Otto. [35]	$MDEA - H_2O - H_2S$	11.9, 23.7, 50.0 wt%	40-120 °C	0.0021 - 58.90 bar (P_{H_2S})

The validations were performed by a simple flash tank set up, as illustrated in figure 3.1.1. The first input stream consisted of the solvent (water or MDEA), and the second input stream consisted of the gas (H_2S, CH_4 or CO_2). The flash was specified by the temperature defined in literature and a vapour fraction of 0.0001. The sensitivity analysis was performed by varying the mass flow of the

gas stream.

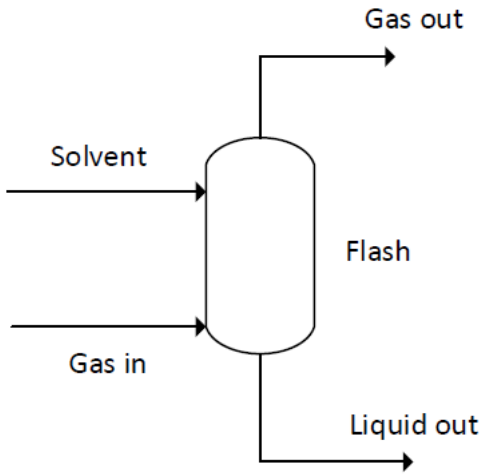

Figure 3.1.1: Illustration of the flash used in VLE validation.

The results from the VLE validation are presented as loadings and partial pressures. The loading was calculated as mole H_2S per mole MDEA. Dalton's law, which is presented in equation 3.1.1 [36], was used to calculate the partial pressures from Aspen. p_A represents the partial pressure of A in vapour phase, while P_{tot} is the total pressure and y_A is the mole fraction of A in vapour phase.

$$p_A = P_{tot} y_A \tag{3.1.1}$$

To find the values corresponding to literature values from Aspen, linear interpolation was used. The equation for linear interpolation is shown in equation 3.1.2 where α represents the loading and P represents the partial pressure.

$$P(\alpha) = P(\alpha_1) + (P(\alpha_2) - P(\alpha_1))\left(\frac{\alpha - \alpha_1}{\alpha_2 - \alpha_1}\right) \tag{3.1.2}$$

The average deviation for each system was calculated as the average of all deviations for each temperature. The deviation was calculated as the absolute value of the difference between the literature value and the value interpolated from Aspen, relative to literature values, as shown in equation 3.1.3.

$$\text{Deviation } [\%] = \frac{|(Value_{Literature} - Value_{AspenPlus})|}{Value_{Literature}} \cdot 100\% \tag{3.1.3}$$

3.1.1 Solubility of H_2S in Water

Aspen Plus provides several combinations of thermodynamic models and models to predict the activity coefficients in the liquid. Four of the available models were compared: NRTL, ENRTL-RK, ELECNRTL and UNIQUAC. NRTL and UNIQUAC uses the Ideal gas law and Henry's law to calculate the liquid activity coefficients. Both models are recommended for highly non-ideal systems [20][37]. ENRTL-RK is an unsummetric electrolyte NRTL model, and uses the Redlich-Kwong equation of state in addition to Henry's law to predict the activity coefficients [37]. The ELECNRTL model is the electrolytic NRTL model with the Redlich-Kwong equation of state. ELECNRTL is an extension, and a more complicated method than the NRTL model. ELECNRTL has added a description of the ionic associations and dissociations along molecular species.[20] This model is mostly used for aqueous and mixed solvent applications.

The validation graphs for each temperature are given in Appendix A.1.1. Overall it can be said that all of the four models provide good results at low pressures (up to 10 bar) for temperatures between 25 and 65 °C. The model that deviates most from the literature data appears to be ELECNRTL, while NRTL is the model that provides the best overall result. Based on the findings it was decided to use the activity coefficient model called NRTL to model the activities of the liquid phase components. The gas phase is modelled using the Ideal gas law [37]. In this chapter results with this model are presented.

The solvent and gas feed streams in the current validation consisted of pure water and H_2S-gas respectively. Figure 3.1.2 presents the result of the total pressure plotted as a function of the H_2S mole fraction in liquid. In this binary system, the total pressure equals the sum of the partial pressure of water and the partial pressure of H_2S. Since water has a boiling point of 100 °C, the partial pressure of H_2S will be high, and the total pressure will therefore be approximately equal to the partial pressure of H_2S. The validation was checked with partial pressures for the highest and lowest temperature, to make sure that the results did not deviate significantly. The partial pressure of H_2S was then found by using the water vapor pressure. Mole fraction of H_2S in liquid represents the absorbed H_2S in the liquid stream out of the absorber (rich loading).

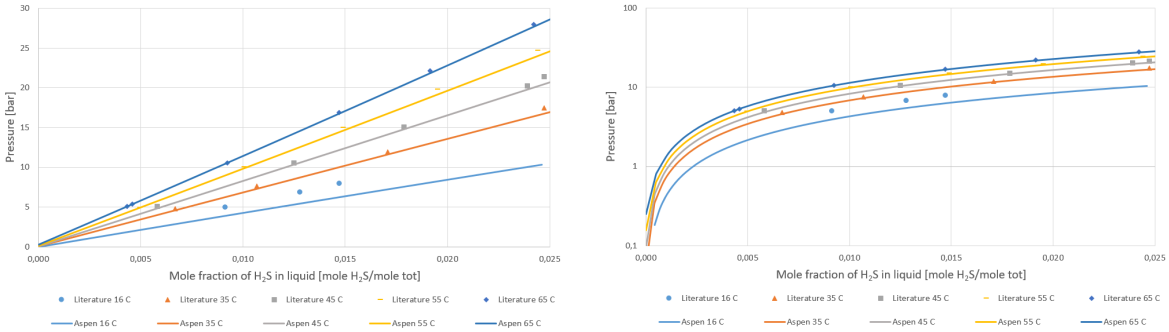

Figure 3.1.2: Validation of the binary $H_2S - H_2O$ system at different temperatures compared to literature data [29]. The graph on the right hand side shows the same result presented on logscale.

The deviation of the results from Aspen compared to literature data were calculated to get the average deviation percentages. The values from Aspen corresponding to the given literature data was calculated by linear interpolation as shown in equation 3.1.2. The average deviations from the validation of the $H_2S - H_2O$ binary system are listed in table 3.1.2.

Table 3.1.2: Average deviations from literature data for the binary $H_2S - H_2O$ system [29].

Temperature [°C]	**Average deviation [%]**	
	Mole fraction of H_2S in liquid	**Total pressure**
16	28	21
35	5	5
45	4	3
55	3	3
65	1	1

The deviations in both mole fraction and pressure are highest for the lowest temperature, 16 °C. The deviations at this temperature exceeds 20 %, which is not a particularly good result. However, this temperature is relatively low in relation to the absorber temperature to be used. The deviations are decreasing with increasing temperature, with <1 % deviation at 65 °C. Since the absorber temperature to be used in this current task is 40 °C, the deviations for the absorber relevant area will be approximately 3-5 %, and can be seen as a good enough result to proceed with the simulations.

3.1.2 Solubility of CH_4 in Water

Solubility of methane is of importance, since methane that is dissolved into water in the absorber will reduce the amount of produced biomethane.

The flash simulations of the $CH_4 - H_2O$ binary system compared to literature data is presented in figure 3.1.3. The average deviations in mole fraction and total pressure from literature are listed in table 3.1.3. Mole fraction of CH_4 in liquid represents the absorbed methane, while pressure represents the total pressure.

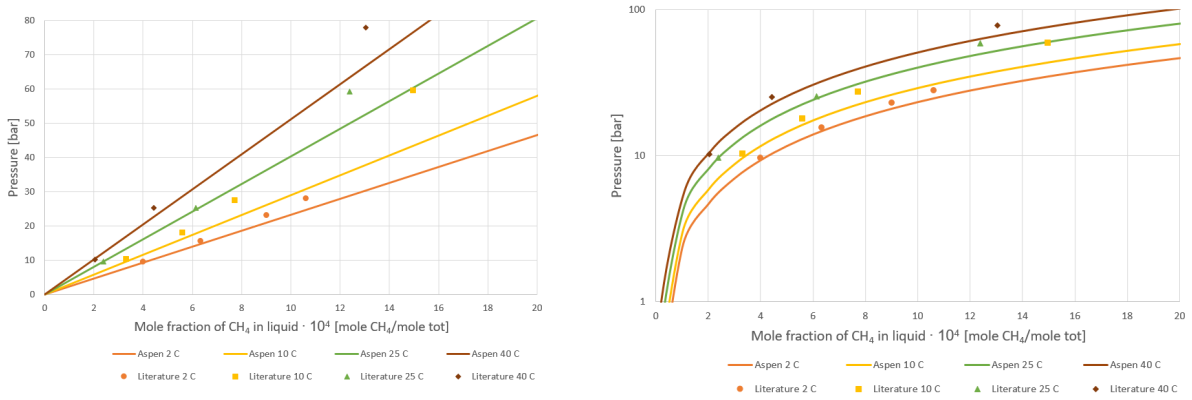

Figure 3.1.3: Validation of the binary $CH_4 - H_2O$ system at different temperatures compared to literature data [30].

Table 3.1.3: Average deviations from literature data [30].

Temperature [°C]	Average deviation [%]	
	Mole fraction of CH_4 in liquid	Total pressure
2	10	8
10	20	16
25	21	14
40	21	15

From table 3.1.3 it appears that the average deviations are quite high. However, since the solubility of methane in water is very small as seen from figure 3.1.3, the absolute deviations are small. Thus, it can be concluded that the selected model can be used to estimate methane solubility during the process simulations.

3.1.3 Solubility of CO_2 in Water

CO_2 is important for the production of biomethane in the same way as CH_4, and validation was therefore also carried out on the binary $CO_2 - H_2O$-system. Aspen simulation results were compared to literature data from Carroll et al. (1991) [31] (low partial pressures of CO_2), and Valtz et al. (2004) [32] (high partial pressures). The result from the validation is presented in figure 3.1.4 and 3.1.5.

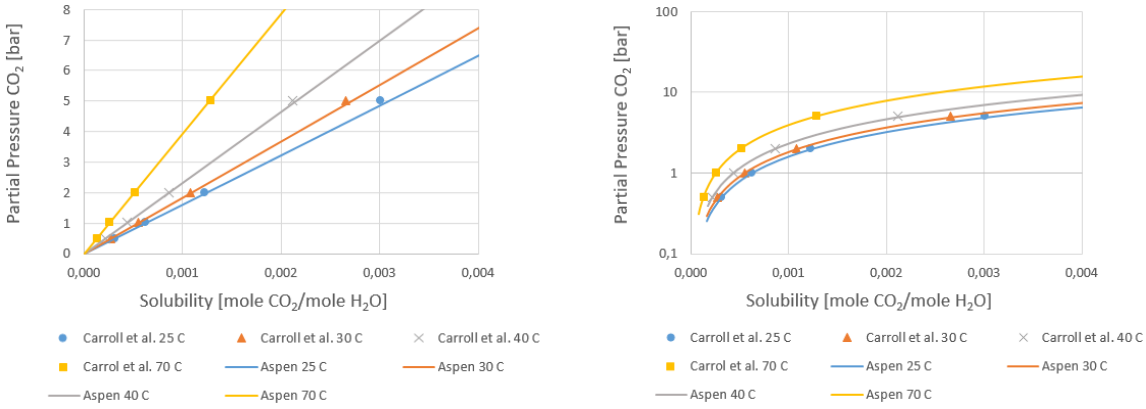

Figure 3.1.4: Aspen simulation at low partial pressures of CO_2 compared to literature data of Carroll et al. [31]. The right graph presents the data in logscale.

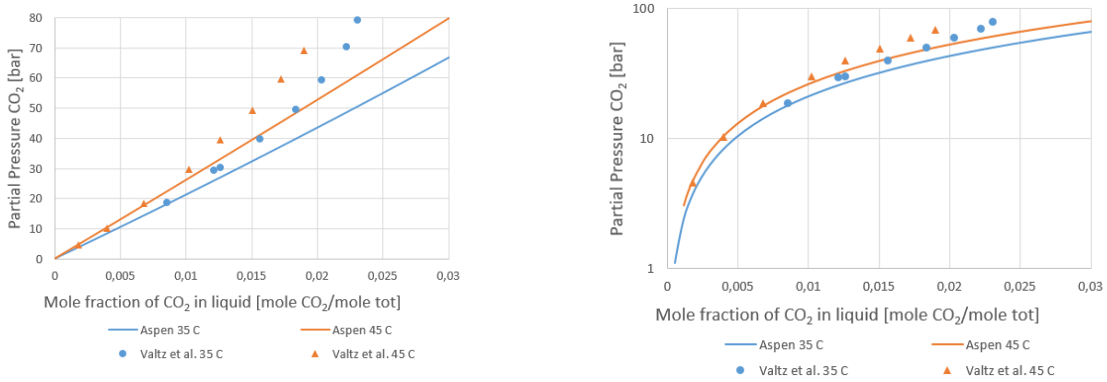

Figure 3.1.5: Aspen simulation at high partial pressures of CO_2 compared to literature data of Valtz et al. [32]. The right graph presents the data with logscale.

The graph deviates most from literature data when the partial pressure of CO_2 exceeds 30 bar. In the water scrubbing system the pressure will be highest in the absorber, where the pressure is set to 8 bar. The model will therefore be accurate enough to complete the simulations for water scrubbing. The average deviations for the validation is presented in table 3.1.4

Table 3.1.4: Average deviations from literature data of Carroll et al. [31] (low partial pressures) and Valtz et al. [32] (high partial pressures).

Temperature [°C]	**Average deviation [%]**	
	Solubility/mole fraction CO_2	**Partial pressure** CO_2
Low partial pressure		
25	2	2
30	1	1
40	1	1
70	3	3
High partial pressure		
35	25	20
45	17	14

CO_2 solubility was calculated for low partial pressures of CO_2, while the mole fraction of CO_2 in the liquid stream out of the absorber was calculated for the high partial pressures. Table 3.1.4 shows that the deviations for the binary $CO_2 - H_2O$-system are low. The deviations from literature data at high partial pressures are higher than the deviations at low partial pressures. The reason for this is that the model deviates from the literature data when the partial pressure exceeds 30 bar. This is included in the average deviation, which will then increase. Since the model deviates at pressures that are so much higher than what is used in the simulation of water scrubbing, it was concluded that the model works well and can be used to predict CO_2 solubility.

3.1.4 Solubility of H_2S in Aqueous MDEA Solutions

In this validation the Aspen Plus template "ELECNRTL_Rate_Based_MDEA_Model", was used. The system was compared to literature data for MDEA concentrations of 11.9 wt%, 23.7wt % and 50.0 wt%.

Figure 3.1.6 presents the results for the validation at an MDEA concentration of 11.9 wt%.

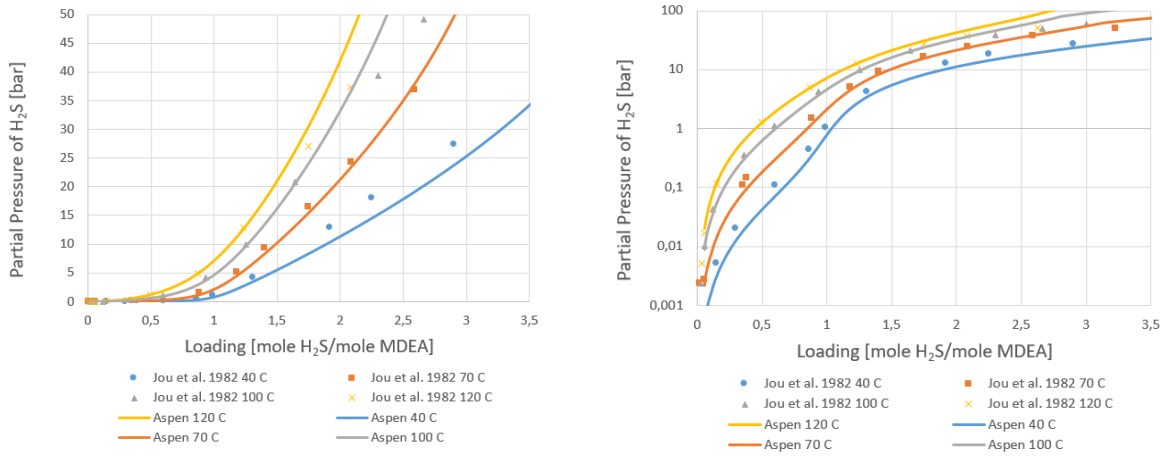

Figure 3.1.6: Validation at 11.9 wt% MDEA [35]. The graph on the right side presents the same graph with log scale.

As can be seen, the results from Aspen seem to correlate well with the literature data for low partial pressures of H_2S in absolute values. The deviation is not significant before the pressure reaches $\sim$ 25 bar. However, the relative deviations are higher at low pressures. The lowest temperature gives higher deviations than for higher temperatures. The average deviations in loading and partial pressure were calculated and are present in table 3.1.5.

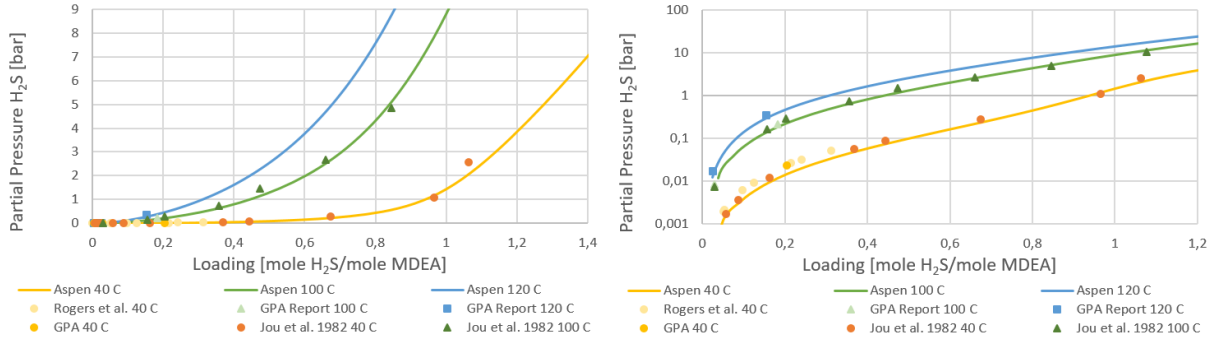

Figure 3.1.7: Validation at 23.7 wt% MDEA [34]. The graph on the right side presents the same graph with log scale.

The results from Aspen coincide well with the literature data. For 40 °C the results from Aspen seem to correlate very well with the literature for partial pressures below 10 bar. The average deviations for the validation with 23.7 wt% MDEA are present in table 3.1.5. The result from the validation with 50.0 wt% MDEA is presented in figure 3.1.8.

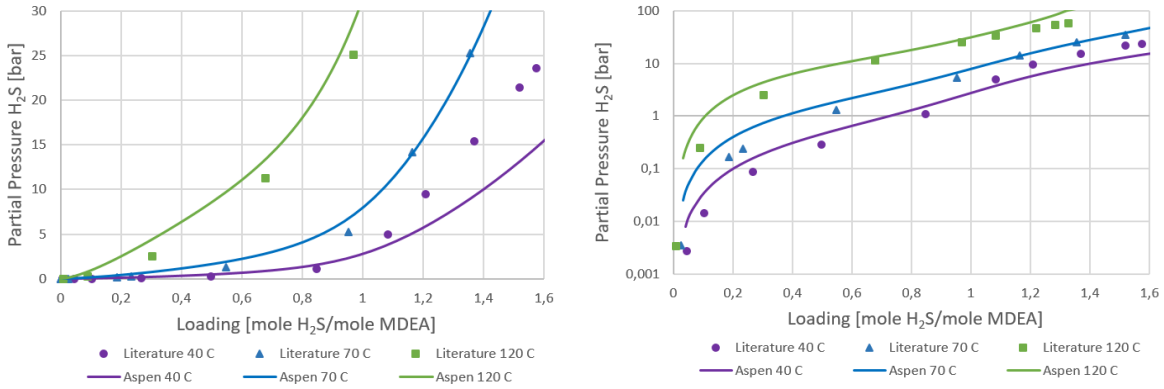

Figure 3.1.8: Validation at 50.0 wt% MDEA [35]. The graph on the right side presents the same graph with log scale.

As can be seen from figure 3.1.8 the model predicts the most inaccurate results for a temperature of 40 °C. For this temperature the model deviates significantly for partial pressures above 5 bar. This is not very fortunate as the absorber temperature to be used in the simulations is also 40 °C. The model seems to correlate well with literature data for higher temperatures. The average deviations in loading and partial pressure for MDEA concentrations of 11.9, 23.7 and 50.0 wt% are listed in table 3.1.5.

Table 3.1.5: Average deviations from literature data of Rogers et al., (1998) [33] (23.7 wt%), GPA report, (1998) [34] (23.7 wt%) and Jou et al., (1982) [35] (11.9, 23.7 and 50 %).

wt%	Temperature [°C]	Average deviation [%]	
		Loading	Partial pressure H_2S
11.9	40	22	60
	70	30	150
	100	14	39
	120	14	49
23.7	40 (Rogers et al.)	32	137
	40 (GPA Report)	29	48
	40 (Jou et al.)	19	68
	100 (GPA Report)	21	65
	100 (Jou et al.)	8	15
	120 (GPA Report)	23	39
50.0	40	42	248
	70	40	560
	100	35	217
	120	24	138

As can be seen in table 3.1.5, the average deviations are quite high, especially for the partial pressure of H_2S. The highest deviations can be found at 70 °C (11.9 and 50.0 wt%). This temperature is relatively high compared to the absorber temperature to be used in this thesis. For 40 °C, the deviation in loading and pressure are 42 and 248 % at an MDEA concentration of 50.0 %. This is a high deviation, but is however not the MDEA concentration to be used in the final model. It was therefore concluded that the model was good enough to carry out the simulations with MDEA concentrations of 23.7 wt%.

The average deviations were compared to the average relative deviation reported for Jou et al. in Modeling Gas Solubilities in the Aqueous Solution of Methyldiethanolamine by Zhang and Chen [38]. The average relative deviation reported was 31.9 % for 108 points and a pressure range of 0.13-5900 kPa (0.0013-59.00 bar). Using the same pressure and loading range, a total of 117 points were found with an average relative deviation of 62.2 %. This must mean that several points have been taken out in the deviation calculation without this being reported, and thus it cannot be compared. All points were therefore included which resulted in an average relative deviation of partial pressure of 155.8 % and a total of 150 points. The deviation in partial pressure of H_2S was plotted as a function of loading to check if there is any correlation. The results for 11.9, 23.7 and 50.0 wt% is presented in figure 3.1.9, 3.1.10 and 3.1.11.

The deviation in partial pressure of H_2S is highest for low loadings. The nine highest points are taken out of the chart for 11.9 wt% to make a clearer view of the majority of the points.

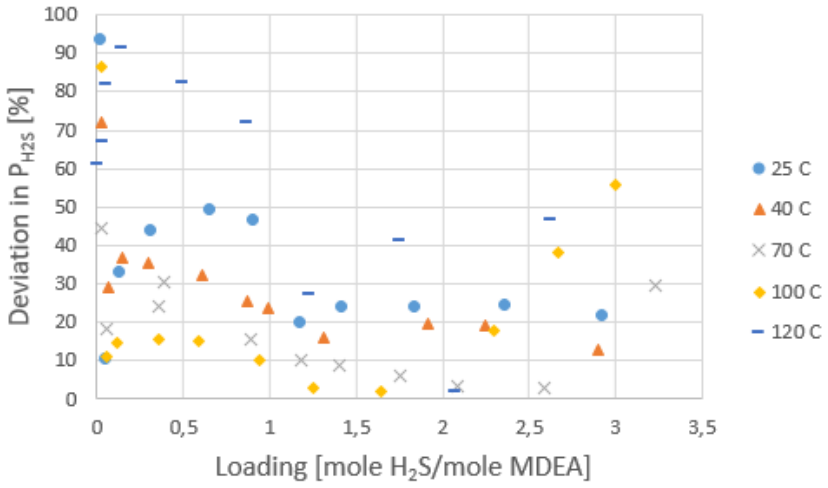

Figure 3.1.9: Average deviation in partial pressure of H_2S from literature Jou et al. [35] as a function of loading for an MDEA concentration of 11.9 wt %.

Three points are taken out in the chart for 23.7 wt %.

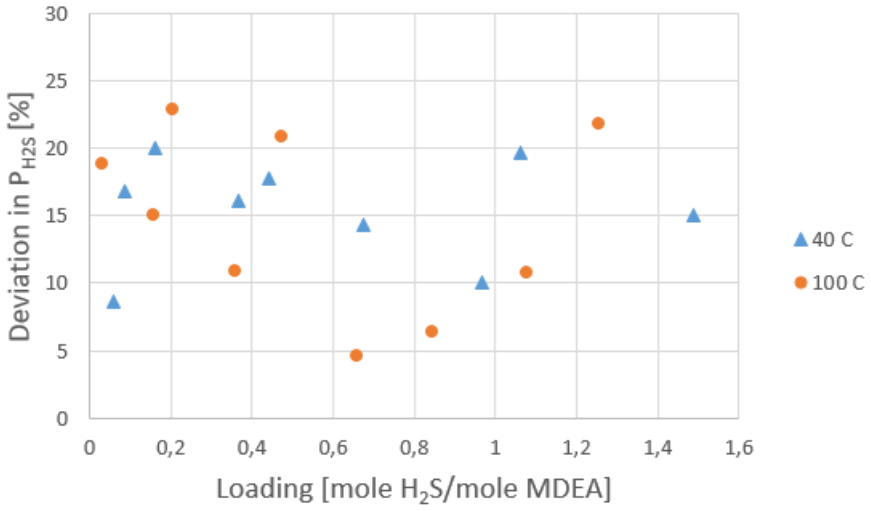

Figure 3.1.10: Average deviation in partial pressure of H_2S from literature Jou et al. [35] as a function of loading for an MDEA concentration of 23.7 wt %.

Sixteen points are taken out in the chart for 50.0 wt % as they have a much higher deviation percentage than the rest of the points.

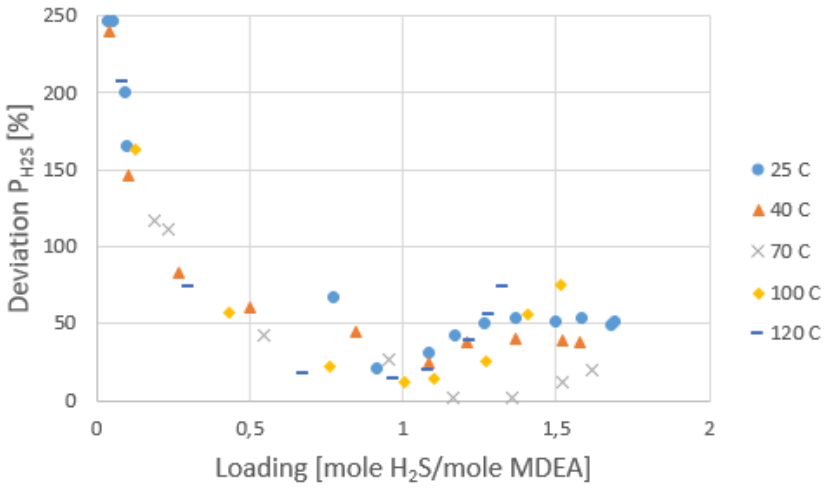

Figure 3.1.11: Average deviation in partial pressure of H_2S from literature Jou et al. [35] as a function of loading for an MDEA concentration of 50.0 wt %.

It seems that the highest deviation in partial pressure of H_2S is presents for low loadings. The general trend for the three MDEA concentrations is that the deviation in partial pressure decrease for increasing loading. For low loadings, the partial pressure is low, which means that the relative deviation gets very high. Usually, it is also more difficult to get accurate experimental results for low partial pressures. The combination of this may be the reason for the decreasing trend in partial pressure deviation. Figure 3.1.10 is more even, and does not decrease significantly. This graph, on the other hand, has only points for two temperatures, and will thus not show an equally clear trend as the other two graphs.

3.2 Water Scrubbing

Three main cases were investigated to examine the possibility of H_2S removal by water scrubbing. The absorber column was implemented as a RadFrac column. The biogas flow was 572.11 kg/hr into the compressor train, consisting of 40 % CO_2 (mole basis), 500 ppm H_2S, 53.25 % CH_4, and was saturated with water. The biogas entered the compressor train at 1.1 bar at 40 °C, and was compressed to 8 bar before the absorber inlet. The main process requirement was to obtain a maximum H_2S content of <5 ppm (mole basis) in the purified gas. It was also desired to keep the methane loss at a minimum. Several parameters were examined, but mainly L/G-ratios, column diameter in terms of flooding and energy requirements. The simulations are performed by rate-based calculations. There will be no chemical reactions in the case of water scrubbing, as the absorption happens through physical absorption.

Initial tests were conducted in order to find the approximate dimensions of the absorber column. The absorber was implemented and simulations were run for different L/G-ratios and heights. The results from the initial tests are presented in Appendix A.1.1. It was decided to use an absorber height of 10 m. The dimensions were adjusted in each case if necessary.

3.2.1 Simple Flash, C-1

The first case that was implemented in Aspen Plus was water scrubbing with regeneration of water by a simple flash tank. Prior to absorption, the biogas was introduced into a compressor train to compress the gas to 8 bar. After each of the heat exchangers, a flash was implemented to remove the liquid from the gas. The compressed gas was then introduced into the absorption column along with regenerated water. The purified gas left the top of the absorber while the liquid was withdrawn at the bottom and further passed into a heat exchanger with subsequent flash to remove the absorbed impurities. The process flow diagram is illustrated in figure 3.2.1. Absorber specifications are presented in table 3.2.1.

The system was tested at various L/G-ratios and flash temperatures to see if it was possible to reach the target of a maximum H_2S-concentration of 5 ppm in the purified gas out of the absorber. The absorber diameter was first increased to 0.6 m to avoid flood in the column. Flooding was detected at L/G-ratios around 150, and the diameter was therefore further increased to 0.8 m. The flash temperature was increased from 40 °C to 60 °C, 80 °C and 90 °C. An attempt was made to improve this case by introducing a water drain that was replaced by introducing pure water into the loop (see section 3.2.2).

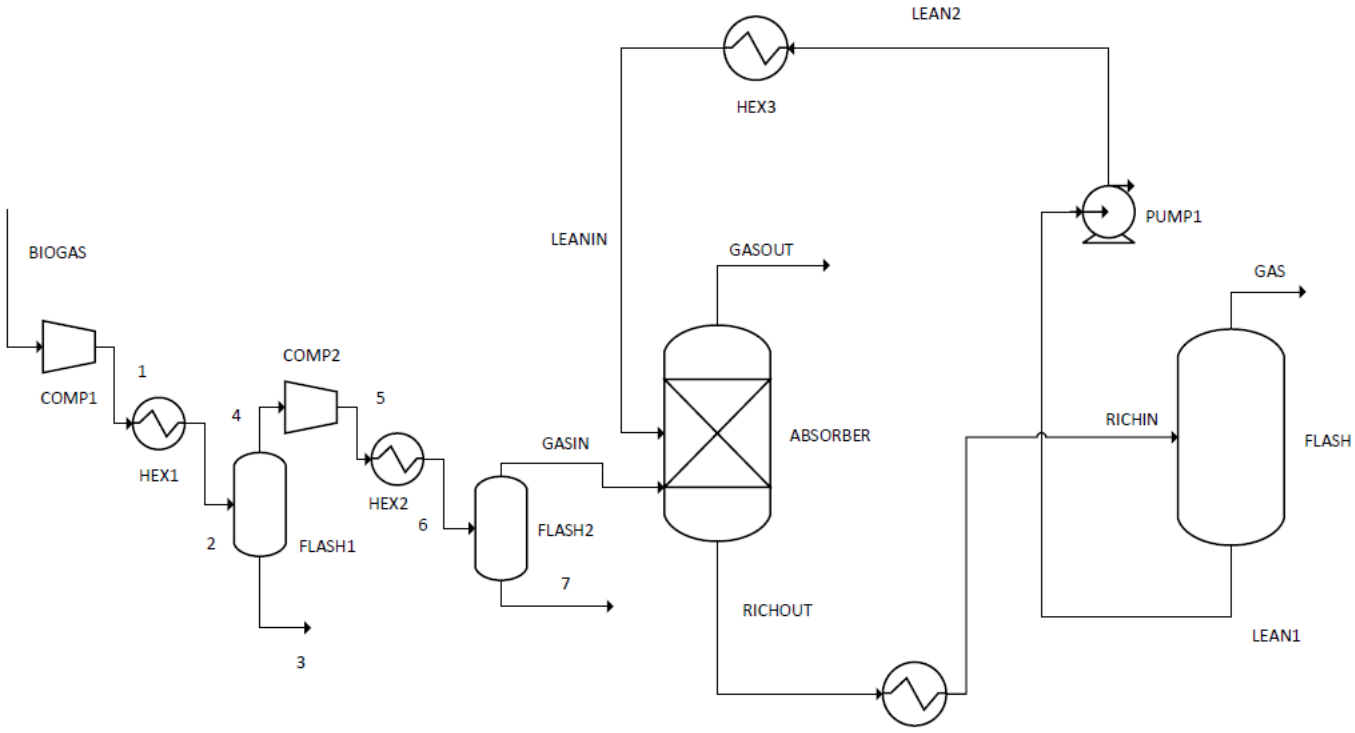

Figure 3.2.1: Water scrubbing with regeneration of water with a simple flash tank.

Table 3.2.1: Absorber specifications in the case with regeneration through a simple flash.

	Absorber	
Object	**Value**	**Unit**
Diameter	0.8	m
Packing dimension	250Y	-
Packing height	10	m
Packing type	FLEXIPAC	-
Stages	20	-
Temperature	-	-
Pressure	8	bar

3.2.2 Flash with Purge, C-2

The effect of a purge was investigated by introducing a split after the absorber and a new water stream that corresponded to the outlet split stream (see figure 3.2.2). By introducing a pure water stream to the lean stream out of the flash, the concentration of H_2S in the loop will decrease. The split ratio required to reach the target at different L/G-ratios was checked to see if this technique could be suitable. The absorber diameter was increased to 0.8 m to avoid flooding in the column.

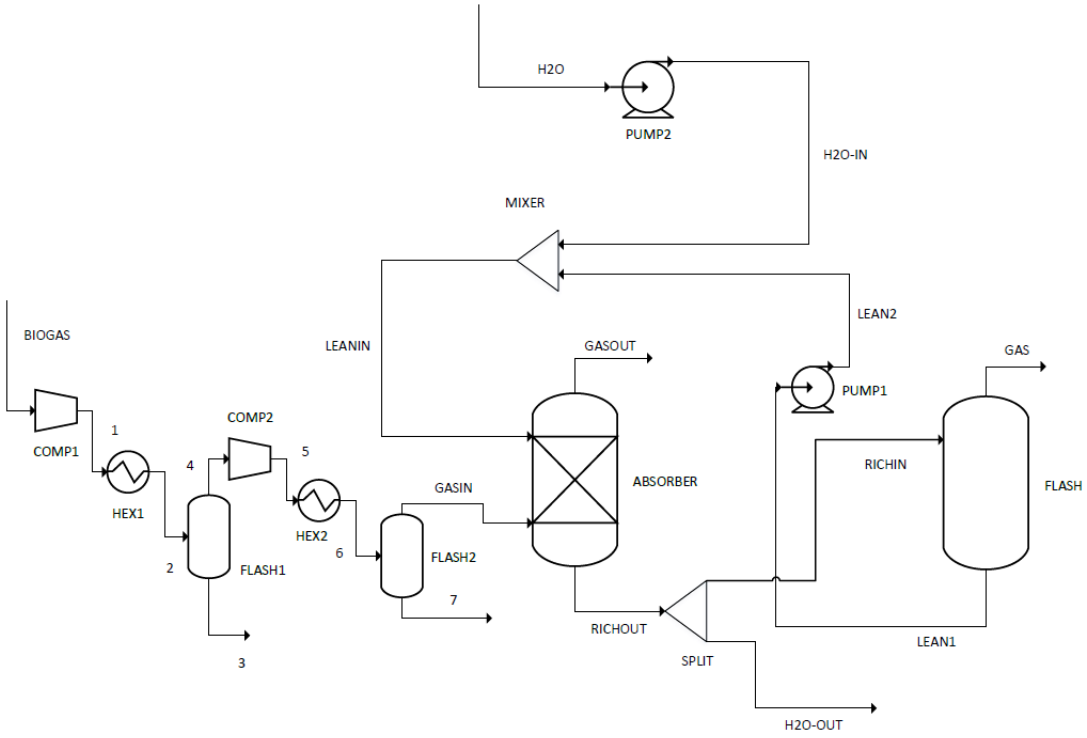

Figure 3.2.2: Water scrubbing with regeneration of water by a flash and a water purge.

In figure 3.2.3 the split is implemented after the flash tank. This was done due to environmental reasons in terms of H_2S disposal. The possibility of optimization of the methane loss was investigated by the implementation of a gas-recycling stream. The gas out of the top of the flash was recycled back and mixed with the biogas inlet stream. The pressure in the flash was changed from 1 bar to 1.1 bar to avoid an extra compressor. The purging system including gas recycle is presented in figure 3.2.4.

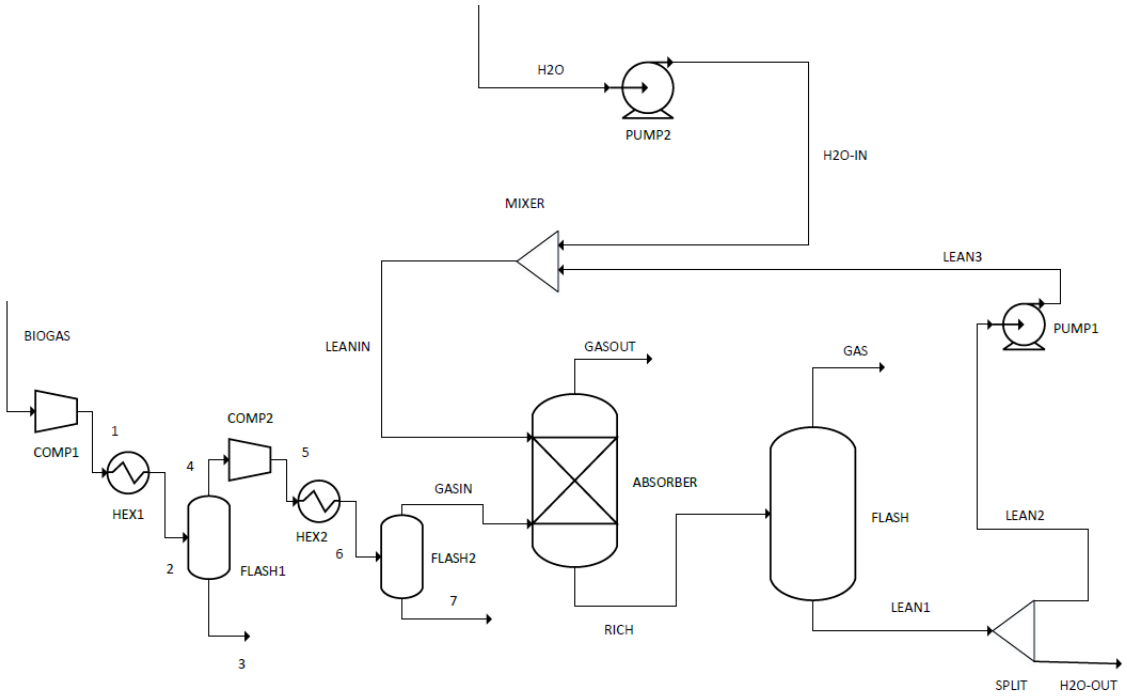

Figure 3.2.3: Process flow diagram of the system including water purge excluding gas recycle, where the split is inserted after the flash tank.

Table 3.2.2: Absorber specifications in the case with regeneration through a flash including a water purge.

	Absorber	
Object	**Value**	**Unit**
Diameter	0.8	m
Packing dimension	250Y	-
Packing height	10	m
Packing type	FLEXIPAC	-
Stages	20	-
Pressure	8	bar

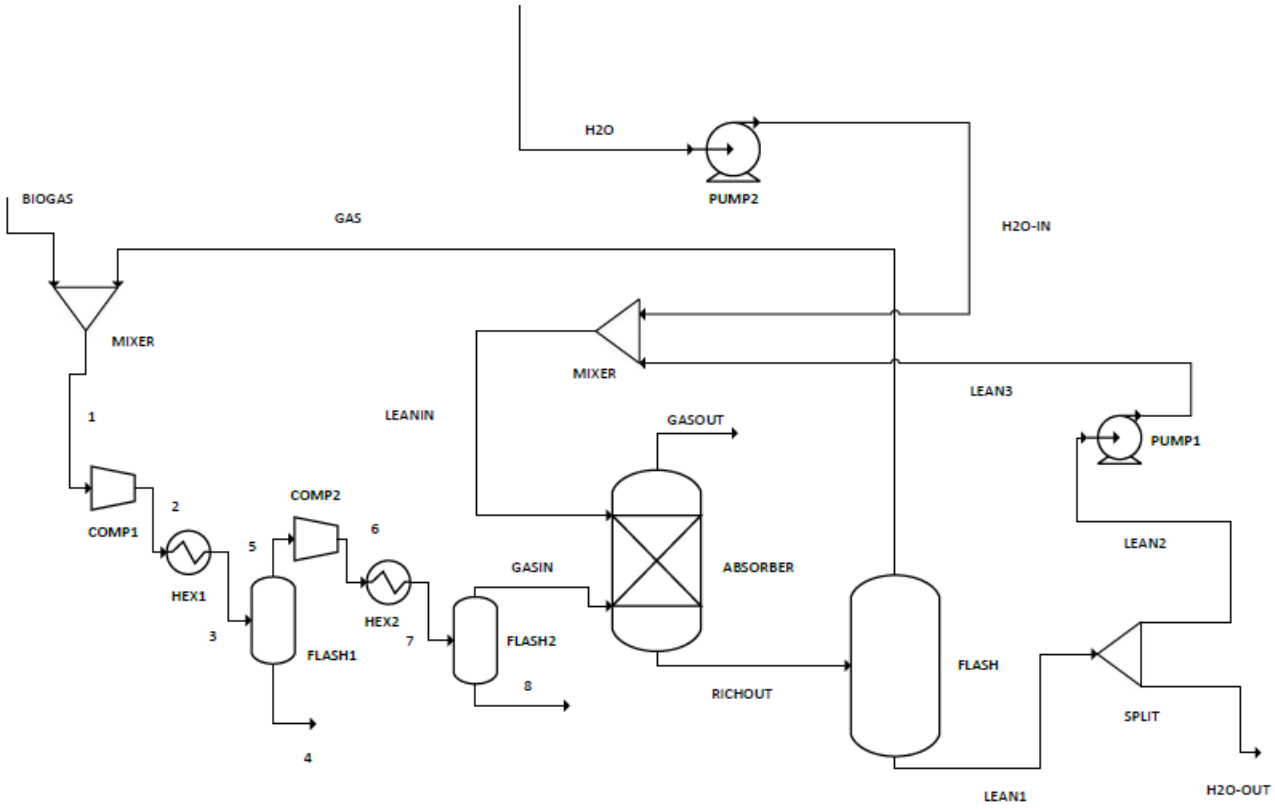

Figure 3.2.4: Water scrubbing with regeneration of water by a flash. A water purge was implemented as well as a gas recycle.

Based on the results of the water scrubbing system with regeneration by a flash, including a water purge, it was decided to investigate the performance of a water scrubbing system with no regeneration (C-3). This case requires a continuously supply of water, as the rich stream does not undergo a regeneration process. Since fresh water is used to absorb the H_2S without any recycling, the water entering the H_2S absorption tower is free from H_2S (lean loading = 0).

The results from the purging system proved that the methane loss could be optimized by introducing a gas recycle, as expected. It was therefore decided to implement a gas recycle in the case with no regeneration of lean solution. The system including gas recycle is displayed in figure 3.2.5.

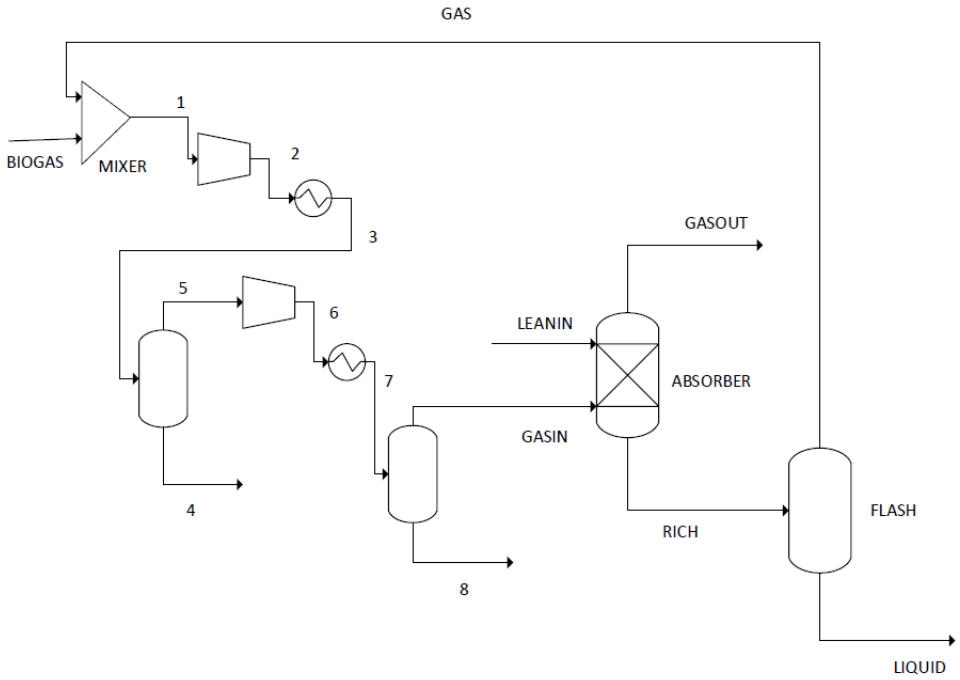

Figure 3.2.5: Absorber system including gas recycling.

Table 3.2.3: Absorber specifications in the case with no regeneration of the lean stream. The gas out of the flash is recycled back to the absorber.

	Absorber	
Object	**Value**	**Unit**
Diameter	0.5	m
Packing dimension	250Y	-
Packing height	10	m
Packing type	FLEXIPAC	-
Stages	20	-
Temperature	-	-
Pressure	8	bar

3.2.3 Air Stripping, C-4

The last case included examination of an air stripping system. In this case the desorber was implemented as a RacFrac column in Aspen Plus as an alternative to the flash used in the two previous cases. The absorber diameter was 0.6 m. The air stream consisted of nitrogen and oxygen and was saturated with water at 20 °C. In the same way as in the previous case, the system can be

optimized for methane losses. Therefore, a recirculation stream of the gas from the top of the flash was implemented in this case as well. The flash was placed between the absorber and the desorber, and was operated at 2 and 5 bars, where the latter provided the best results. The final air stripping arrangement is presented in figure 3.2.6.

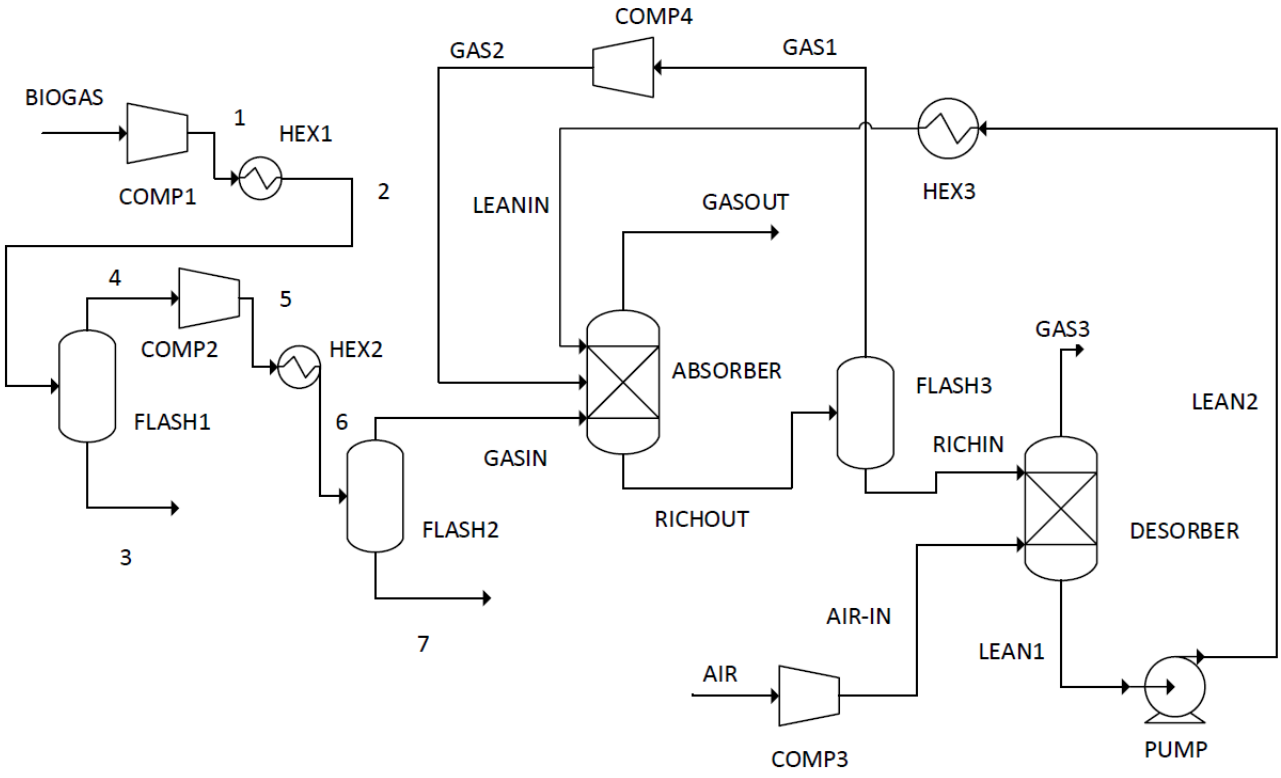

Figure 3.2.6: Water scrubbing system with air stripping and gas recycle.

Table 3.2.4 lists the most important specifications for the absorber and desorber.

Table 3.2.4: Absorber and desorber specifications in the case with air stripping.

	Absorber		**Desorber**	
Object	**Value**	**Unit**	**Value**	**Unit**
Diameter	0.6	m	0.7	m
Packing dimension	250Y	-	250Y	-
Packing height	10	m	7	m
Packing type	FLEXIPAC	-	FLEXIPAC	-
Stages	20	-	20	-
Pressure	8	bar	2 and 5	bar

3.3 Amine Scrubbing

The biogas content was specified as described in water scrubbing, section 3.2. The biogas entered the absorber at 1.1 bar, and there was no compressor train prior to the absorber. Before the implementation of the complete amine scrubbing system, the absorber was analyzed to find the right dimensions. The result from this can be found in Appendix A.1.2. It was decided to use a column height of 20 m and a column diameter of 0.35 m. Both the absorber and the desorber were implemented as RadFrac columns.

3.3.1 Reactions

The reactions for the amine scrubbing system as presented in the template are listed in table 3.3.1.

Table 3.3.1: Reactions from Aspen Plus for the amine scrubbing system using the ELECNRTL_Rate_Based_MDEA_Model template.

Reaction type	Reaction number	Stoichiometry
EQUIL	1	MDEAH+ + H2O $\longleftrightarrow$ MDEA + H3O+
EQUIL	2	2 H2O $\longleftrightarrow$ H3O+ + OH-
EQUIL	3	HCO3- + H2O $\longleftrightarrow$ CO3-2 + H3O+
KINETIC	4	CO2 + OH- $\longrightarrow$ HCO3-
KINETIC	5	HCO3- $\longrightarrow$ CO2 + OH-
EQUIL	6	H2S + H2O $\longleftrightarrow$ HS- + H3O+
EQUIL	7	HS- + H2O $\longleftrightarrow$ S-2 + H3O+
KINETIC	8	MDEA + CO2 + H2O $\longrightarrow$ MDEAH+ + HCO3-
KINETIC	9	MDEAH+ + HCO3- $\longrightarrow$ MDEA + CO2 + H2O

The reactive absorption of gases involves chemical reactions. Therefore, in this system chemical and phase equilibrium needs to be solved. In table 3.3.1 the set of reactions are shown where EQUIL indicates the equilibrium reactions and KINETIC the kinetic reactions, as this work uses the rate-based approach. The equilibrium reactions are modelled by equilibrium constants.[25] In Aspen Plus, the equilibrium constant K_{eq} can be calculated from Gibbs energy, or from the in-built expression shown in equation 3.3.1.

$$lnK_{eq} = A + \frac{B}{T} + Cln(T) + DT \tag{3.3.1}$$

A, B, C and D can be determined from data banks in Aspen Plus, or be defined by the user. The T symbolizes the temperature, and should be stated in Kelvin. Kinetic reactions are irreversible, and the reactions are determined by final rates. Kinetic factors in Aspen Plus can be specified by an in-built Power Law expression, as shown in equation 3.3.2, or by using a user kinetic subroutine. k, n and E can be obtained from Aspen data banks or defined by the user. R is the Ideal gas constant.

$$\text{Kinetic factor} = kT^n e^{\frac{-E}{RT}} \tag{3.3.2}$$

The reaction between MDEA and H_2S is not a part of the reaction system. This is because the reaction happens rather rapidly, which means that the system will be limited by equilibrium, and not this specific reaction.

Reaction 1 illustrates the protonation of MDEA, and reaction 2 shows the protonation of water. Reaction 4 illustrates the reaction between CO_2 and OH^- from the dissociation of water. Reaction 3 shows that bicarbonate, HCO_3^-, reacts further with water to form carbonate, CO_3^{2-} and H_3O^+. Reaction 5 is the reverse of reaction 4. Reaction 6 is the dissociation reaction of H_2S, and reaction 7 is the dissociation of HS^-. Reaction 8 gives the reaction between MDEA and CO_2, and reaction 9 is the same reaction reversed. H_2S and CO_2 will react with MDEA through chemical absorption, and also be dissolved in the solvent through physical absorption. CH_4 will only be absorbed through physical absorption.

After the initial tests to decide the absorber dimensions, the absorber was investigated further in terms of loadings, L/G-ratio and removal efficiency. The system consisted of the absorber with two input streams, one with the aqueous MDEA solution and one with biogas. Temperature and concentration profiles were also examined for the absorber, and the results are described in chapter 4.

After the absorber analysis, the complete amine scrubbing system was implemented to Aspen Plus, as illustrated in figure 3.3.1. Absorber and desorber specifications can be found in table 3.3.2. The biogas is led into the absorber at 1.1 bar. The purified gas exits the top of the absorber, where it is cooled down to 40 °C to regenerate any MDEA solution that may be in the gas. The remaining purified gas is then compressed to 8 bar in two steps to get the same outlet pressure as for water scrubbing. The gas is cooled down to 40 °C after each compressor, and any liquid is separated by a flash. The rich stream out of the absorber, containing the absorbed H_2S, continues into a pump as the pressure in the desorber is 2 bar. A heat exchanger ensures that the rich stream is heat exchanged with the hot lean stream out of the desorber. The rich stream enters the desorber where H_2S is supposed to be stripped off. The gas leaves the desorber at the top, where it is cooled down

to 25 °C and liquid is recycled back to the desorber. The lean stream leaves the desorber in the bottom, and enters the heat exchanger. Then, the lean stream is cooled down to 40 °C, before it is recycled back to the absorber.

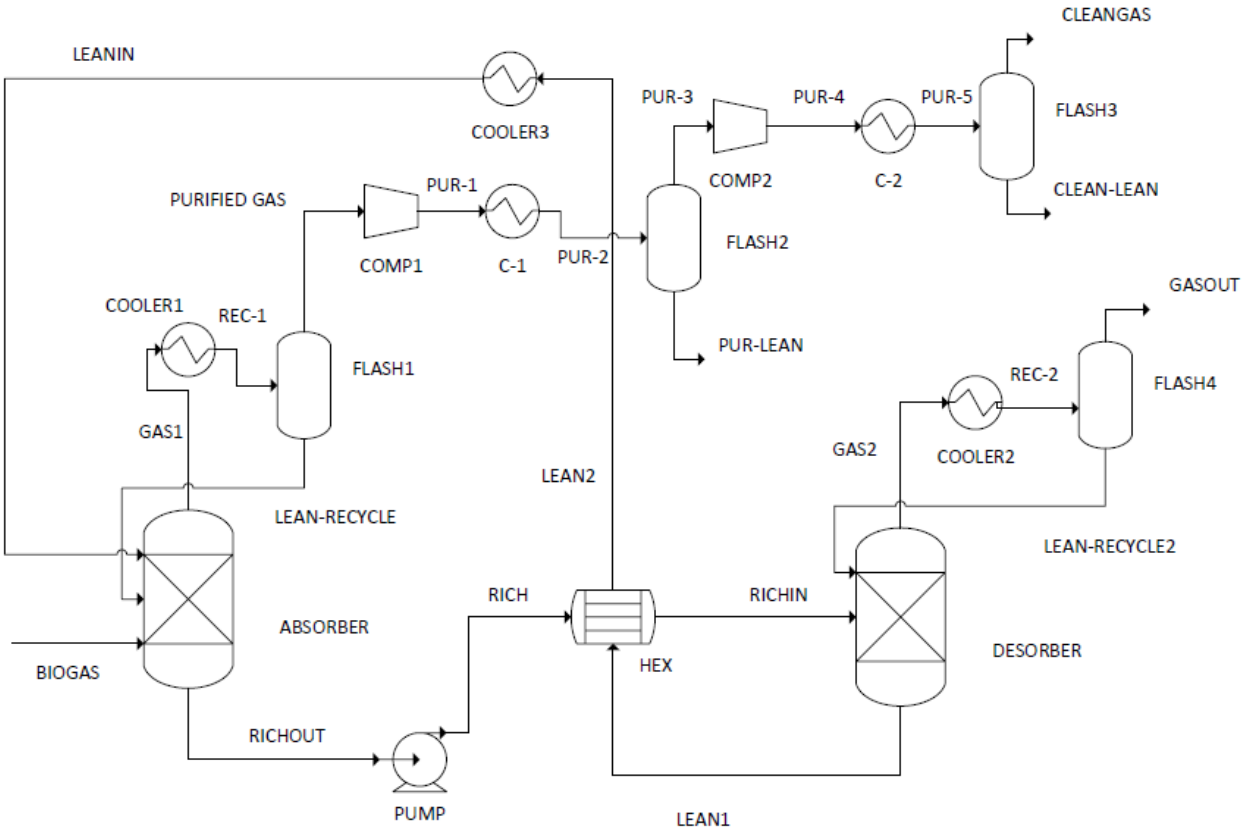

Figure 3.3.1: Process flow diagram of the amine scrubbing system.

Table 3.3.2: Absorber and desorber specifications for amine scrubbing.

	Absorber		**Desorber**	
Object	**Value**	**Unit**	**Value**	**Unit**
Diameter	0.35	m	0.65	m
Packing dimension	250Y	-	250Y	-
Packing height	20	m	20	m
Packing type	FLEXIPAC	-	FLEXIPAC	-
Stages	20	-	20	-
Pressure	1.1	bar	2	bar

It was difficult to optimize the amine scrubbing simulation in terms of reboiler duty and convergence. It was therefore determined that two cases, respectively, for L/G = 14 (C-5) and L/G = 16 (C-6) should be examined. These cases were also taken into account when the energy demand was calculated.

After the comparison of the two amine scrubbing cases, the case with L/G-ratio at 16 (C-6) was used as the final case, as this case obtained the purify target of maximal 5 ppm H_2S in the purified gas. The reboiler duty was adjusted down from 1000 kW to 350 kW. It should be noticed that this case obtained a purity far within the target.

An overview of the main cases investigated can be found in table 3.3.3.

Table 3.3.3: The main cases implemented in Aspen Plus.

Case label	**Case**
Case 1 (C-1)	Simple flash
Case 2 (C-2)	Flash w/purge
Case 3 (C-3)	Absorber w/gas-recycle
Case 4 (C-4)	Air Stripping w/gas-recycle
Case 5 (C-5)	Amine Scrubbing L/G = 14
Case 6 (C-6)	Amine Scrubbing L/G = 16

Chapter 4

Results and Discussion

4.1 Water Scrubbing

4.1.1 Simple Flash, C-1

The starting point for the water scrubbing simulation model was a system consisting of an absorber and a simple flash for regeneration. The best result was obtained with a high flash temperature (90°C), which was expected as the stripping is favored by high temperatures. The result is shown in figure 4.1.1.

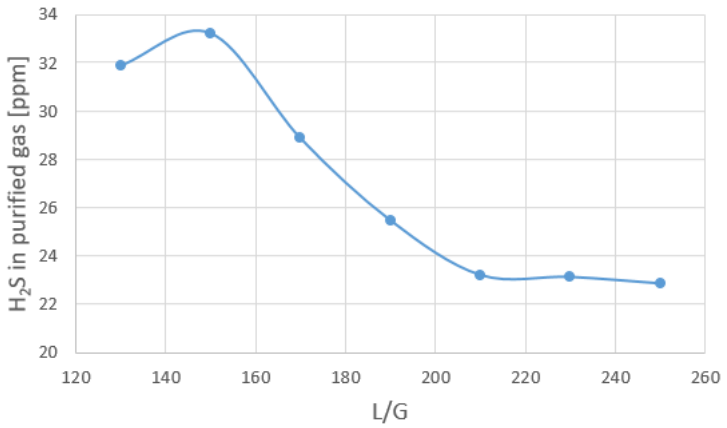

Figure 4.1.1: Mole fraction of H_2S in the purified biogas as a function of L/G-ratio when water is regenerated through a flash at 90 °C.

The H_2S in the purified gas represents the amount of H_2S in the purified biogas on mole basis. The general trend is that a higher L/G-ratio (mass basis) gives a lower H_2S content in the biogas, which makes sense as there is more solvent to absorb H_2S. The absorbed amount of H_2S for this case stabilizes at an L/G-ratio above 200 for a flash at 90 °C. Higher flash temperature gives better absorption performance, but will also increase the energy demand. In addition, there will be a need for large amounts of water to achieve a significant decrease in the H_2S content in the biogas. It is

also important to consider that water has a boiling point of 100 °C and will thus evaporate at this temperature. It should be noticed that this case did not fulfill the target of less than 5 ppm H_2S in the purified gas out of the absorber. The energy demand and type for all equipment included in this case is listed in table 4.1.1, together with the other water scrubbing cases.

Table 4.1.1: Comparison of energy demand and type for four different water scrubbing cases.

Case	Equipment	Duty [kW]	Type
Simple flash C-1	COMP1	21.8	Electricity
	HEX1	32.2	Cooling
	COMP2	23.7	Electricity
	HEX2	27.9	Cooling
	HEX3	6480.9	Heating
	PUMP	31.1	Electricity
	HEX4	6260	Cooling
	SUM	**12877.6**	**kW**
Flash with purge C-2	COMP1	21.8	Electricity
	HEX1	32.2	Cooling
	COMP2	23.7	Electricity
	HEX2	27.9	Cooling
	PUMP1	1.6	Electricity
	PUMP2	20.1	Electricity
	SUM	**127.3**	**kW**
Absorber with recycle C-3	COMP1	29.1	Electricity
	HEX1	43.3	Cooling
	COMP2	31.7	Electricity
	HEX2	37.3	Cooling
	SUM	**141.4**	**kW**
Air Stripping C-4	COMP1	21.7	Electricity
	HEX1	21.1	Cooling
	COMP2	23.6	Electricity
	HEX2	22.5	Cooling
	COMP3	40.3	Electricity
	PUMP	16.0	Electricity
	HEX3	31.2	Cooling
	COMP4	0.3	Electricity
	SUM	**176.7**	**kW**

Table 4.1.1 shows that the case with regeneration through a simple flash gives a total energy demand of 12877.6 kW. 50 % of this energy is required by HEX3. The reason for this is that a high temperature is used in the flash to remove impurities, thus requires a lot of energy to heat the stream before it enters the flash. HEX4 requires almost the same amount of energy in terms of cooling. This is because the stream has to be cooled down to 40 °C before the absorber inlet. It is possible to lower the energy demand in this case by lowering the flash temperature, but this will then be at the expense of the absorption performance. For this current task, the regeneration through a simple flash did not meet the requirement for a purified biogas with less than 5 ppm H_2S content.

4.1.2 Flash with Purge, C-2

In the case with water purge and pure water mixing, the split fractions required to obtain the purity at different L/G-ratios were plotted. The split fractions represent the fraction that will stay in the loop. The result is presented in figure 4.1.2.

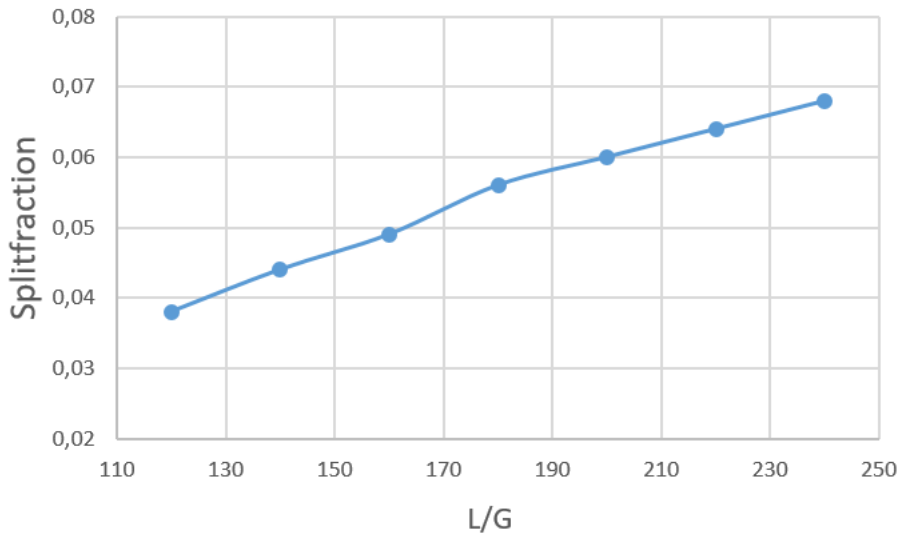

Figure 4.1.2: The split fractions needed to obtain the target of 5 ppm in the gas out of the absorber as a function of L/G-ratio.

From figure 4.1.2 it can be seen that over 90 % of the water must be replaced to reach the requirement of a maximum H_2S content of 5 ppm. This means that the extra cost of implementing a split and purge may not give much benefit, as most of the water must be replaced anyway. In addition, the content of H_2S in the water flow out of the split must be taken into account, as there are regulations on sulfur content of liquid disposal into the sea. It may be more profitable to implement a

system without regeneration. This was therefore investigated as a sub-case (C-3).

It was decided to use the purging case to check if the methane loss could be optimized by introducing a gas recycle to the system. The results are shown in table 4.1.2.

Table 4.1.2: Effect of a gas recycle to the system containing a water purge.

L/G	Splitfraction	P_{Flash} [bar]	Mole frac. of H_2S in purified gas	Methane loss [%]	Gas recycle
120	0.033	1	4.78 ppm	3.1	No
120	0.041	1	5.91 ppm	3.1	No
120	0.041	1.1	13.9 ppm	0.03	Yes

Table 4.1.2 clearly shows that the implementation of a gas recycle can provide a significant decrease in methane losses from 3.1 % to 0.03 %. This makes sense as the L/G-ratio is fixed. It should be noticed that the pressure in the flash is slightly increased in the case with gas recycle to avoid an additional compressor. The purity of the gas decreases with the gas recycle as some of the impurities left in the gas will be recycled back to the absorber. It will therefore be a matter of judgment what is desired in each case and if a gas recycle should be implemented.

The energy requirement for the case with a water purge is listed in table 4.1.1. The energy calculations are based on the case with split fraction of 0.033 without a gas recycle, as the target can be reached. From the table it can be seen that the energy demand in this case is low. It is possible to reach the target of maximum 5 ppm in the purified gas when there is no recycle to minimize the methane loss. It will, however, be costly with equipment to remove parts of the rich stream in addition to mixing the lean stream with clean water. A system with no regeneration of water may therefore be a better alternative.

Absorber with Gas Recycle, C-3

Since the case with a water drain was dependent on replacing almost all the water to reach the target, it was investigated how much energy was required for the case without water regeneration. Figure A.1.7 in Appendix A.1 shows that the target can be reached for an L/G-ratio between 90 and 100 with an absorber of 10 m.

Figure 4.1.3 presents the removal efficiency of an absorber containing a compressor train and a gas recycle. The height of the absorber was 10 m, and the diameter was adjusted to 0.5 m. It can be seen that the removal efficiency stabilizes at 100 % for an L/G-ratio above 100. As can be seen from figure 4.1.4 the purity target is obtained for an L/G-ratio of $\sim$ 125. The target of 5 ppm is marked with an orange, dashed line.

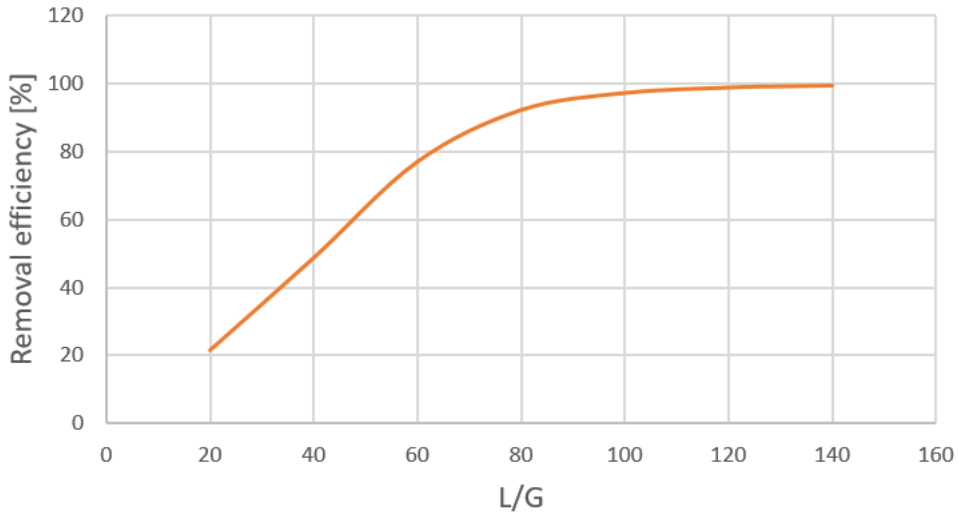

Figure 4.1.3: Removal efficiency as a function of L/G-ratio for an absorber system including a compressor train for compression of biogas, and a gas recycle to minimize the methane loss.

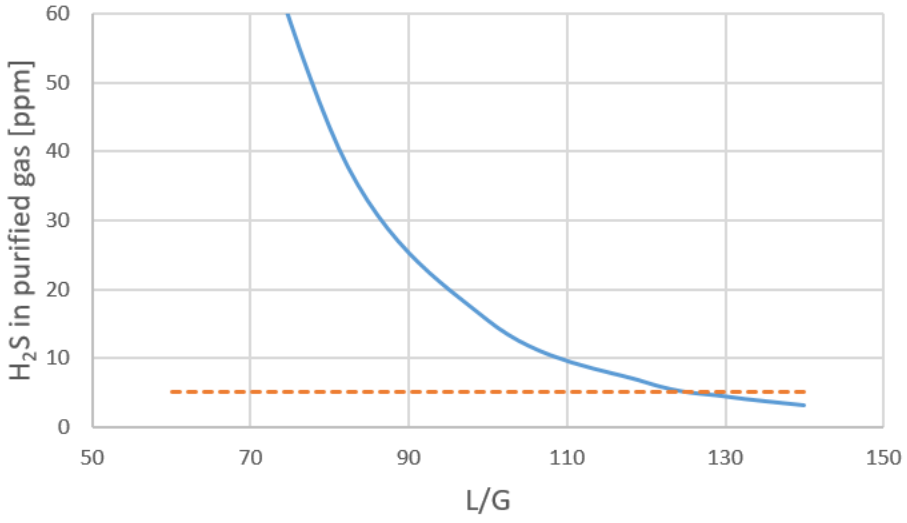

Figure 4.1.4: Amount of H_2S in the purified gas plotted as a function of L/G-ratio when the biogas is compressed in a compressor train and the gas is recycled.

Figure 4.1.5 and 4.1.6 present the rich loading and methane loss as a function of L/G-ratio. The rich loading has a peak for L/G at 60, before it decreases steadily with increasing L/G-ratio. The absorption of H_2S is nearly constant compared to the increase in L/G-ratio, and it therefore makes sense that the rich loading decreases. The methane loss increases with increasing L/G-ratio because the increasing amount of water makes it more easily to absorb the impurities, but also CH_4.

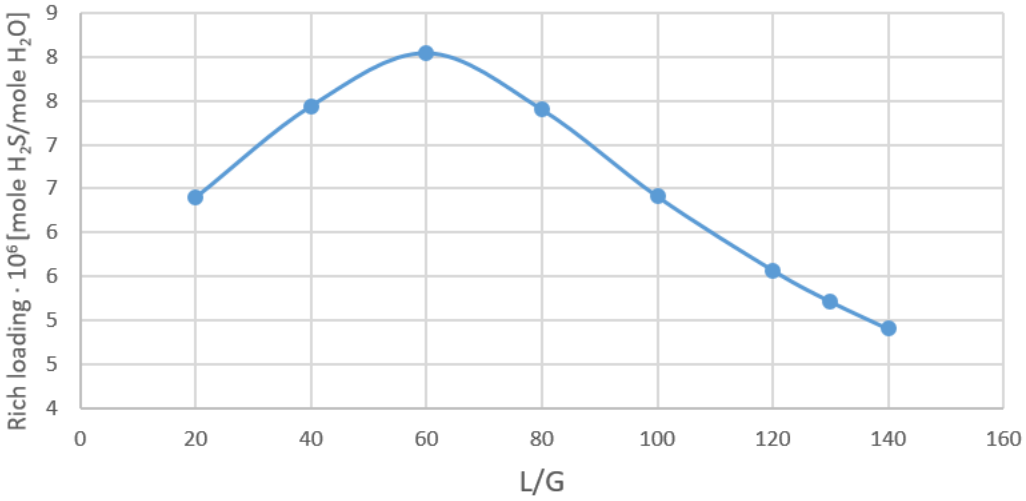

Figure 4.1.5: Rich loading plotted as a function of L/G-ratio when a compressor train for the biogas is implemented as well as a gas recycle.

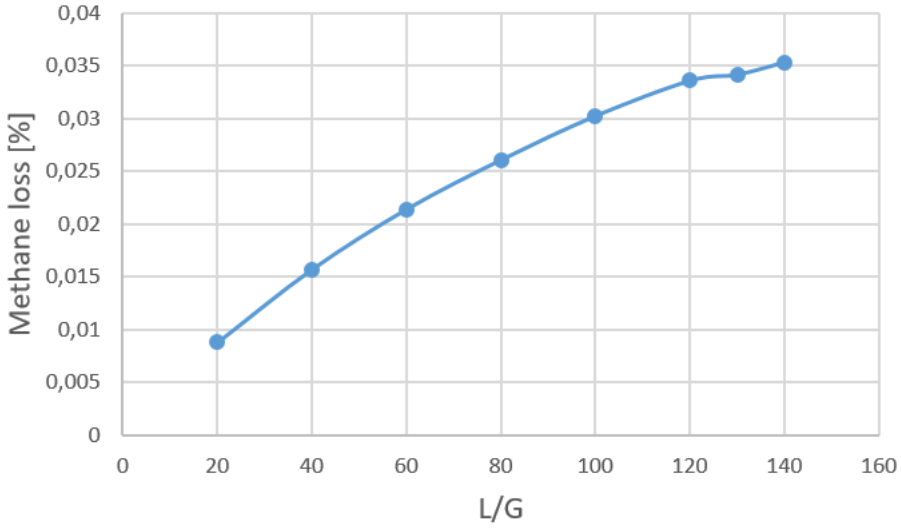

Figure 4.1.6: Methane loss plotted as a function of the L/G-ratio when the absorber system includes a compressor train to compress the biogas and a gas recycle.

Equipment with associated energy demand and type is listed in table 4.1.1. It can be seen from the table that the total energy demand is 141.4 kW. More than half of this energy is cooling, and therefore there are no large amounts of electricity needed.

The main disadvantage with this technique is the amount of pure water required, as this technique needs a continuous water supply. However, it is more cost efficient to only implement an absorber and not an additional regeneration unit.

4.1.3 Air Stripping, C-4

The air stripping case was implemented both with and without gas recirculation. The air-to-water volumetric ratio was kept at $\sim$ 25 at all times [39]. The results are summarized in the following paragraphs.

No Gas Recirculation

Figure 4.1.7, 4.1.8 and 4.1.9 present the mole fraction of H_2S in the purified gas out of the absorber, rich loading and methane loss as a function of the L/G-ratio. The orange, dashed line in figure 4.1.7 illustrates the target of 5 ppm.

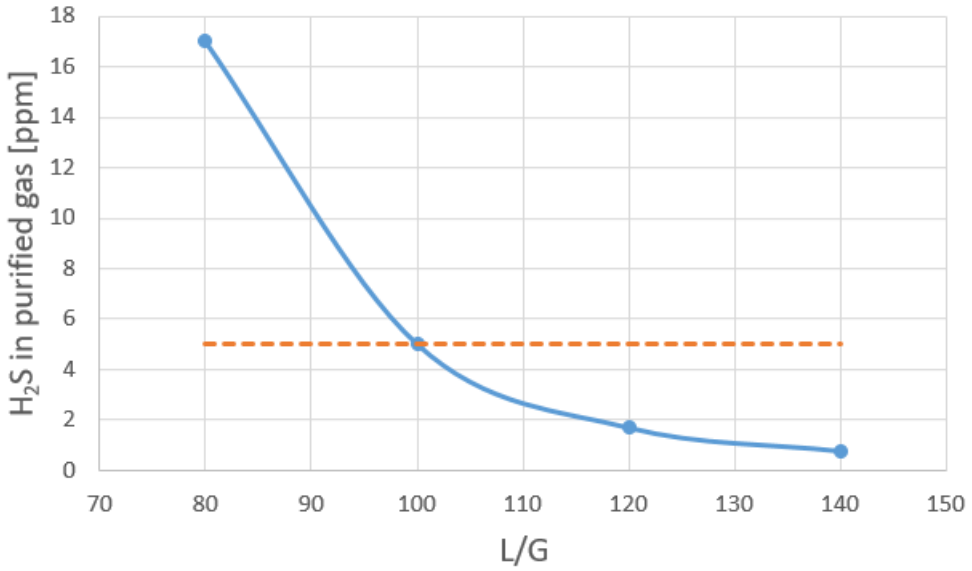

Figure 4.1.7: Mole fraction of H_2S in the purified gas plotted as a function of L/G-ratio for the air stripping system, excluding gas recycle.

As can be seen from figure 4.1.7 the purity target can be reached for an L/G-ratio of $\sim$ 100 when there is no gas recirculation.

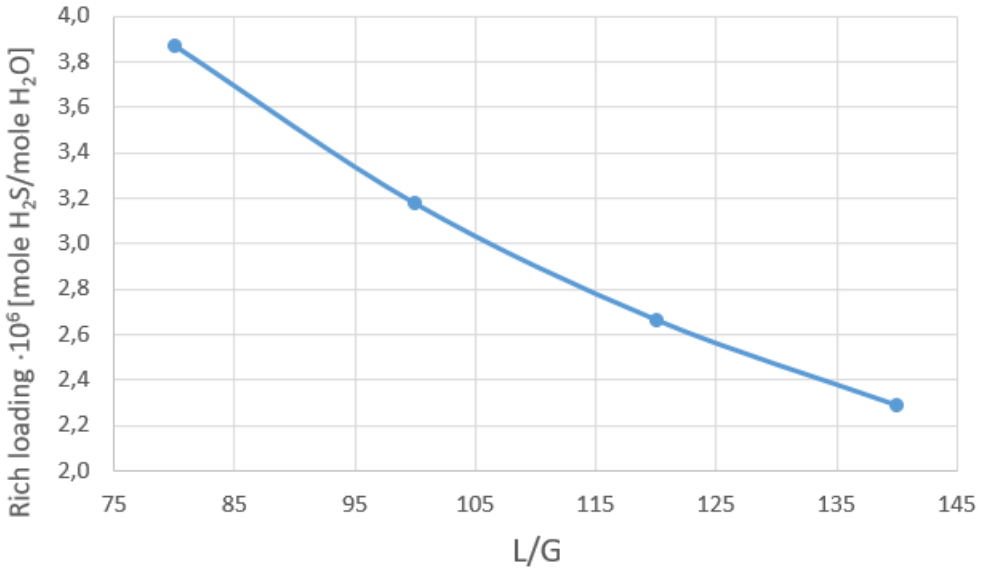

Figure 4.1.8: Rich loading plotted as a function of L/G-ratio for the air stripping system excluding gas recycle.

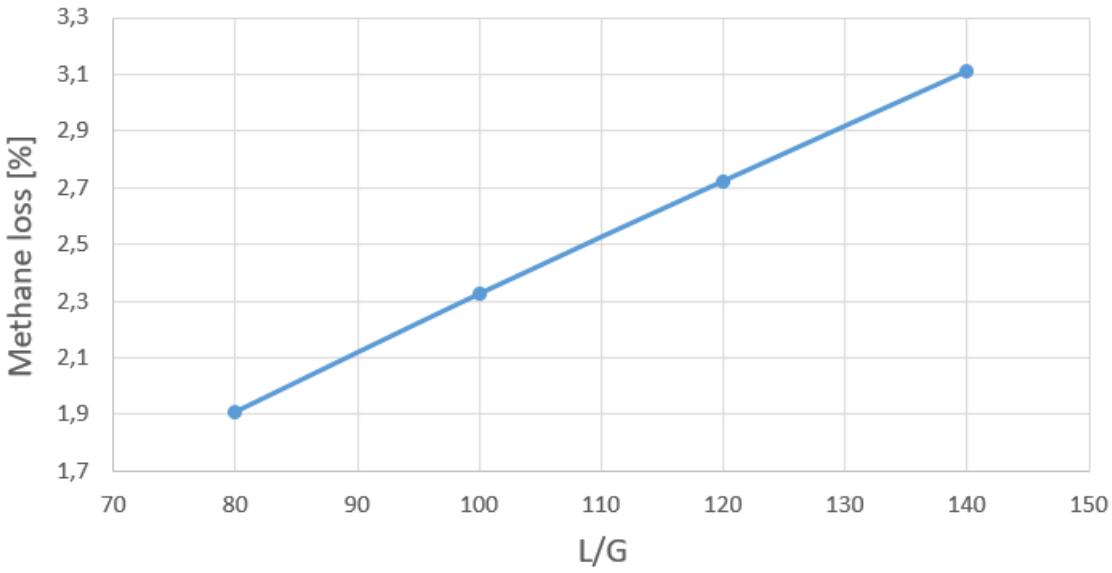

Figure 4.1.9: Methane loss as a function of L/G-ratio for the air stripping system excluding gas recycle.

The rich loading decreases with increasing L/G-ratio. This is because a higher L/G-ratio means more water, for a nearly constant amount of H_2S. It can also be seen that the methane loss will

increase as the L/G-ratio increases. This is reasonable because there will be more water present in the system to dissolve CH_4.

Gas Recirculation

Mole fraction of H_2S in the purified gas, rich loading and methane loss were plotted as a function of L/G-ratio for the system including a gas recycle, and are presented in 4.1.10, 4.1.11 and 4.1.12.

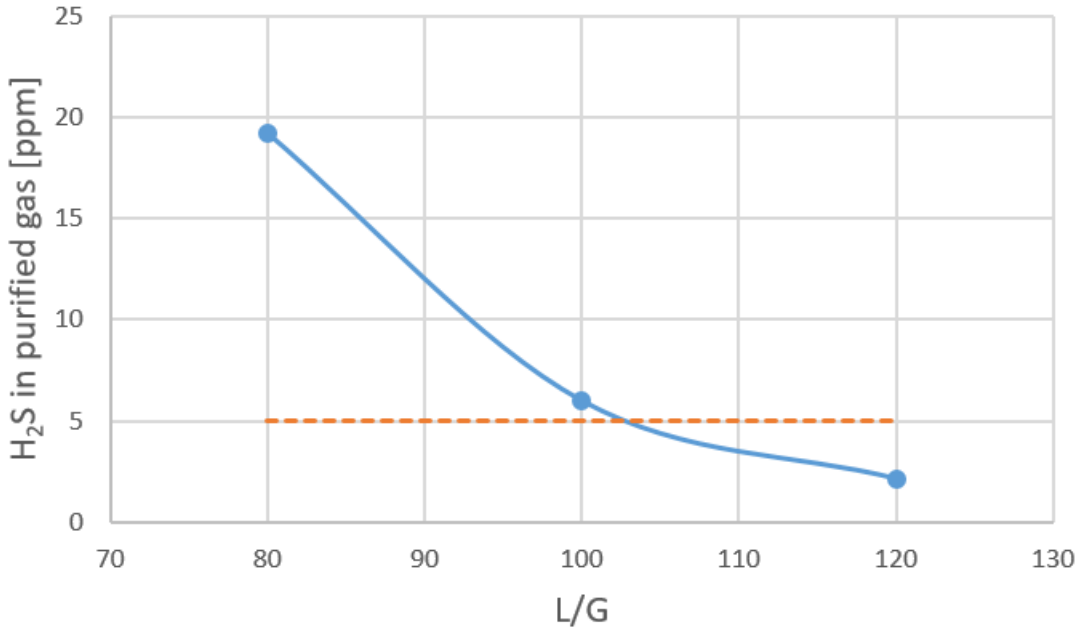

Figure 4.1.10: Mole fraction of H_2S in purified gas plotted as a function of the L/G-ratio.

Figure 4.1.10 shows that a higher L/G-ratio is needed when the gas is recirculated. This is because the amount of impurities present in the gas will be recirculated back to the absorber, which makes the loading increase. The required L/G-ratio to reach the target is $\sim$ 103. The rich loading and the methane loss follow the same trend as in the system with no gas recirculation.

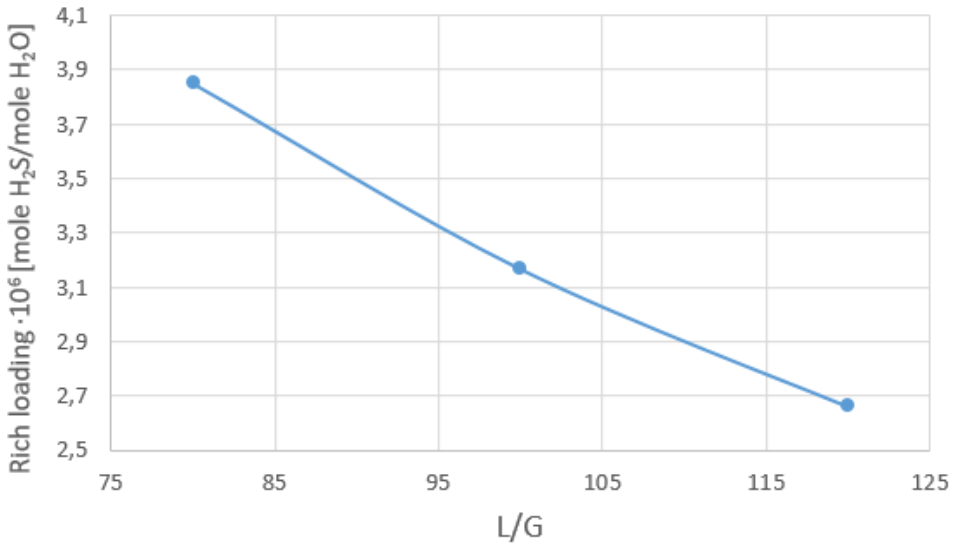

Figure 4.1.11: Rich loading plotted as a function of L/G-ratio in the system with a gas recycle.

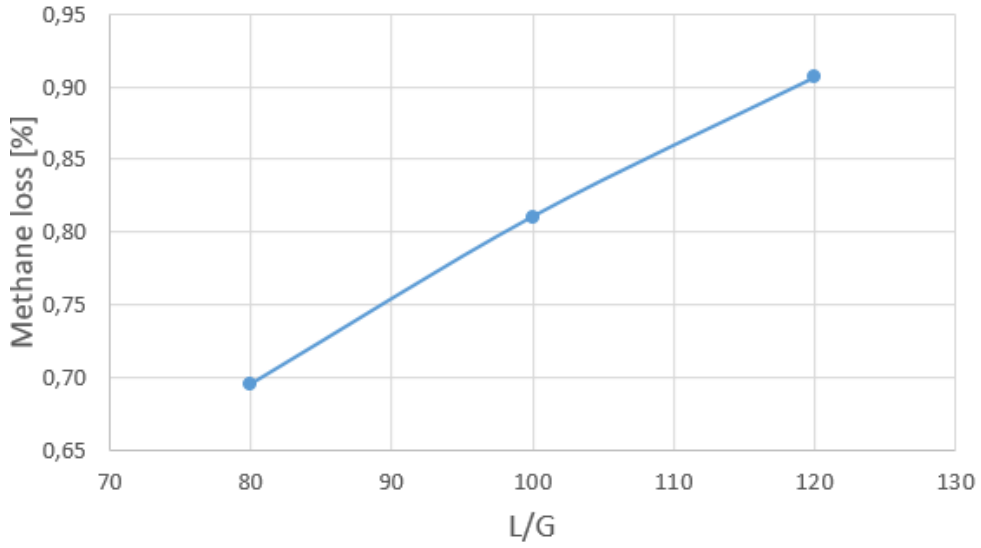

Figure 4.1.12: Methane loss at different L/G-ratios for the system including gas recycling.

The different equipment used in the air stripping technique with corresponding energy demand and duty type for the gas with gas recirculation can be found in table 4.1.1. The energy calculations are performed based on the case with L/G = 105 and a pressure in the flash of 5 bar. The total energy demand was summarized to 176.7 kW. This is slightly higher than in the case with an absorber and no regeneration of water. Considering that the air stripping system is more complex, this increase is not very high. Most of the energy required is also electricity and cooling which is more cost

efficient than steam needed for heating.

4.1.4 Comparison of the Different Water Scrubbing Techniques

From the various implementations of water scrubbing, it was found that the absorber without regeneration of lean solution and air stripping yielded the best results in terms of purity. The case with the simple flash regeneration did not reach the target of 5 ppm H_2S in the purified gas. The case with a flash with water purge was able to reach the target, but over 90 % of the water had to be replaced, making it inefficient and costly. This is the reason why the case with no water regeneration was examined. In this case it will be possible to achieve the desired purity in the gas, but large amounts of fresh water is required. This technique will therefore be best suited in locations where there is an adequate access of water. It will also fit better for smaller biogas flows, as the amount of water required to purify the biogas will be less than for larger gas flows. Besides, the cost related to such a large water supply will be an important factor. The air stripping case will also make it possible to reach the purity target. The main disadvantage in this case is that the electricity demand is increased compared to the other cases. On the other hand, the cost of the equipment and operating costs have not been taken into account. This should also be evaluated in accordance with energy demand. It was found that gas recycling to the absorber could minimize the methane loss. The most important parameters from the various techniques can be compared from table 4.1.3.

Table 4.1.3: Results from the main cases of the water scrubbing technique.

	Methane loss [%]	**Energy demand steam [kW]**	**Energy demand electricity [kW]**	**Energy demand cooling [kW]**	**Total energy demand [kW]**	**Gas recycle**	**Amount of H_2S in the purified gas**
Simple flash	4.8	6480.9	76.6	6320.1	12877.6	No	24.2 ppm
Flash with Purge	3.1	0	67.2	60.1	127.3	No	4.8 ppm
Absorber	0.04	0	60.8	80.6	141.4	Yes	4.5 ppm
Air Stripping	0.8	0	101.9	74.8	176.7	Yes	4.6 ppm

The results from these cases indicate that the setup with only an absorber and gas recirculation (C-3), and air stripping (C-4) are promising. These cases are therefore listed with more detail in this chapter. More information about the remaining cases are presented in Appendix A.1.1.

4.2 Amine Scrubbing, C-5 and C-6

Before the entire system was implemented, the absorber was examined. Simulations were first made without any loading, and results from this can be found in Appendix A.1.2. In a real system, a lean loading will occur as a result of the regeneration, and the absorber was therefore implemented with loading as reported in Moioli et al. (2013) [40]. Figure 4.2.1 and 4.2.2 represents the removal efficiency and rich loading as a function of the absorber height when the L/G-ratio was fixed at 10 (mass basis). The diameter was adjusted to 0.3 m, and the lean loading was $3,7 \cdot 10^{-4}$ mole H_2S/mole MDEA.

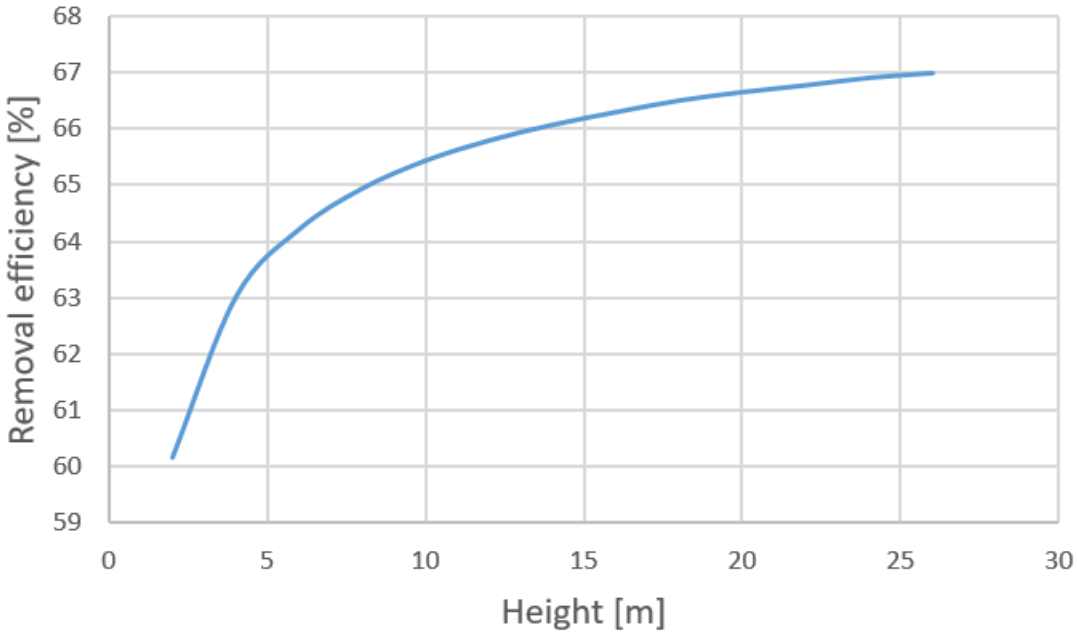

Figure 4.2.1: Removal efficiency plotted as a function of absorber height when L/G = 10 and D = 0.3 m.

It can be seen that the removal efficiency stabilizes at approximately 67 %. This removal efficiency is too low to reach the target, but this may be due to the low L/G-ratio at 10. The rich loading increases with increasing height, which is in agreement with the increasing removal efficiency. The removal efficiency increases with increasing absorption, and thus there will be more H_2S per MDEA when the L/G-ratio is kept constant. It was decided that the absorber height should be implemented as 20 m, and the diameter was adjusted to 0.35 m.

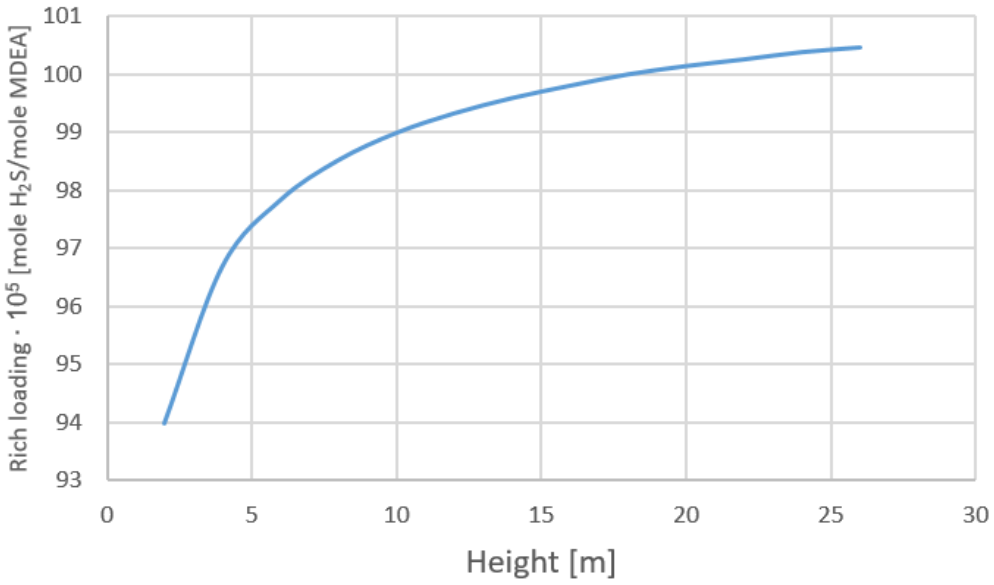

Figure 4.2.2: Rich loading of H_2S plotted as a function of height when L/G = 10 m and D = 0.3 m.

After the height was increased, the removal efficiency was plotted as a function of L/G-ratio. As can be seen from figure 4.2.3, the removal efficiency is increasing with increasing L/G-ratio and stabilizes around 100 % as expected.

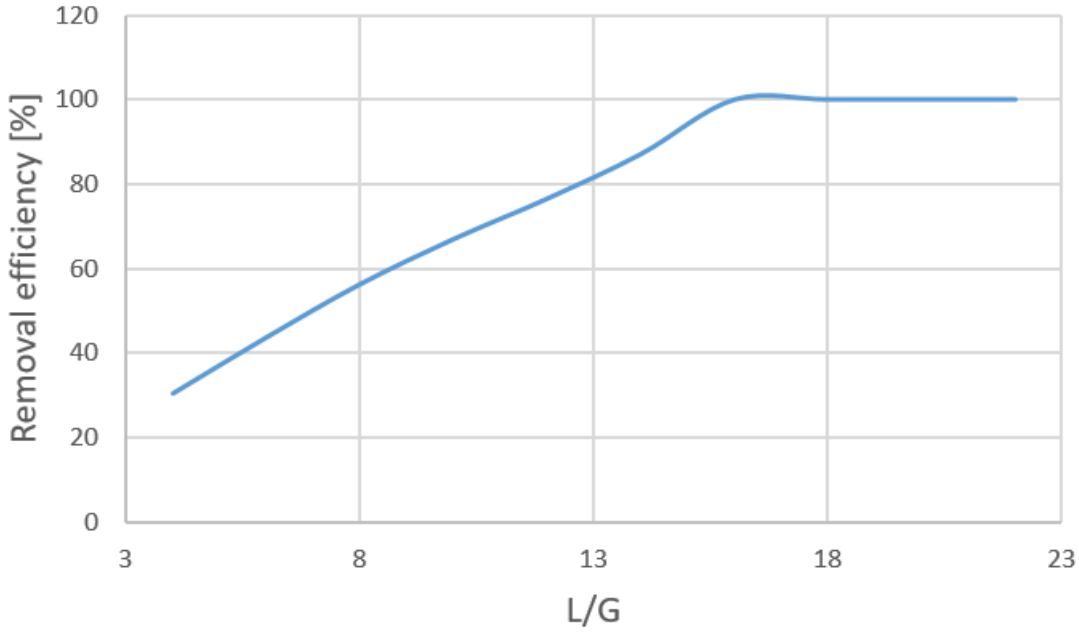

Figure 4.2.3: Removal efficiency as a function of L/G-ratio when H = 20 m and D = 0.35 m

Figure 4.2.4 represents how the rich loading changes with increasing L/G-ratio. The lean loading was fixed, and is shown as the orange, dashed line. The rich loading is located above the lean loading at all points in the graph. Thus, there is more H_2S per MDEA in the liquid flow out of the absorber than in the liquid flow into the absorber, because H_2S has been absorbed through the column. It can be seen that the rich loading is decreasing with increasing L/G-ratio, and has an inconsistency around L/G = 16.

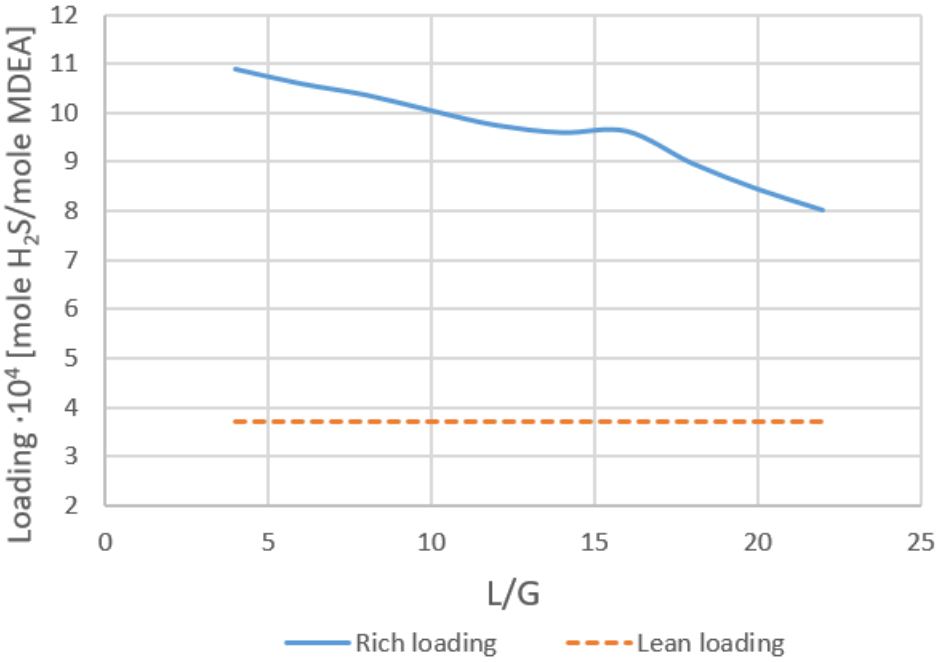

Figure 4.2.4: Rich loading plotted as a function of L/G ratio when H = 20 m D = 0.35 m. The lean loading was fixed and is marked as a dashed, orange line.

The rich loading decreases for an increasing L/G-ratio. This makes sense as the rich loading is calculated as mole H_2S per mole MDEA. When the L/G-ratio increases, the amount of aqueous MDEA solution increases, but the amount of H_2S absorbed is nearly constant in comparison. There is a clear inconsistency at L/G between 15 and 16. At L/G-ratios above 16, the graph seems to follow the same trend as for L/G below 15.

As the L/G-ratio increases, the absorption and therefore the removal efficiency increases. This means that more of the H_2S-impurities in the biogas are absorbed and removed. The H_2S content in the purified gas is therefore decreasing as can be seen in figure 4.2.5. Between L/G = 14 and 16, the value for the H_2S amount falls more than for the previous ones. The last four points are equal, and therefore lies on a straight line. The removal efficiency and the H_2S content in the purified gas out of the absorber have the same value for an L/G-ratio of 18, 20 and 22. It may seem that Aspen

is unable to distinguish the points when the removal efficiency is so close to 100 %. The inconsistency in the graph may therefore occur due to precision limits in Aspen, as the mole fraction of H_2S gets too low. It can be seen that the inconsistency in figure 4.2.4 and 4.2.5 appear at the same L/G-ratio, and it is therefore likely that it represents the same error.

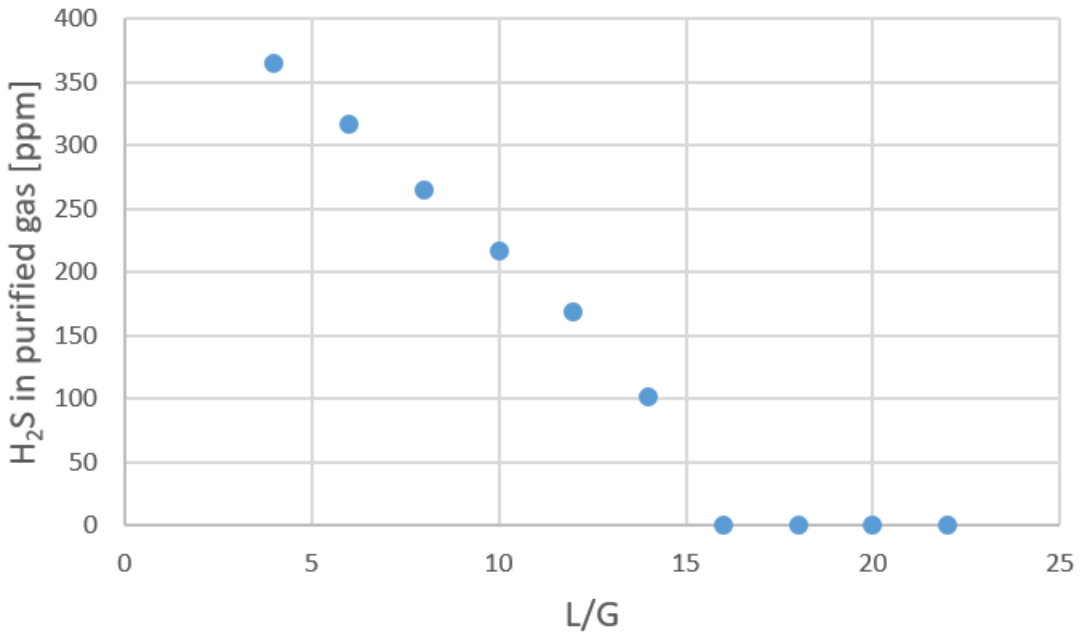

Figure 4.2.5: Amount of H_2S in purified gas plotted as a function of L/G ratio when H = 20 m and D = 0.35 m.

As can be seen in table 3.3.1 reaction 8, CO_2 will react with MDEA. It will therefore also exist a CO_2 loading in the liquid stream out of the absorber (rich loading). Figure 4.2.6 presents the rich loading of CO_2 as a function of L/G-ratio. It can be seen that the shape of this graph is similar to the one for H_2S, except that the loading values are higher. This makes sense as the amount of CO_2 present in the system will be higher, thus higher loading.

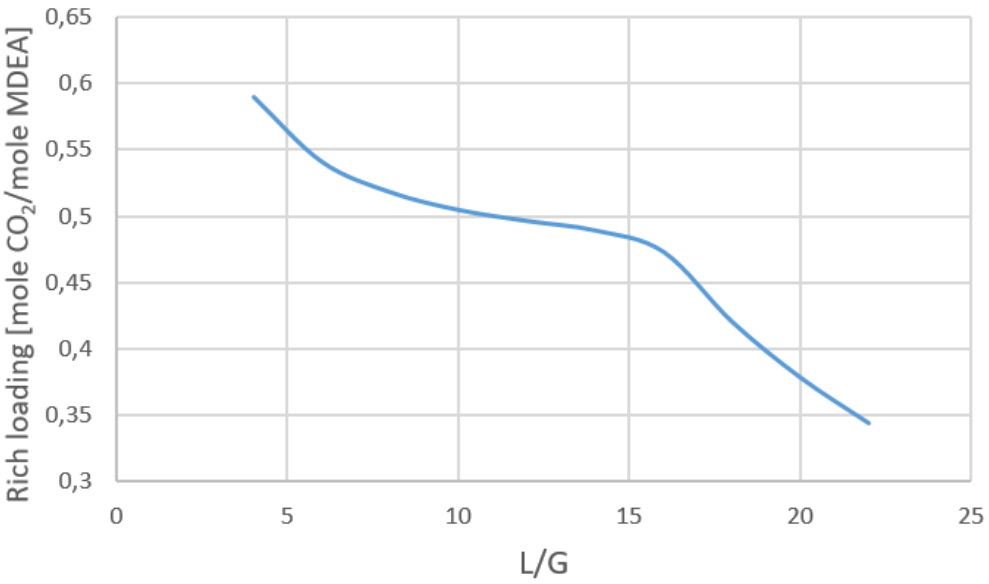

Figure 4.2.6: Rich loading of CO_2 plotted as a function of L/G-ratio when H = 20 m and D = 0.35 m.

The methane loss plotted as a function of the L/G-ratio is presented in figure 4.2.7.

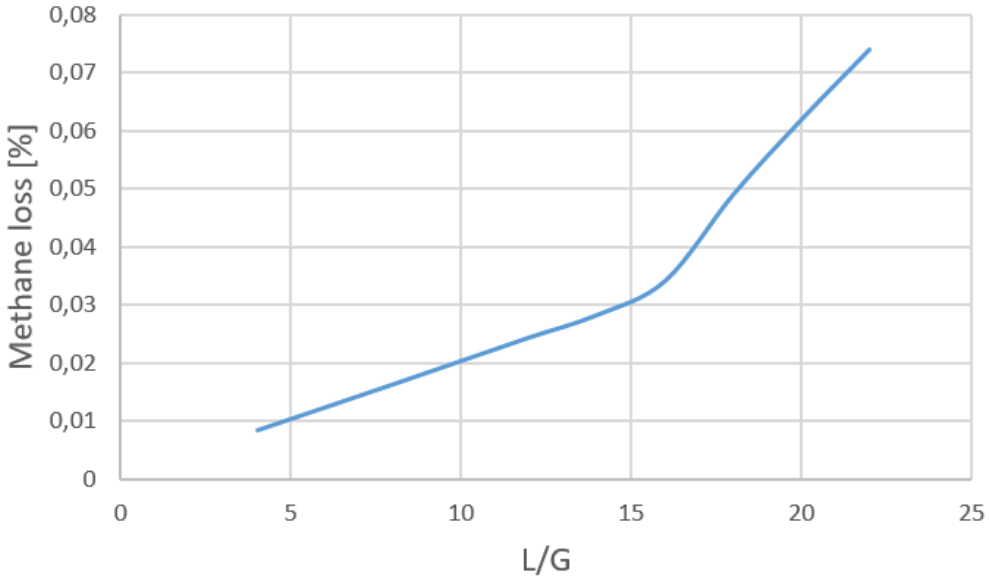

Figure 4.2.7: Methane loss plotted as a function of L/G-ratio when H = 20 m and D = 0.35 m.

The methane loss increases with increasing L/G-ratio. This is the same trend as in the previous cases, and occurs because there is more solvent and thus water for the methane to be dissolved in. The aqueous MDEA solution absorbs H_2S by chemical absorption. Since the reactions between MDEA and H_2S, as well as MDEA and CO_2 are exothermic, heat will be released and the tem-

perature will therefore increase. The reaction will most easily occur when the solvent enters the absorber, that is, at the top of the column. The rate of reaction will decrease as H_2S reacts, which can be seen in the temperature profiles in figure 4.2.8. In accordance with the graphs presented earlier, it can be seen that the system changes behaviour for L/G-ratios above 14. Since physical absorption reactions are not very exothermic, there is a possibility that the formation of bicarbonate is the reason for the difference in the temperature profiles. The formation of bicarbonate releases a lot of heat, and since the lean stream contains a lot of bicarbonate already for an L/G-ratio of 16, there is a possibility that this will cause large variations in the temperature profiles.

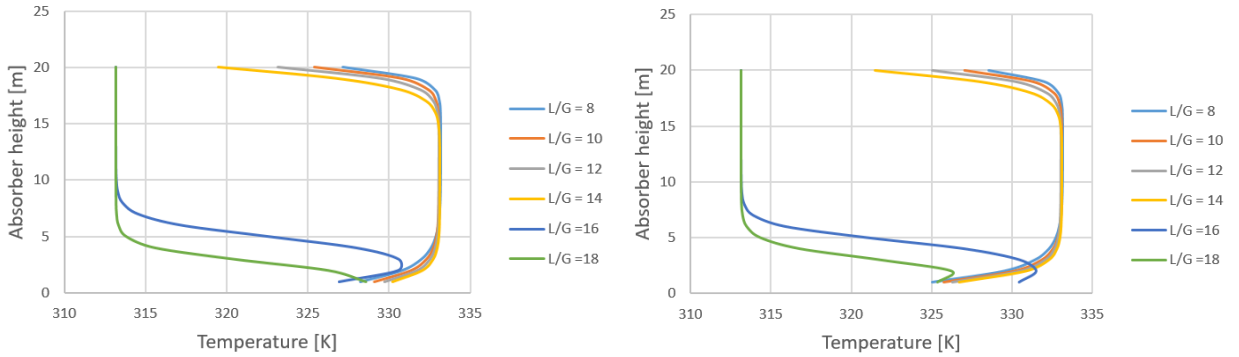

Figure 4.2.8: Temperature profiles for the absorber. The left graph presents the liquid temperature profile, and the right graph represents the vapor temperature profile.

Biogas enters the absorber in the bottom, and H_2S reacts with MDEA in the lean solution that enters on the top. This means that H_2S reacts and thus passes into the liquid phase. This mass transfer happens with a low rate in the bottom of the column as a great amount of the MDEA already has reacted. In the top of the column, the lean solution enters, and the reaction will occur more rapidly as can be seen in figure 4.2.9.

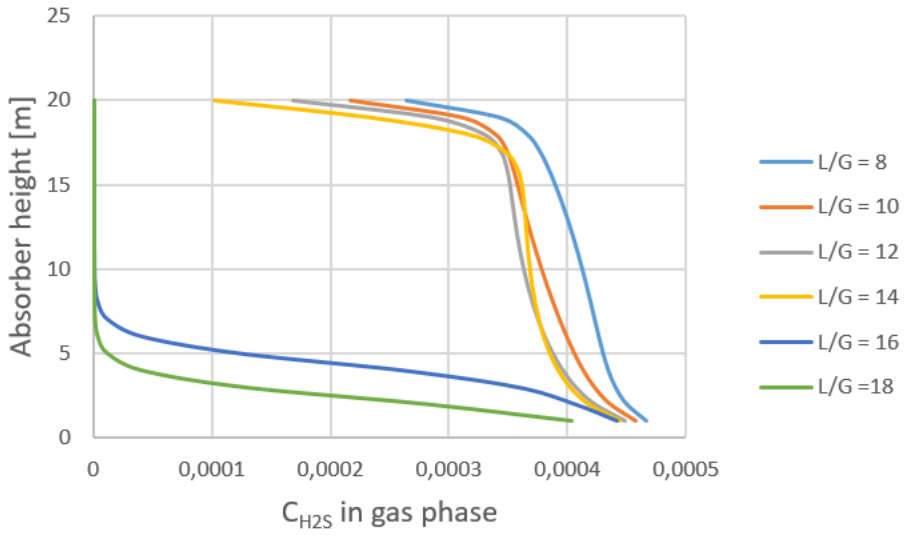

Figure 4.2.9: Concentration profile for H_2S in vapor phase.

Figure 4.2.10 shows that CO_2 follows the same trend as H_2S. The CO_2 content in the liquid increases from the top of the absorber to the bottom as CO_2 reacts with MDEA.

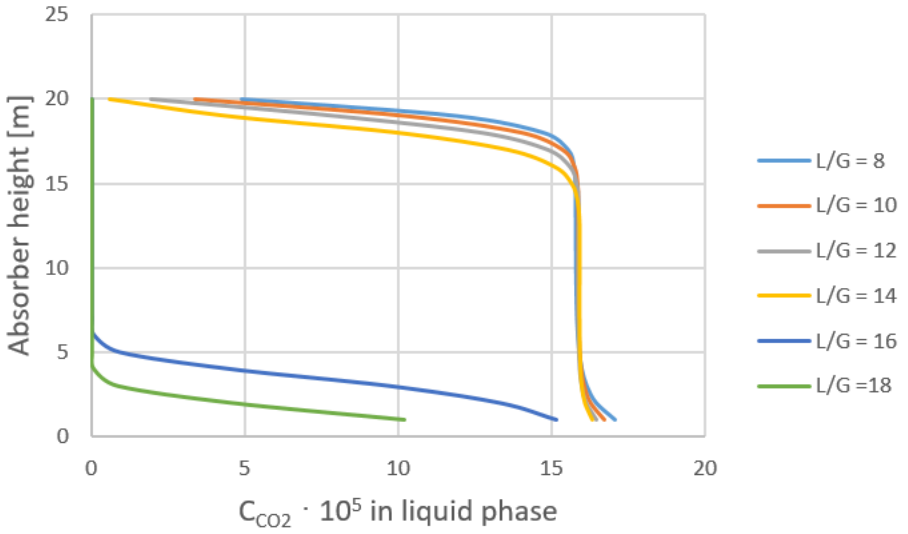

Figure 4.2.10: Concentration profile for CO_2 in liquid phase.

Absorption of CH_4 is physical unlike the absorption of CO_2 and H_2S. There is also a clear difference in the concentration profile, as can be seen in figure 4.2.11. For an L/G-ratio lower than 16, the CH_4 content in the liquid phase seems to decrease. This may be because the solubility depends on the temperature, and the amount of CH_4 in the liquid will therefore decrease as the temperature increases.

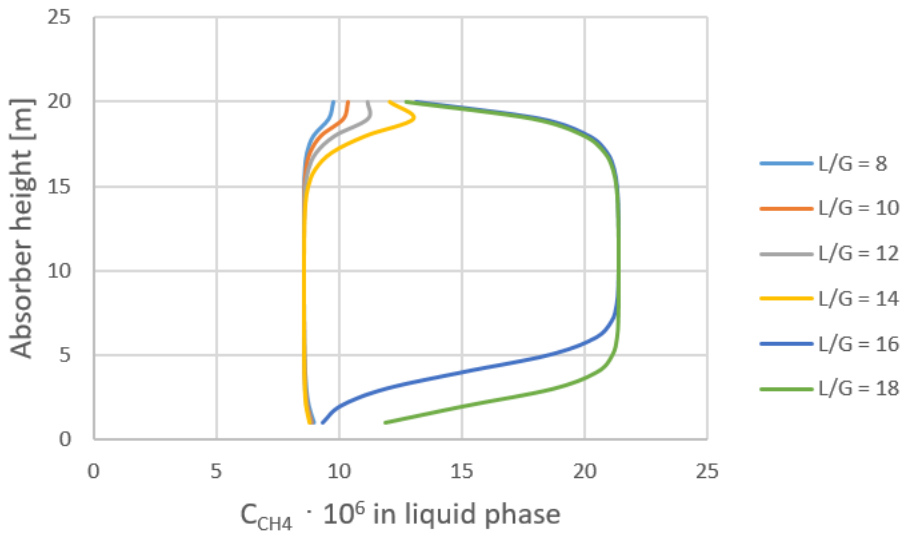

Figure 4.2.11: Concentration profile for CH_4 in liquid phase.

Because the temperature and concentration profiles show a change in trend between L/G = 14 and L/G = 16, the absorber was investigated at a low L/G-ratio to see the effect of CO_2 absorption. L/G = 2 was used, and the absorber was operated with no initial loading. Removal of the reaction between MDEA and CO_2 gave no effect, but when all of the reactions with CO_2 were removed, the amount of H_2S removed in the absorber increased. It therefore seems that the formation of bicarbonate causes less H_2S to be absorbed, which supports the hypothesis that bicarbonate formation gives the great behavioral change in temperature and concentration profiles.

The total amine scrubbing system was implemented, but the system caused problems in the boundary between L/G = 14 and L/G = 16. The lean stream was therefore implemented with no initial loading and a fixed reboiler duty of 1000 kW to compare the two cases. From Aspen simulations it can be seen that the physical absorption of CO_2, the formation of bicarbonate and the physical absorption of H_2S falls when L/G-ratio is increased from 14 to 16. Physical absorption processes are not very exothermal, so it seems that the formation of bicarbonate is the reason for the change. It may also be possible that the CO_2 content in the biogas is too high for H_2S to be selectively absorbed.

The energy demand and type for the two amine scrubbing cases are presented in table 4.2.1.

Table 4.2.1: Energy demand and type for the amine scrubbing simulation at L/G = 14 and L/G = 16.

Case	Equipment	Duty [kW]	Type
L/G = 14	COMP1	14.9	Electricity
	C-1	21.9	Cooling
	COMP2	13.8	Electricity
	C-2	16.4	Cooling
	COOLER1	6.6	Cooling
	PUMP	0.5	Electricity
	HEX	488.0	Heat transfer
	DESORBER	1000.0	Heating
	COOLER2	786.3	Cooling
	COOLER3	215.2	Cooling
	SUM	**2563.7**	**kW**
L/G = 16	COMP1	13.8	Electricity
	C-1	19.9	Cooling
	COMP2	12.9	Electricity
	C-2	15.3	Cooling
	COOLER1	0.0 [a]	Cooling
	PUMP	0.6	Electricity
	HEX	555.4	Heat transfer
	DESORBER	350.0	Heating
	COOLER2	111.3	Cooling
	COOLER3	248.2	Cooling
	SUM	**1327.4**	**kW**

[a] 0.019, is set to 0 due to rounding.

4.3 Water Scrubbing vs. Amine Scrubbing

The results showed that the case with only an absorber including a gas recycle, and the air stripping case were the most promising water scrubbing techniques in terms of purity. For amine scrubbing, the case with an L/G-ratio of 16 provided the best results. This case is however not properly optimized, and is far within the target. This means that the energy demand might be over-estimated. The energy demands for each case divided in heating, electricity and cooling are listed in table 4.3.1.

Table 4.3.1: Comparison of energy demand for the three most promising cases.

	Heating [kW]	**Electricity [kW]**	**Cooling [kW]**
Absorber	-	60.8	80.6
Air Stripping	-	101.9	74.8
Amine scrubbing L/G = 16	350	27.3	394.7

When it comes to energy consumption in the different cases, it can be seen that amine scrubbing differs from water scrubbing in terms of heating requirement. In addition, air stripping uses most electricity and amine scrubbing requires the largest amount of cooling. Heating is expensive and will therefore affect energy costs the most. Cooling water, on the other hand, is cheap and can be easily accessed depending on the plant location. Table 4.3.2 includes how much energy in terms of heating and electricity that is used per kg H_2S and CO_2 removed. Among the water scrubbing cases, the absorber seems to provide the lowest energy consumption per kg H_2S removed. Considering this, it may seem that water scrubbing with an absorber containing gas recirculation is a good choice of technique. On the other hand, this technique will require a large supply of water, and it is also dependent on the lean stream having an acceptable H_2S content for disposal.

Table 4.3.2: Energy demand per kg H_2S and CO_2 removed for the three most promising techniques.

Case	**Energy [kW]**	**H_2S absorbed [kg/s]**	**CO_2 absorbed [kg/s]**	**Energy/kg H_2S absorbed [MJ/kg]**	**Energy/kg CO_2 absorbed [MJ/kg]**	**Energy/kg H_2S+CO_2 absorbed [MJ/kg]**
Absorber	60.8	9.8E-5	0.02	620.4	3.0	3.0
Air Stripping	101.9	6.8E-5	0.05	1498.5	2.0	2.0
Amine Scrubbing L/G = 16	377.3	1.0E-4	0.1	3773	3.8	3.8

Table 4.3.3 presents values for energy consumption from literature for both water scrubbing and amine scrubbing. As most sources for water scrubbing stated energy consumption per amount of biogas, energy consumption per impurity was calculated based on the water scrubbing simulations in this current thesis. The mass flows for the case with only an absorber and a gas recycle, in addition to the air stripping case were calculated, and the used value is the average of these two. Calculations can be found in Appendix A.2.1.

Table 4.3.3: Energy demand per kg impurity absorbed from literature for water scrubbing and amine scrubbing [16][41].

	Energy/kg H_2S absorbed [MJ/kg H_2S]	**Energy/kg CO_2 absorbed [MJ/kg CO_2]**	**Energy/kg H_2S+CO_2 absorbed [MJ/kg H_2S+CO_2]**
Water Scrubbing	1258.8	3.5	3.5
Amine Scrubbing	25.1-43.0	2.9-3.7	-

Table 4.3.2 and 4.3.3 clearly show that most of the energy (as absolute values) is used for the absorption of CO_2. This fits well with the results that more CO_2 is absorbed than what was expected. Water scrubbing in the literature uses more energy per H_2S and CO_2 removed than what was used in the simulations in this thesis. There may be several reasons for this, including that the H_2S removal unit in the literature uses two absorption columns at high pressure, which will require a lot of energy[41]. Two absorbers are also used in the CO_2 removal unit. In addition to this, sour syngas is used in the literature that was found. Syngas consists of less CO_2 than biogas, and the energy per kg CO_2 will increase with decreasing CO_2 absorbed. On the other hand, the gas consisted of more H_2S, but the proportion of H_2S and CO_2 combined is still greater in the estimated biogas for this current project. A more precisely comparison would be possible with a more similar H_2S and CO_2 removal unit from literature.

The results from amine scrubbing showed that a lot of CO_2 was absorbed, and the energy consumption per H_2S and CO_2 absorbed will thus be approximately equal to the energy consumption per kg CO_2 absorbed. This means that the simulations coincide well with the literature. The amine scrubbing simulation in this task, however, is not optimized, and it will probably be possible to optimize the energy consumption further.

It was difficult to find good sources of regulations for legal disposal of sulfide-containing liquids. Therefore, a source that follows Brazilian laws was used, and it is assumed that other countries will follow similar specifications. As can be seen from table 4.3.4, the absorber with gas recycle has a lean stream that exceeds the maximum sulfur content of 2 ppm for disposal according to Brazilian

law. If this technique is to be used, the stream must be further treated before disposal. In the amine scrubbing simulations, the lean stream is regenerated, and the only liquid streams to be disposed will be the PUR-LEAN and C-LEAN from the compression train of the purified gas. It can be seen that the sulfide contents are far below 2 ppm. Disposal of these streams will therefore be possible without further treatment for sulfide removal. However, since a significantly amount of CO_2 is absorbed in addition to H_2S, the gas stream out of the desorber will most likely require a separation between H_2S and CO_2. The two disposal streams from the compressor train will also contain small amounts of MDEA that might require further treatment.

Table 4.3.4: Sulfide content in lean disposal streams.

Case	Sulfide content [ppm]
Flash with purge H2O-OUT	2.45
Absorber with gas recycle LEAN	4.33
Amine scrubbing PUR-LEAN	0.01
Amine scrubbing C-LEAN	0.03

It is important to emphasize that costs have not been taken into account in this work, and that the cost for MDEA, water, electricity, heating and process equipment will have an impact on the choice of technique.

Chapter 5

Summary and Recommendations for Further Work

5.1 Conclusion

The objective of this thesis was to examine two techniques for H_2S removal from biogas, respectively water scrubbing and amine scrubbing. All simulations were performed by Aspen Plus.

First, a VLE validation was performed to investigate the accuracy of the simulation models compared to literature data. From this validation it was found that the solubility of H_2S in water deviates 4 % from literature data in loading, and 3 % in the total pressure at 45 °C. The solubility of H_2S in aqueous MDEA at 45 °C had an average deviation of 19-32 % in loading and 68-137 % in partial pressure of H_2S.

Three cases of water scrubbing and two cases of amine scrubbing were mainly examined. In the first case, water scrubbing was implemented with regeneration through a simple flash. This case was then improved in a new case, by implementing a split to remove portions of the lean stream from the absorber, and replace it with clean water. A sub-case with only an absorber and no regeneration unit was also created. The last case with water scrubbing was air-stripping regeneration. For amine scrubbing, two cases with L/G = 14 and L/G = 16, were examined. The regeneration in amine scrubbing was obtained by a desorber column. It was found that the target of less than 5 ppm H_2S in the purified gas could be reached for all cases except for simple flash regeneration. The flash with purge case was excluded as a well-functioning method as over 90 % of the water had to be taken out in the split to reach the target. An absorber without lean regeneration including a gas recycle and air stripping therefore provided the best results in terms of purity and methane loss for water scrubbing. Air stripping provided the most promising energy result. For amine scrubbing, the case with an L/G-ratio at 16 was used to achieve the desired purity, but this case was not fully optimized. The overall absorption performance may therefore be further improved, and this case

should be more deeply investigated. The effect of a gas recycle should be analyzed in the same way as for water scrubbing to see if it is possible to achieve the purity target.

In the work with amine scrubbing, it was found that the absorption of CO_2 has a higher impact on the absorption of H_2S than expected. This may be due to the high formation of bicarbonate in the process. It is also a possibility that the biogas has a too high CO_2 content to selectively absorb H_2S.

Overall it was found that both water scrubbing and amine scrubbing are promising methods for H_2S removal from biogas. Water scrubbing provided results with relatively low energy requirements. Amine scrubbing seemed to provide low sulfide-containing liquid disposal streams. The streams will contain small amounts of MDEA that may require further treatment, but this case needs to be optimized before any conclusions can be drawn. However, the costs associated with the two techniques should be investigated to determine the profitability.

5.2 Further Work

In the work on this thesis, there were problems with the influence of CO_2 in the amine scrubbing simulation. In any further work on this system, the influence of CO_2 on the system should be investigated further before the complete system is implemented. Studies on the desorber should be performed so that its dimensions are properly optimized in addition to the reboiler duty.

To get a complete analysis of the difference and profitability of the two techniques studied, a cost analysis should be conducted. In this way, any cost differences with regard to energy, solvents and processing equipment will be taken into account.

Bibliography

[1] International Energy Agency. *Key World Energy Statistics*. URL: https://www.iea.org/statistics/kwes/supply/.

[2] *Global Greenhouse Gas Emissions Data | Greenhouse Gas (GHG) Emissions | US EPA*. URL: https://www.epa.gov/ghgemissions/global-greenhouse-gas-emissions-data.

[3] T.A Boden, G. Marland, and R.J. Andres. *Global, Regional, and National Fossil-Fuel CO2 Emissions*. 2017. URL: https://ourworldindata.org/co2-and-other-greenhouse-gas-emissions.

[4] Ayhan Demirbas. *Potential applications of renewable energy sources, biomass combustion problems in boiler power systems and combustion related environmental issues*. 2005. DOI: 10.1016/j.pecs.2005.02.002.

[5] International Energy Agency. *Renewables*. URL: https://www.iea.org/topics/renewables/.

[6] N.L. Panwar, S.C. Kaushik, and Surendra Kothari. "Role of renewable energy sources in environmental protection: A review". In: *Renewable and Sustainable Energy Reviews* 15.3 (Apr. 2011), pp. 1513–1524. ISSN: 1364-0321. DOI: 10.1016/J.RSER.2010.11.037.

[7] Gary W Frey and Deborah M Linke. "Hydropower as a renewable and sustainable energy resource meeting global energy challenges in a reasonable way Frey, G. W. and Linke, D. M. Energy Policy, 2002, 30, (14), 1261–1265". In: *Fuel and Energy Abstracts* 44.4 (2003), pp. 240–241. ISSN: 01406701. DOI: 10.1016/S0140-6701(03)83044-8.

[8] Mita Bhattacharya et al. "The effect of renewable energy consumption on economic growth: Evidence from top 38 countries". In: *Applied Energy* 162 (2016), pp. 733–741. ISSN: 03062619. DOI: 10.1016/j.apenergy.2015.10.104.

[9] Olumide Wesley Awe et al. "A Review of Biogas Utilisation, Purification and Upgrading Technologies". In: *Waste and Biomass Valorization* 8.2 (2017), pp. 267–283. ISSN: 1877265X. DOI: 10.1007/s12649-016-9826-4.

[10] M. Balat and H. Balat. "Biogas as a renewable energy sourcea review". In: *Energy Sources, Part A: Recovery, Utilization and Environmental Effects* 31.14 (2009), pp. 1280–1293. ISSN: 15567036. DOI: 10.1080/15567030802089565.

[11] Laura Bailón Allegue and Jørgen Hinge. "Biogas and bio-syngas upgrading". In: *DTI Report* December (2012), pp. 1–97.

[12] E. Ryckebosch, M. Drouillon, and H. Vervaeren. "Techniques for transformation of biogas to biomethane". In: *Biomass and Bioenergy* 35.5 (2011), pp. 1633–1645. ISSN: 09619534. DOI: 10.1016/j.biombioe.2011.02.033.

[13] Raúl Muñoz et al. "A review on the state-of-the-art of physical/chemical and biological technologies for biogas upgrading". In: *Reviews in Environmental Science and Biotechnology* 14.4 (2015), pp. 727–759. ISSN: 15729826. DOI: 10.1007/s11157-015-9379-1.

[14] John Boesel and Brad Rutledge. *WestStart-CALSTART California Biogas Industry Assessment White Paper President and CEO*. Tech. rep. 2005. URL: https://calstart.org/wp-content/uploads/2018/10/California-Biogas-Industry-Assessment.pdf.

[15] *RESOLUÇÃO N*. Tech. rep. URL: http://www2.mma.gov.br/port/conama/res/res05/res35705.pdf.

[16] Panagiotis Tsapekos et al. "Biogas upgrading and utilization: Current status and perspectives". In: *Biotechnology Advances* 36.2 (2018), pp. 452–466. ISSN: 07349750. DOI: 10.1016/j.biotechadv.2018.01.011.

[17] Petronela Cozma et al. "Modeling and simulation of high pressure water scrubbing technology applied for biogas upgrading". In: *Clean Technologies and Environmental Policy* 17.2 (2014), pp. 373–391. ISSN: 16189558. DOI: 10.1007/s10098-014-0787-7.

[18] Hong Nie et al. "Comparison of Water Scrubbing and Propylene Carbonate Absorption for Biogas Upgrading Process". In: (2013). DOI: 10.1021/ef400233w.

[19] J I Huertas, N Giraldo, and S Izquierdo. *7 Removal of H 2 S and CO 2 from Biogas by Amine Absorption*. Tech. rep.

[20] Petronela Cozma et al. "Analysis and modelling of the solubility of biogas components in water for physical absorption processes". In: *Environmental Engineering and Management Journal* 12.1 (2013), pp. 147–162. ISSN: 15829596.

[21] Debasish Tikadar, Ashish M Gujarathi, and Chandan Guria. "Detailed Analysis of MDEA based Gas Sweetening Process". In: (2017).

[22] Yu. A. Anufrikov, G. L. Kuranov, and N. A. Smirnova. "Solubility of CO2 and H2S in alkanolamine-containing aqueous solutions". In: *Russian Journal of Applied Chemistry* 80.4 (2007), pp. 515–527. ISSN: 1070-4272. DOI: 10.1134/s1070427207040015.

[23] Noman Haimour, Al1 Bidarian, and Orville C Sandall. *KINETICS OF THE REACTION BETWEEN CARBON DIOXIDE AND METHYLDIETHANOLAMINE*. Tech. rep. 6, pp. 1393–1398. DOI: 10.1016/0009-2509(87)85011-X.

[24] Morteza Afkhamipour and Masoud Mofarahi. "Experimental measurement and modeling study on CO2 equilibrium solubility, density and viscosity for 1-dimethylamino-2-propanol (1DMA2P) solution". In: *Fluid Phase Equilibria* 457 (Feb. 2018), pp. 38–51. ISSN: 0378-3812. DOI: 10.1016/J.FLUID.2017.09.019.

[25] Markus Bolhàr-Nordenkampf et al. "Modelling selective H 2 S absorption and desorption in an aqueous MDEA-solution using a rate-based non-equilibrium approach". In: *Chemical Engineering and Processing* 43 (2004), pp. 701–715. DOI: 10.1016/S0255-2701(03)00011-4.

[26] Jacob A. Moulijn, Michiel Makkee, and Annelies E. Van Diepen. *Chemical Process Technology*. 2nd ed. 2014, pp. 162–163.

[27] Mohammad R M Abu-Zahra et al. "Experimental verification of Equilibrium-Stage and Rate-Based Simulations". In: *INTERNATIONAL JOURNAL OF ENHANCED RESEARCH IN SCIENCE TECHNOLOGY & ENGINEERING* 1 (2012). ISSN: 2319-7463.

[28] K Ramesh et al. *Dynamic Rate-Based and Equilibrium Model Approaches for Continuous Tray Distillation Column*. Tech. rep. 12. 2007, pp. 2030–2041. URL: http://www.aensiweb.com/old/jasr/jasr/2007/2030-2041.pdf.

[29] Antonin Chapoy et al. "Experimental measurement and phase behavior modeling of hydrogen sulfide-water binary system". In: *Industrial and Engineering Chemistry Research* 44.19 (2005), pp. 7567–7574. ISSN: 08885885. DOI: 10.1021/ie050201h.

[30] Antonin Chapoy et al. "Gas solubility measurement and modeling for methane-water and methane-ethane-n-butane-water systems at low temperature conditions". In: *Fluid Phase Equilibria* 220.1 (2004), pp. 111–119. ISSN: 03783812. DOI: 10.1016/j.fluid.2004.02.010.

[31] John J. Carroll, John D. Slupsky, and Alan E. Mather. "The Solubility of Carbon Dioxide in Water at Low Pressure". In: 20 (1991).

[32] Alain Valtz et al. "Vapour-liquid equilibria in the carbon dioxide-water system, measurement and modelling from 278.2 to 318.2 K". In: (2004).

[33] William J Rogers, Jerry A Bullin, and Richard R Davison. "FTIR Measurements of Acid-Gas-.pdf". In: 44.11 (1998), pp. 2423–2430.

[34] S. H. Huang and H.-J. Ng. *Solubility of H2S and CO2 in Alkanolamines*. Tech. rep. 1998.

[35] Fang Yuan Jou, Alan E. Mather, and Frederick D. Otto. "Solubility of hydrogen sulfide and carbon dioxide in aqueous methyldiethanolamine solutions". In: *Industrial & Engineering Chemistry Process Design and Development* 21.4 (2005), pp. 539–544. ISSN: 0196-4305. DOI: 10.1021/i200019a001.

[36] Christie John Geankoplis. *Transport Processes and Separation Process Principles*. 4th ed. Prentice Hall, 2003, p. 696.

[37] Aspen Technology. "Aspen Physical Property System Physical Property Models". In: *Aspen Technology, Inc.* V9 (2016), Bedford, MA.

[38] Ying Zhang and Chau Chyun Chen. "Modeling gas solubilities in the aqueous solution of methyldiethanolamine". In: *Industrial and Engineering Chemistry Research* 50.10 (2011), pp. 6436–6446. ISSN: 08885885. DOI: 10.1021/ie102150h.

[39] Don D. Ratnayaka, Malcolm J. Brandt, and K. Michael Johnson. "Specialized and Advanced Water Treatment Processes". In: *Water Supply*. Elsevier, 2009, pp. 365–423. DOI: 10.1016/B978-0-7506-6843-9.00018-4.

[40] Stefania Moioli et al. "Improved Rate-Based Modeling of H 2 S and CO 2 Removal by Methyldiethanolamine Scrubbing". In: (2013). DOI: 10.1021/ie301967t.

[41] Stefania Moioli et al. "Assessment of MDEA absorption process for sequential H2S removal and CO2 capture in air-blown IGCC plants". In: *Applied Energy* 183 (Dec. 2016), pp. 1452–1470. ISSN: 03062619. DOI: 10.1016/j.apenergy.2016.08.155.

Appendix A

Additional Information

A.1 Simulations

A.1.1 Water Scrubbing

Different property base methods in Aspen were evaluated to decide which one to be used in the simulations. Aspen Plus contains several, but only NRTL, ENRTL-RK, ELECNRTL and UNIQUAC were evaluated. The validation graphs are shown in figure A.1.1, A.1.2, A.1.3, A.1.4 and A.1.5.

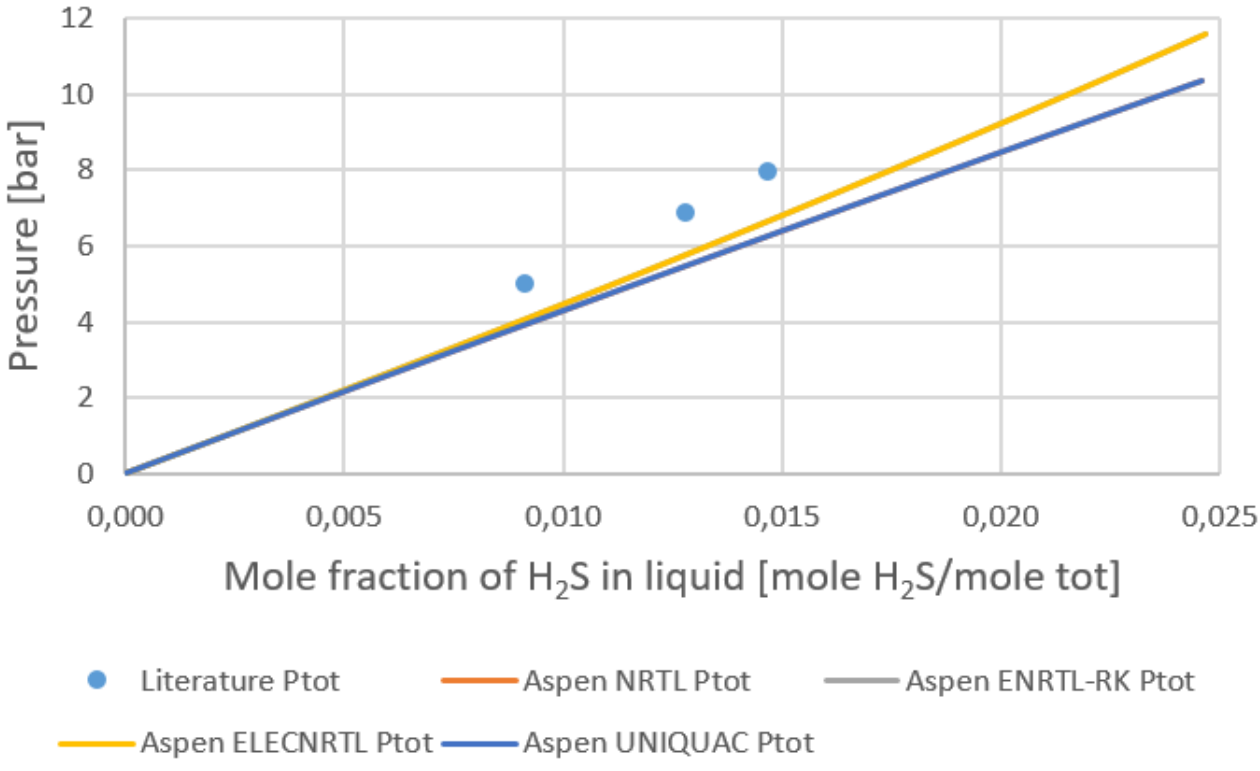

Figure A.1.1: Validation at 16 °C.

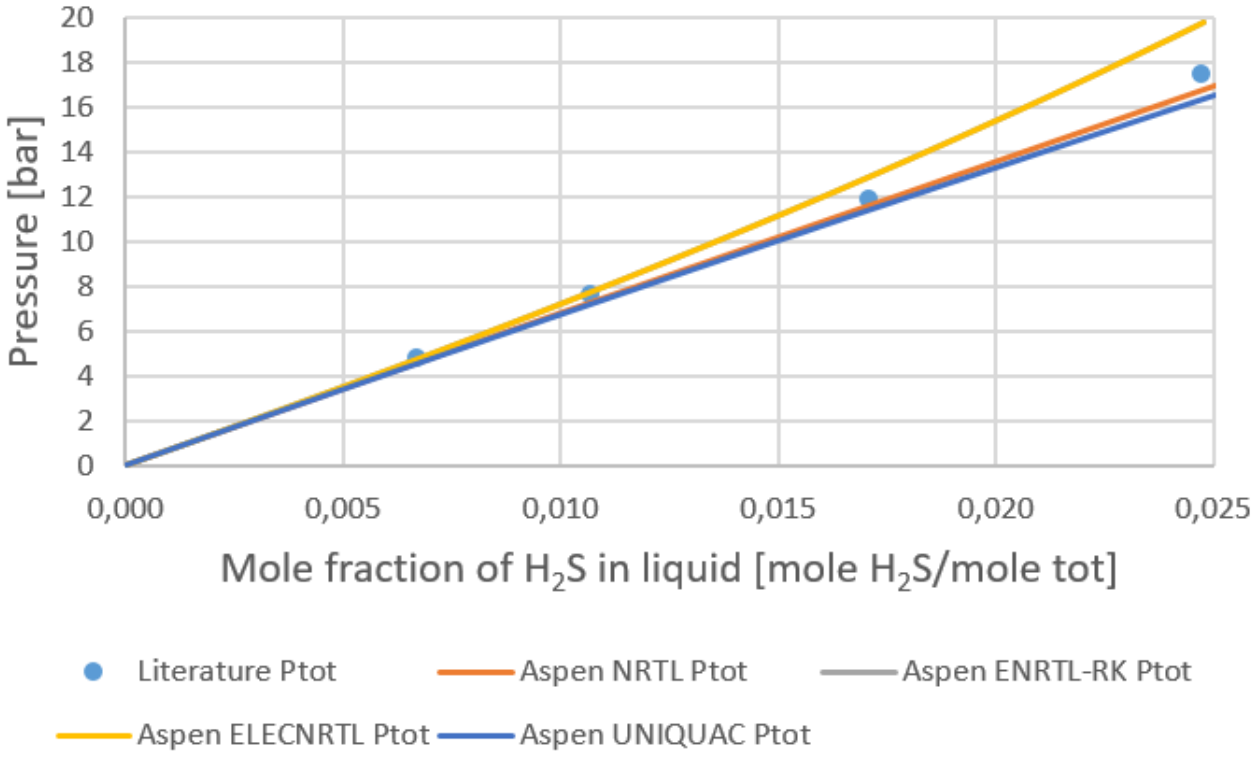

Figure A.1.2: Validation at 35 °C.

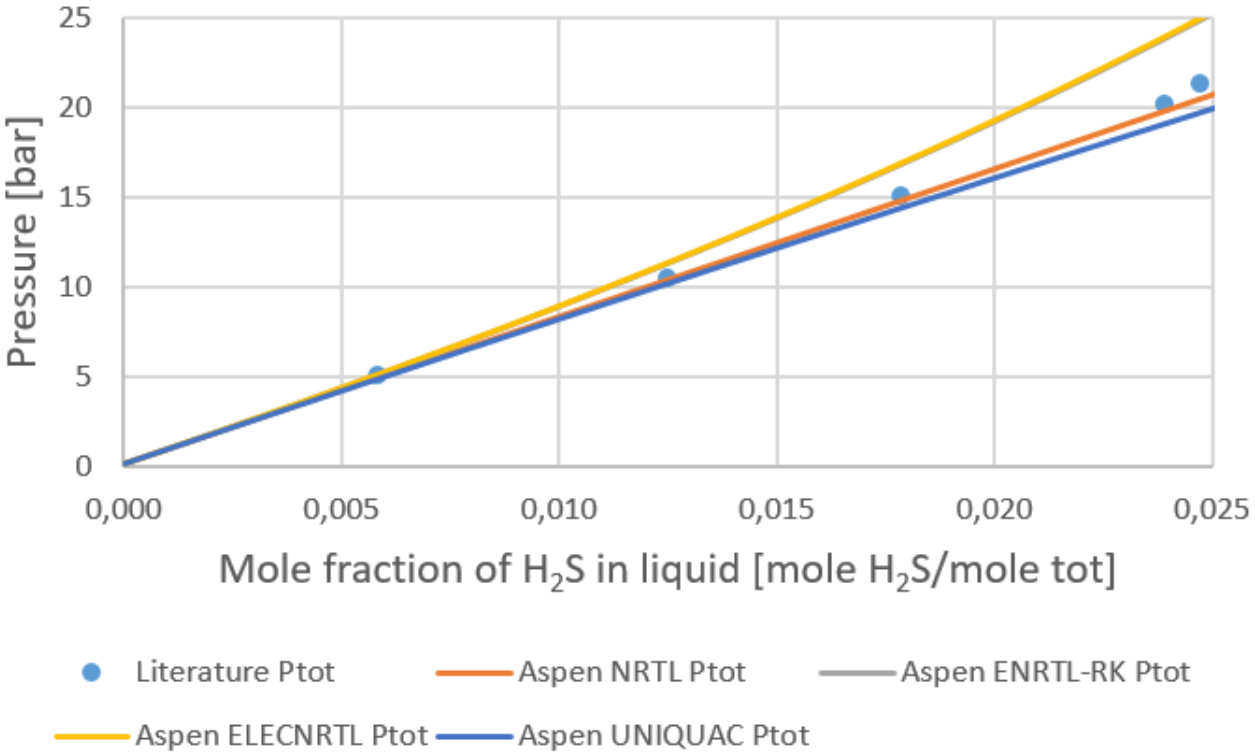

Figure A.1.3: Validation at 45 °C.

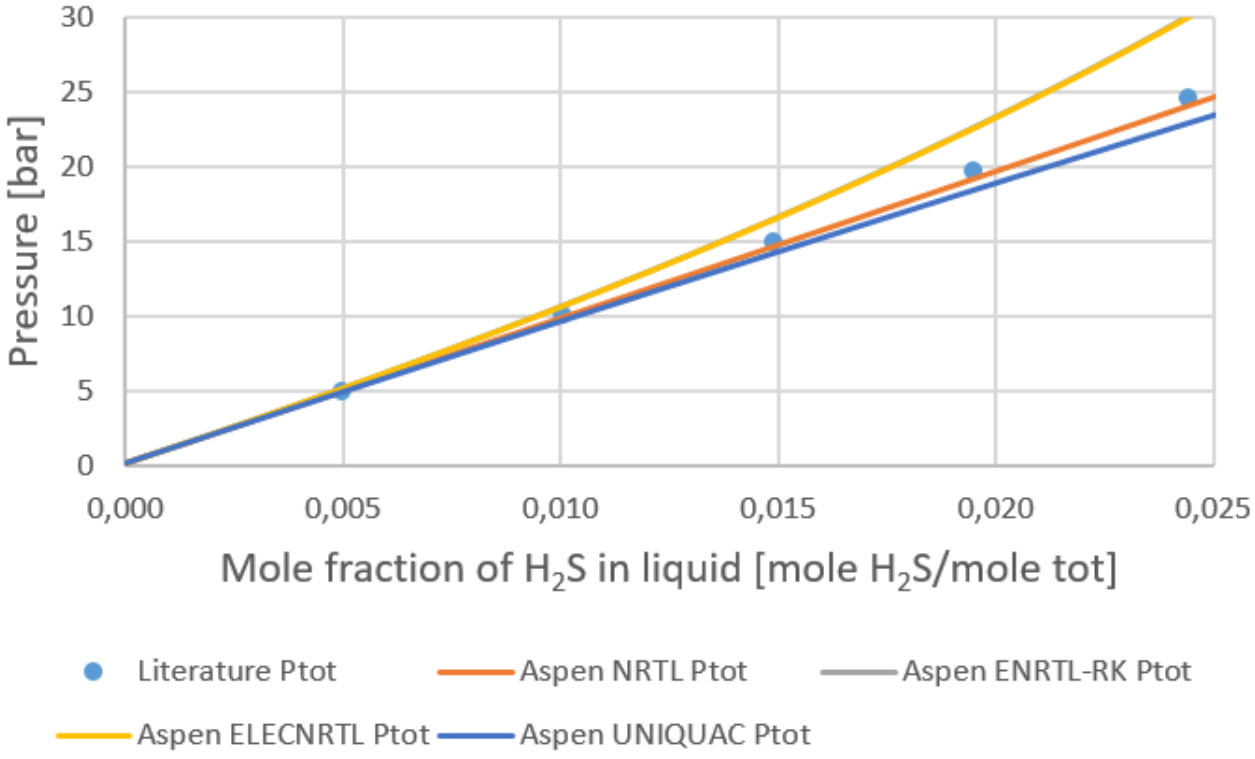

Figure A.1.4: Validation at 55 °C.

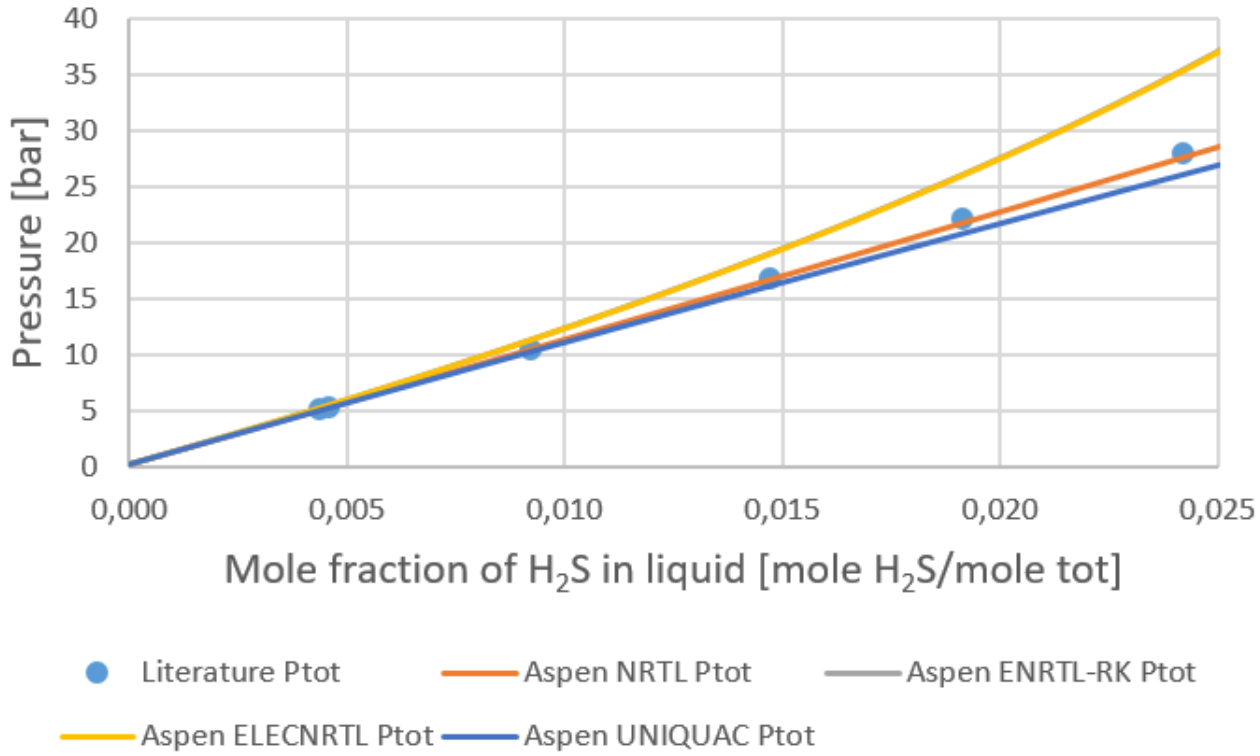

Figure A.1.5: Validation at 65 °C.

Initial tests were performed to check approximately what dimensions the column should have and what L/G-ratio that was reasonable. Figure A.1.6 illustrates the removal efficiency as a function of the L/G-ratio for a fixed absorber height of 10 m. The diameter was set to 0.5 m.

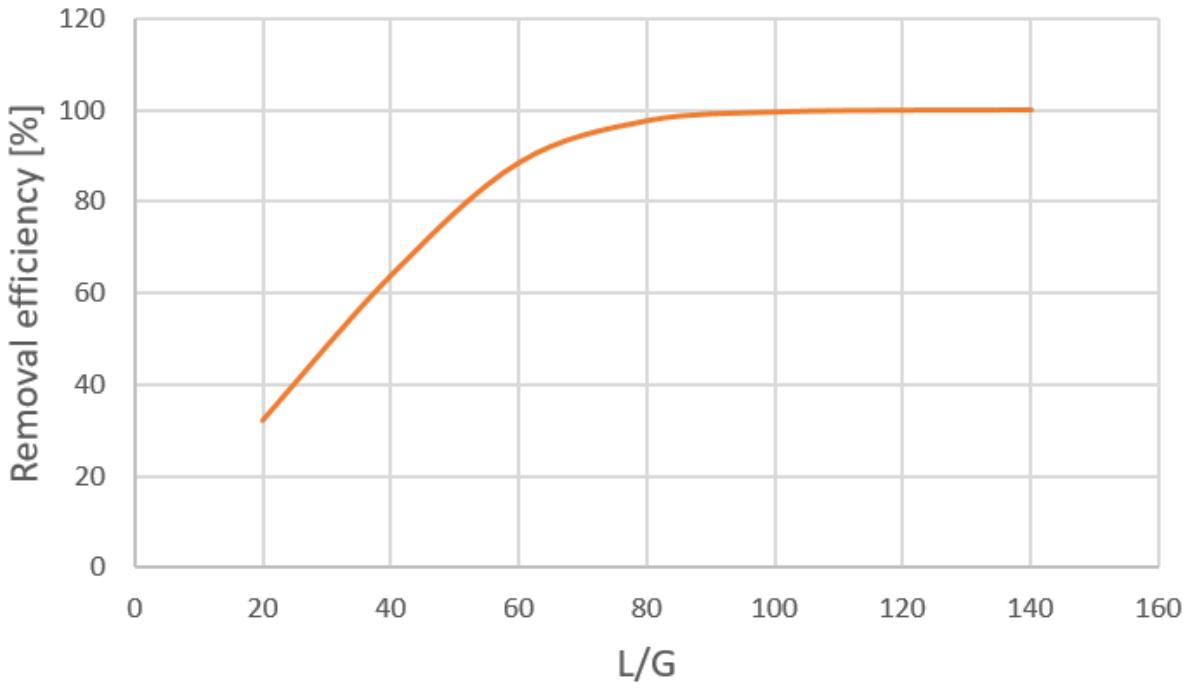

Figure A.1.6: Removal efficiency as a function of L/G-ratio.

In figure A.1.7, the target of 5 ppm in the purified gas is marked as an orange line. It can be observed that the L/G-ratio should be around and above 100 to reach the target, when there is no lean loading and no gas recycle. The L/G-ratio will of course depend on the system, and parameters such as and if it contains gas recycling, has high or low loading, temperature and pressure.

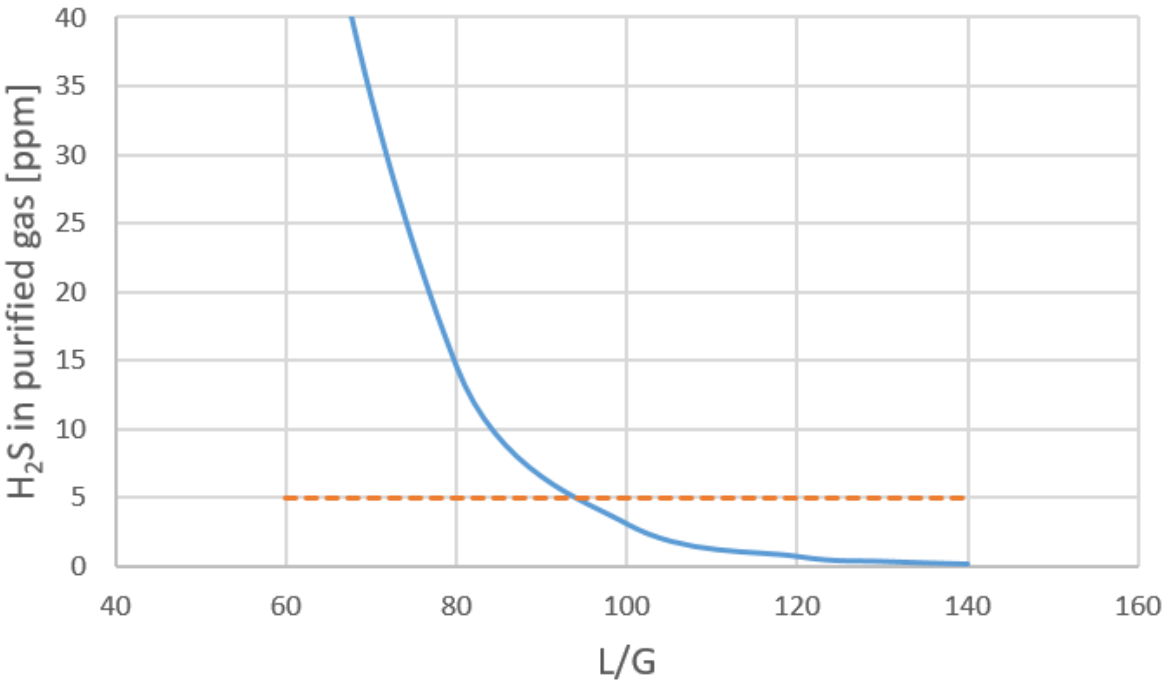

Figure A.1.7: Mole fraction of H_2S in gas out of the absorber as a function of L/G-ratio. The target of 5 ppm is illustrated by the dashed, orange line.

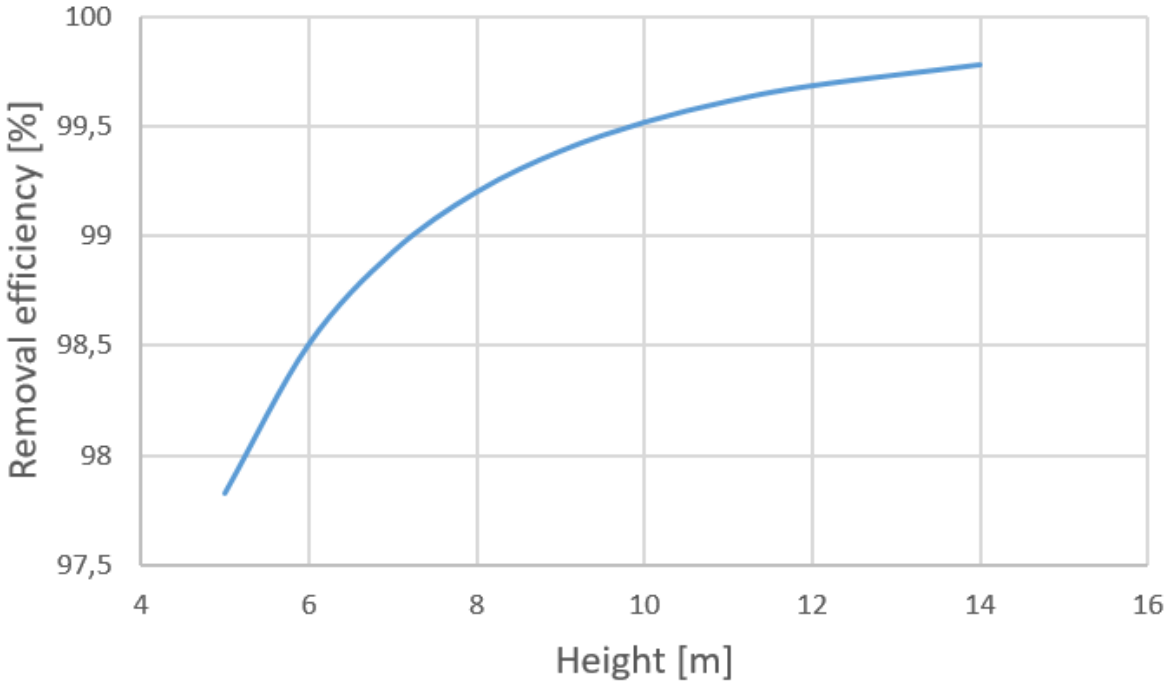

Figure A.1.8: Removal efficiency plotted as a function of the absorber height when the L/G-ratio is fixed at 100.

The rich loading was plotted as a function of the L/G-ratio, and the result is presented in figure A.1.9.

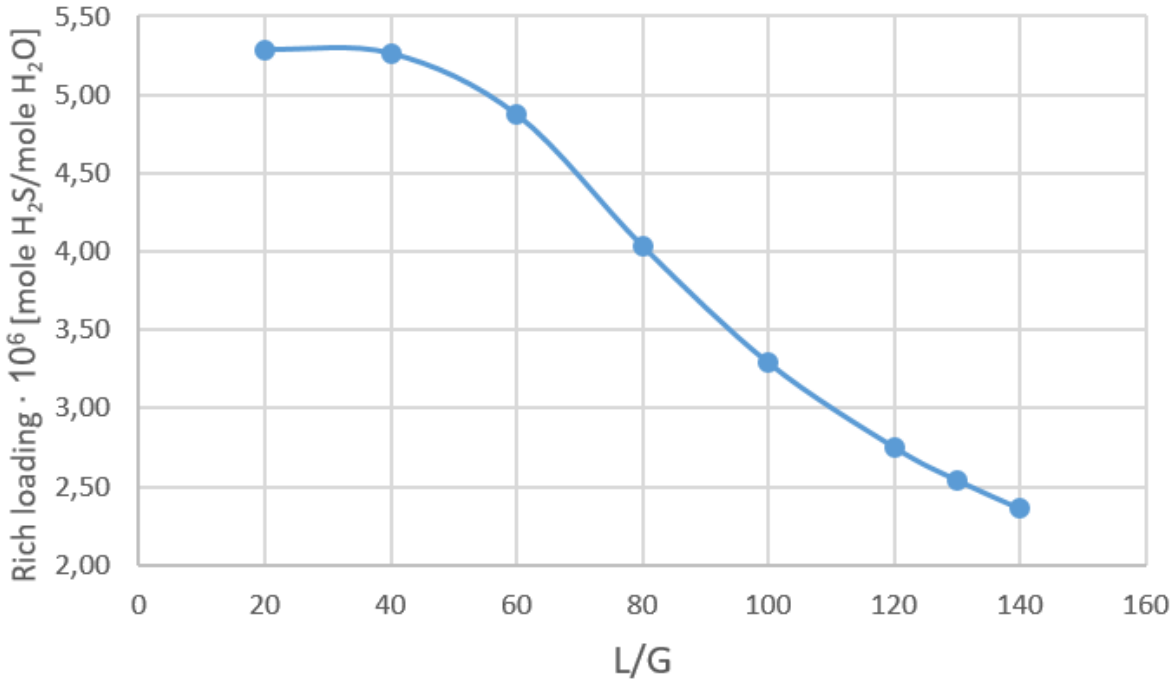

Figure A.1.9: Rich loading as a function of L/G-ratio.

Simple Flash

The flash was operated at different temperatures to check how this affected the system. Figure A.1.10 and A.1.11 present the results for flash temperatures of 60 and 80 °C respectively.

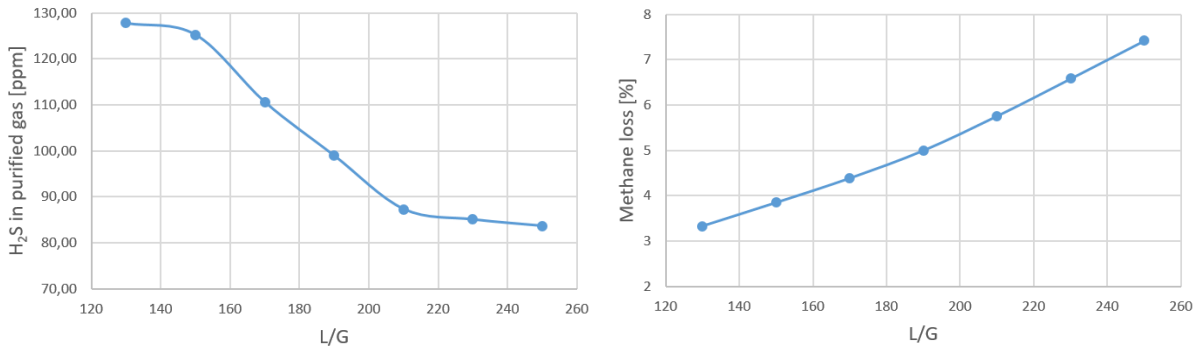

Figure A.1.10: Mole fraction of H_2S and methane loss plotted as a function of L/G-ratio for a flash temperature of 60 °C.

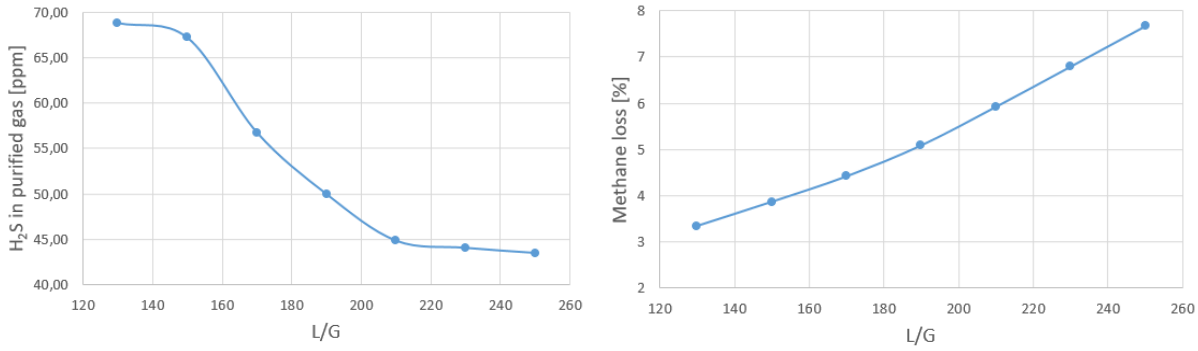

Figure A.1.11: Mole fraction of H_2S and methane loss plotted as a function of L/G-ratio for a flash temperature of 80 °C.

Table A.1.1 gives an overview of the temperatures, pressures, mole flows, mass flows and mole fractions for the different streams.

Table A.1.1: Stream overview in the case with regeneration through a simple flash.

					Mole fractions									
	Temperature	**Pressure**	**Mole Flows**	**Mass Flows**	**CO2**	**H2O**	**H2S**	**CH4**	**H3O+**	**OH-**	**HS-**	**HCO3-**	**S–**	**CO3–**
	C	bar	kmol/hr	kg/hr										
BIOGAS	40	1.1	20.902	572.110	0.400	0.067	5.0E-4	0.533	-	-	-	-	-	-
1	136	2.8	20.902	572.110	0.400	0.067	5.0E-4	0.533	-	-	-	-	-	-
2	40	2.8	20.902	572.110	0.400	0.067	5.0E-4	0.533	8.9E-8	1.8E-13	1.1E-10	8.9E-8	3.6E-21	4.5E-14
3	40	2.8	0.871	15.705	5.0E-4	0.999	1.9E-6	3.0E-5	2.1E-6	4.4E-12	2.5E-9	2.1E-6	8.7E-20	1.1E-12
4	40	2.8	20.031	556.405	0.417	0.026	5.2E-4	0.556	-	-	-	-	-	-
5	148	8.0	20.031	556.405	0.417	0.026	5.2E-4	0.556	-	-	-	-	-	-
6	40	8.0	20.031	556.405	0.417	0.026	5.2E-4	0.556	6.3E-8	4.5E-14	7.5E-11	6.3E-8	1.5E-21	1.9E-14
7	40	8.0	0.348	6.288	0.001	0.998	5.6E-6	8.8E-5	3.6E-6	2.6E-12	4.3E-9	3.6E-6	8.7E-20	1.1E-12
GASIN	40	8.0	19.683	550.117	0.425	0.009	5.3E-4	0.565	-	-	-	-	-	-
LEANIN	40	8.0	5890.314	106124.400	5.6E-5	1.000	2.5E-7	2.7E-7	7.1E-7	1.3E-11	9.9E-10	7.1E-7	1.0E-19	1.1E-12
GASOUT	40	8.0	11.145	191.358	0.040	0.009	2.4E-5	0.951	-	-	-	-	-	-
RICHOUT	40	8.0	5898.835	106483.200	0.001	0.999	2.0E-6	9.0E-5	3.6E-6	2.7E-12	1.6E-9	3.6E-6	4.6E-19	1.1E-12
RICHIN	90	1.0	5898.852	106483.200	0.001	0.999	2.0E-6	9.0E-5	6.6E-7	1.9E-10	2.2E-9	6.6E-7	1.0E-17	1.3E-12
GAS	90	1.0	28.342	715.577	0.279	0.702	3.6E-4	0.019	-	-	-	-	-	-
LEAN1	90	1.0	5870.510	105767.600	5.6E-5	1.000	2.5E-7	2.7E-7	6.7E-7	1.9E-10	2.2E-9	6.6E-7	1.1E-17	1.3E-12
LEAN2	90	8.0	5870.510	105767.600	5.6E-5	1.0	2.5E-7	2.7E-7	6.7E-7	1.9E-10	2.2E-9	6.6E-7	1.1E-17	1.3E-12

Flash with Purge

Table A.1.2: Stream overview in the case with a flash and a water purge.

					Mole fractions									
	Temperature	**Pressure**	**Mole Flows**	**Mass Flows**	**CO2**	**H2O**	**H2S**	**CH4**	**H3O+**	**OH-**	**HS-**	**HCO3-**	**S–**	**CO3–**
	C	bar	kmol/hr	kg/hr										
BIOGAS	40	1.1	20.902	572.110	0.400	0.067	5.0E-4	0.533	-	-	-	-	-	-
1	136	2.8	20.90224	572.110	0.400	0.067	5.0E-4	0.533	-	-	-	-	-	-
2	40	2.8	20.902	572.110	0.400	0.067	5.0E-4	0.533	8.9E-8	1.8E-13	1.1E-10	8.9E-8	3.6E-21	4.5E-14
3	40	2.8	0.871	15.705	5.0E-4	0.999	1.9E-6	3.0E-5	2.1E-6	4.4E-12	2.5E-9	2.1E-6	8.7E-20	1.1E-12
4	40	2.8	20.031	556.405	0.417	0.026	5.2E-4	0.556	-	-	-	-	-	-
5	148	8.0	20.031	556.405	0.417	0.026	5.2E-4	0.556	-	-	-	-	-	-
6	40	8.0	20.031	556.405	0.417	0.026	5.2E-4	0.556	6.3E-8	4.5E-14	7.5E-11	6.3E-8	1.5E-21	1.9E-14
7	40	8.0	0.348	6.288	0.001	0.998	5.6E-6	8.8E-5	3.6E-6	2.6E-12	4.3E-9	3.6E-6	8.7E-20	1.1E-12
GASIN	40	8.0	19.683	550.117	0.425	0.009	5.3E-4	0.565	-	-	-	-	-	-
LEANIN	40	8.0	3927.129	70749.600	1.2E-5	1.000	4.5E-8	4.4E-8	3.3E-7	2.9E-11	3.8E-10	3.3E-7	8.5E-20	1.1E-12
GASOUT	40	8.0	13.634	295.098	0.200	0.009	4.8E-6	0.791	-	-	-	-	-	-
RICHOUT	40	8.0	3933.165	71004.620	0.001	0.998	2.7E-6	8.8E-5	3.6E-6	2.6E-12	2.1E-9	3.6E-6	4.3E-20	1.1E-12
H2S	40	1.0	4.950	198.763	0.856	0.074	0.001	0.069	-	-	-	-	-	-
LEAN1	40	1.0	3928.222	70805.860	3.7E-4	1.000	1.4E-6	1.3E-6	1.8E-6	5.1E-12	2.1E-9	1.8E-6	8.4E-20	1.1E-12
H2O-OUT	40	1.0	3798.591	68469.260	3.7E-4	1.000	1.4E-6	1.3E-6	1.8E-6	5.1E-12	2.1E-9	1.8E-6	8.4E-20	1.1E-12
LEAN2	40	1.0	129.631	2336.593	3.7E-4	1.000	1.4E-6	1.3E-6	1.8E-6	5.1E-12	2.1E-9	1.8E-6	8.4E-20	1.1E-12
LEAN3	41	8.0	129.631	2336.593	3.7E-4	1.000	1.4E-06	1.3E-6	1.8E-6	5.3E-12	2.1E-9	1.8E-6	8.9E-20	1.1E-12
H2O	40	1.1	3800.622	68469.260	-	1.000	-	-	3.1E-9	3.1E-9	-	-	-	-
H2O-IN	40	8.0	3800.622	68469.260	-	1.000	-	-	3.1E-9	3.1E-9	-	-	-	-

Absorber with Gas Recycle

Table A.1.3: Stream overview in the case with an absorber and no lean stream recycle.

					Mole fractions									
	Temperature	**Pressure**	**Mole Flows**	**Mass Flows**	**CO2**	**H2O**	**H2S**	**CH4**	**H3O+**	**OH-**	**HS-**	**HCO3-**	**S–**	**CO3–**
	C	bar	kmol/hr	kg/hr										
BIOGAS	40	1.1	20.902	572.110	0.400	0.067	5.0E-4	0.533	-	-	-	-	-	-
1	40	1.1	27.900	859.781	0.523	0.067	7.9E-4	0.409	-	-	-	-	-	-
2	136	2.8	27.900	859.781	0.523	0.067	7.9E-4	0.409	-	-	-	-	-	-
3	40	2.8	27.900	859.781	0.523	0.067	7.9E-4	0.409	1.0E-7	1.6E-13	1.5E-10	1.0E-7	4.4E-21	4.5E-14
4	40	2.8	1.165	21.016	6.5E-4	0.999	3.1E-6	2.3E-5	2.4E-6	3.8E-12	3.5E-9	2.4E-6	1.1E-19	1.1E-12
5	40	2.8	26.735	838.766	0.546	0.026	8.3E-4	0.427	-	-	-	-	-	-
6	148	8.0	26.735	838.766	0.546	0.026	8.3E-4	0.427	-	-	-	-	-	-
7	40	8.0	26.735	838.766	0.546	0.026	8.3E-4	0.427	7.2E-8	3.9E-14	1.0E-10	7.2E-8	1.8E-21	1.9E-14
8	40	8.0	0.465	8.401	0.002	0.998	8.9E-6	6.8E-5	4.1E-6	2.3E-12	6.0E-9	4.1E-6	1.1E-19	1.1E-12
GASIN	40	8.0	26.270	830.364	0.555	0.009	8.4E-4	0.435	-	-	-	-	-	-
LEANIN	40	8.0	4254.466	76645.400	-	1.00	-	-	3.1E-9	3.1E-9	-	-	-	-
GASOUT	40	8.0	17.862	470.615	0.368	0.009	4.5E-6	0.623	-	-	-	-	-	-
RICH	40	8.0	4262.860	77005.310	0.002	0.998	5.2E-6	6.8E-5	4.1E-6	2.3E-12	3.5E-9	4.1E-6	6.4E-20	1.1E-12
LIQUID	40	1.1	4255.871	76717.630	4.2E-4	1.000	2.4E-6	8.7E-7	2.0E-6	4.8E-12	3.5E-9	2.0E-6	1.3E-19	1.1E-12
GAS	40	1.1	6.998	287.671	0.890	0.067	0.002	0.041	-	-	-	-	-	-

Air Stripping

Table A.1.4: Stream overview in the air stripping case.

					Mole fractions										
	Temperature	**Pressure**	**Mole Flows**	**Mass Flows**	**CO2**	**H2O**	**H2S**	**CH4**	**H3O+**	**OH-**	**HS-**	**HCO3-**	**S–**	**CO3–**	**O2**	**N2**
	C	bar	kmol/hr	kg/hr												
BIOGAS	40	1.1	20.902	572.110	0.400	0.067	5.0E-4	0.533	-	-	-	-	-	-	-	-
1	136	2.8	20.902	572.110	0.400	0.067	5.0E-4	0.533	-	-	-	-	-	-	-	-
2	55	2.8	20.902	572.110	0.400	0.067	5.0E-4	0.533	1.8E-8	1.3E-13	3.0E-11	1.8E-8	4.4E-21	1.3E-14	-	-
3	40	2.8	0.857	15.444	4.9E-4	0.999	1.9E-6	3.0E-5	2.1E-6	4.5E-12	2.5E-9	2.1E-6	9.1E-20	1.1E-12	-	-
4	40	2.8	20.046	556.666	0.417	0.027	5.2E-4	0.555	-	-	-	-	-	-	-	-
5	148	8.0	20.046	556.666	0.417	0.027	5.21E-4	0.555	-	-	-	-	-	-	-	-
6	55	8.0	20.046	556.666	0.417	0.027	5.2E-4	0.555	2.0E-8	4.7E-14	3.2E-11	2.0E-8	2.8E-21	8.4E-15	-	-
7	40	8.0	0.348	6.284	0.001	0.999	5.3E-6	8.6E-5	3.6E-6	2.7E-12	4.2E-9	3.6E-6	9.1E-20	1.1E-12	-	-
GASIN	40	8.0	19.697	550.382	0.424	0.010	5.3E-4	0.565	-	-	-	-	-	-	-	-
LEANIN	40	8.0	3429.625	61905.900	4.3E-8	0.997	5.0E-10	7.3E-10	1.9E-8	4.6E-10	6.8E-11	1.9E-8	2.4E-19	9.9E-13	0.001	0.002
GASOUT	40	8.0	21.271	536.617	0.207	0.010	4.6E-6	0.519	-	-	-	-	-	-	0.052	0.212
RICHOUT	40	8.0	3428.649	61940.110	0.001	0.997	3.1E-6	7.8E-5	3.4E-6	2.8E-12	2.6E-9	3.4E-6	5.9E-20	1.1E-12	9.0E-4	5.1E-4
GAS1	40	5.0	0.609	20.434	0.556	0.016	4.7E-4	0.285	-	-	-	-	-	-	0.058	0.084
GAS2	89	8.0	0.609	20.434	0.556	0.016	4.7E-4	0.285	-	-	-	-	-	-	0.058	0.084
RICHIN	40	5.0	3428.040	61919.670	0.001	0.997	3.0E-6	2.7E-5	3.2E-6	3.0E-12	2.6E-9	3.2E-6	6.2E-20	1.1E-12	8.9E-4	5.0E-5
AIR	20	1.1	63.660	1820.400	-	0.021	-	-	-	-	-	-	-	-	0.199	0.779
AIR-IN	98	2.0	63.660	1820.400	-	0.021	-	-	-	-	-	-	-	-	0.199	0.779
GAS3	40	2.0	63.115	1852.335	0.063	0.038	1.6E-4	0.004	-	-	-	-	-	-	0.183	0.714
LEAN1	40	2.0	3428.596	61887.740	4.4E-8	0.997	5.1E-10	7.5E-10	2.0E-8	4.6E-10	6.9E-11	1.9E-08	2.5E-19	9.9E-13	0.001	0.002
LEAN2	40	8.0	3428.596	61887.740	4.4E-8	0.997	5.1E-10	7.5E-10	2.0E-8	4.6E-10	6.9E-11	1.9E-8	2.5E-19	9.9E-13	0.001	0.002

A.1.2 Amine Scrubbing

The absorber was first implemented to find out approximately what height the absorber should have. The result is illustrated in figure A.1.12 for an L/G-ratio of 10. The simulations are performed without H_2S in the lean stream (lean loading = 0). It can be seen that the removal efficiency stabilizes for an absorber height of 15 m and higher when there is no lean loading. In order to take into account the lean loading that will occur in the complete amine scrubbing system, the height should be further increased.

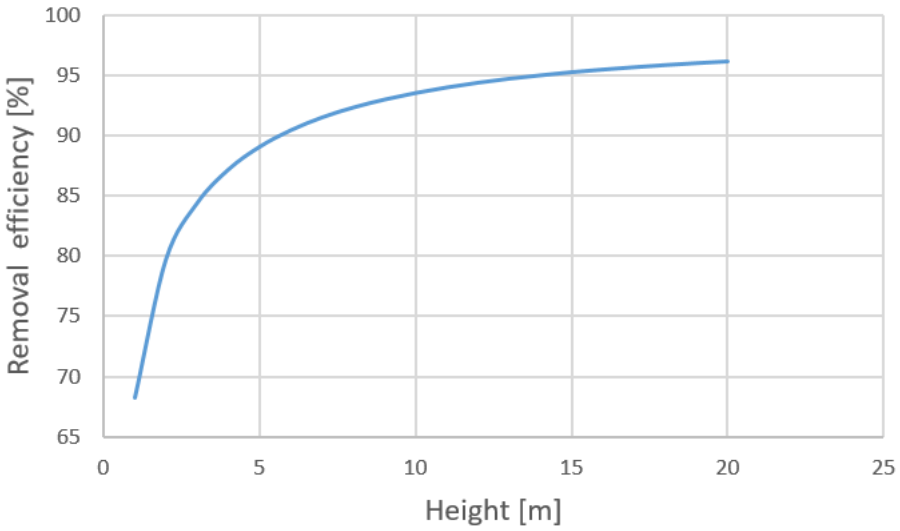

Figure A.1.12: Removal efficiency plotted as a function of the absorber packed height when L/G is fixed at 10 and the diameter at 0.3 m.

Table A.1.5 presents a stream overview for the amine scrubbing system when the L/G-ratio is fixed at 14.

Table A.1.5: Stream overview for Amine scrubbing at L/G = 14.

					Mole fractions											
	Temperature	**Pressure**	**Mole Flows**	**Mass Flows**	**MDEA**	**H2O**	**CO2**	**H2S**	**H3O+**	**OH-**	**HCO3-**	**CO3-2**	**HS-**	**S-2**	**MDEAH+**	**CH4**
	°C	bar	kmol/hr	kg/hr												
BIOGAS	40	1.1	21.541	589.580	-	0.067	0.400	5.0E-4	-	-	-	-	-	-	-	0.533
LEANIN	40	1.1	368.953	8254.120	0.043	0.957	1.9E-10	3.7E-10	1.1E-13	9.1E-5	9.4E-6	1.1E-5	6.6E-6	1.2E-8	1.3E-4	-
LEANREC	40	1.1	0.446	8.032	2.8E-7	1.000	2.9E-5	6.4E-8	5.5E-9	1.9E-9	4.9E-5	1.2E-8	3.7E-8	6.2E-16	4.9E-5	1.9E-5
GAS1	48	1.1	13.633	244.409	1.6E-6	0.098	0.060	4.3E-5	-	-	-	-	-	-	-	0.841
REC1	40	1.1	13.633	244.409	9.0E-9	0.098	0.060	4.3E-5	1.9E-10	6.0E-11	1.6E-6	3.8E-10	1.2E-9	2.0E-17	1.6E-6	0.841
PUR-GAS	40	1.1	13.188	236.377	4.6E-12	0.068	0.0625	4.4E-5	-	-	-	-	-	-	-	0.870
PUR-1	145	3.0	13.188	236.377	4.6E-12	0.068	0.062	4.4E-5	-	-	-	-	-	-	-	0.870
PUR-2	40	3.0	13.188	236.377	1.8E-16	0.068	0.0625	4.4E-5	3.6E-8	4.9E-13	3.6E-8	4.7E-14	2.7E-11	2.5E-21	4.6E-12	0.870
PUR-LEAN	40	3.0	0.577	10.393	4.1E-15	1.000	8.1E-5	1.8E-7	8.3E-7	1.1E-11	8.3E-7	1.1E-12	6.2E-10	5.6E-20	1.1E-10	5.3E-5
PUR-3	40	3.0	12.611	225.983	2.6E-20	0.025	0.065	4.6E-5	-	-	-	-	-	-	-	0.909
PUR-4	142	8.0	12.611	225.983	2.6E-20	0.025	0.065	4.6E-5	-	-	-	-	-	-	-	0.909
PUR-5	40	8.0	12.611	225.983	-	0.025	0.065	4.6E-5	2.1E-8	1.1E-13	2.1E-8	1.7E-14	1.6E-11	8.8E-22	-	0.909
CLEANGAS	40	8.0	12.414	222.444	-	0.010	0.066	4.7E-5	-	-	-	-	-	-	-	0.924
C-LEAN	40	8.0	0.196	3.539	-	1.000	2.1E-4	4.7E-7	1.3E-6	6.9E-12	1.34E-06	1.1E-12	10.0E-10	5.6E-20	-	1.4E-4
RICHOUT	57	1.1	369.573	8607.317	0.022	0.936	1.6E-4	5.6E-7	1.2E-10	8.5E-7	0.021	5.1E-5	3.4E-5	2.79E-09	0.021	8.8E-6
RICH	57	2.0	369.573	8607.317	0.022	0.936	1.64E-4	5.6E-7	1.2E-10	8.5E-7	0.021	5.1E-5	3.4E-5	2.8E-9	0.021	8.8E-6
RICHIN	99	2.0	373.841	8607.317	0.033	0.937	0.012	9.1E-6	4.0E-10	2.1E-6	0.009	2.1E-5	2.5E-5	1.8E-8	0.009	8.7E-6
GAS2	117	2.0	67.502	1422.314	2.0E-4	0.883	0.117	1.6E-4	-	-	-	-	-	-	-	4.8E-5
REC2	25	2.0	67.488	1422.314	4.6E-8	0.883	0.116	1.6E-4	4.3E-8	7.1E-11	2.0E-4	5.0E-9	1.9E-7	1.1E-16	2.0E-4	4.8E-5
GASOUT	25	2.0	7.934	345.656	8.3E-14	0.016	0.982	0.001	-	-	-	-	-	-	-	4.1E-4
LEANREC2	25	2.0	59.554	1076.666	5.2E-8	0.998	0.001	4.7E-6	4.9E-8	8.1E-11	2.3E-4	5.7E-9	2.1E-7	1.3E-16	2.3E-4	2.0E-8
LEAN1	121	2.0	369.369	8261.617	0.043	0.957	3.5E-8	5.6E-9	7.9E-12	1.2E-4	1.9E-5	1.0E-6	6.4E-6	2.4E-7	1.5E-4	1.7E-21
LEAN2	65	2.0	369.369	8261.617	0.043	0.957	1.2E-9	8.8E-10	5.5E-13	1.1E-4	1.4E-5	6.4E-6	6.6E-6	3.3E-8	1.4E-4	-

Information about the streams in the complete amine scrubbing system for L/G = 16 is presented in table A.1.6.

Table A.1.6: Stream overview for Amine scrubbing at L/G = 16.

					Mole fraction											
	Temperature	**Pressure**	**Mole Flows**	**Mass Flows**	**MDEA**	**H2O**	**CO2**	**H2S**	**H3O+**	**OH-**	**HCO3-**	**CO3-2**	**HS-**	**S-2**	**MDEAH+**	**CH4**
	°C	bar	kmol/hr	kg/hr												
BIOGAS	40	1.1	21.541	589.580	-	0.067	0.400	5.0E-4	-	-	-	-	-	-	-	0.533
LEANIN	40	1.1	421.606	9433.280	0.043	0.957	2.8E-9	2.9E-9	2.5E-13	4.3E-5	6.5E-5	3.8E-5	2.4E-5	2.2E-8	2.1E-4	-
LEANREC	40	1.1	6.8E-7	1.5E-5	0.043	0.957	2.8E-9	2.9E-9	2.5E-13	4.3E-5	6.5E-5	3.8E-5	2.4E-5	2.2E-8	2.1E-4	2.1E-5
GAS1	40	1.1	12.263	198.303	7.5E-7	0.065	4.4E-6	1.9E-6	-	-	-	-	-	-	-	0.935
REC1	40	1.1	12.263	198.303	7.5E-7	0.065	4.4E-6	1.9E-6	1.2E-18	1.5E-10	2.4E-10	1.8E-10	9.0E-11	6.5E-14	8.3E-10	0.935
PUR-GAS	40	1.1	12.263	198.303	7.5E-7	0.065	4.4E-6	1.9E-6	-	-	-	-	-	-	-	0.935
PUR-1	146	3.0	12.263	198.303	7.5E-7	0.065	4.4E-6	1.9E-6	-	-	-	-	-	-	-	0.935
PUR-2	40	3.0	12.263	198.303	5.1E-7	0.065	4.2E-6	1.8E-6	5.9E-13	2.6E-8	1.3E-7	1.0E-8	5.9E-8	3.2E-13	2.4E-7	0.935
PUR-LEAN	40	3.0	0.498	8.979	1.3E-5	1.000	5.5E-9	7.3E-9	1.5E-11	6.5E-7	3.2E-6	2.5E-7	1.5E-6	7.9E-12	5.8E-6	5.7E-5
PUR-3	40	3.0	11.764	189.324	8.0E-11	0.025	4.4E-6	1.9E-6	-	-	-	-	-	-	-	0.975
PUR-4	143	8.0	11.764	189.324	8.0E-11	0.025	4.4E-6	1.9E-6	-	-	-	-	-	-	-	0.975
PUR-5	40	8.0	11.764	189.324	2.2E-13	0.025	4.4E-6	1.9E-6	1.7E-10	1.3E-11	1.7E-10	1.6E-14	7.4E-11	4.9E-19	7.9E-11	0.975
CLEANGAS	40	8.0	11.581	186.024	3.9E-17	0.010	4.5E-6	1.9E-6	-	-	-	-	-	-	-	0.990
C-LEAN	40	8.0	0.183	3.300	1.4E-11	1.000	1.4E-8	1.9E-8	1.1E-8	8.1E-10	1.1E-8	1.0E-12	4.8E-9	3.1E-17	5.1E-9	1.5E-4
RICHOUT	57	1.1	422.332	9824.557	0.023	0.936	1.5E-4	7.8E-7	1.1E-10	8.9E-7	0.020	5.3E-5	4.9E-5	4.2E-9	0.020	9.2E-6
RICH	57	2.0	422.332	9824.557	0.023	0.936	1.5E-4	7.8E-7	1.1E-10	8.9E-7	0.020	5.3E-5	4.9E-5	4.2E-9	0.020	9.2E-6
RICHIN	100	2	427.034	9824.557	0.033	0.937	0.011	1.3E-5	4.0E-10	2.1E-6	0.009	2.1E-5	3.6E-5	2.7E-8	0.009	9.1E-6
GAS2	100	2.0	16.841	527.903	6.5E-5	0.487	0.512	5.91E-4	-	-	-	-	-	-	-	2.3E-4
REC2	25	2.0	16.839	527.903	9.3E-9	0.487	0.512	5.9E-4	3.7E-8	2.3E-11	6.5E-5	9.4E-10	5.4E-8	1.8E-17	6.5E-05	2.3E-4
GASOUT	25	2.0	8.772	382.155	3.1E-14	0.016	0.982	0.001	-	-	-	-	-	-	-	4.4E-4
LEANREC2	25	2.0	8.068	145.748	1.9E-8	1.000	0.001	4.1E-6	7.8E-8	4.8E-11	1.4E-4	2.0E-9	1.1E-7	3.7E-17	1.4E-4	2.2E-8
LEAN1	121	2.0	422.113	9442.417	0.043	0.957	3.3E-7	4.2E-8	1.6E-11	6.4E-5	9.8E-5	2.8E-6	2.5E-5	5.4E-7	2.0E-4	2.9E-26
LEAN2	65	2.0	422.113	9442.417	0.043	0.957	1.4E-8	6.6E-9	1.1E-12	5.7E-5	8.1E-5	2.0E-5	2.6E-5	7.2E-8	2.1E-4	-

A.2 Calculations

A.2.1 Energy/kg Impurity Absorbed

The amount of energy per H_2S and CO_2 were calculated from the net energy demand and mass flows of H_2S and CO_2.

$$\frac{\text{Net energy [kW]}}{\text{Mass flow [kg/s]}} = Energy/kg_{impurity} \tag{A.2.1}$$

In order to obtain a basis for comparison from the literature on water scrubbing, the energy consumption per amount of biogas was calculated using the biogas from the water scrubbing simulations in this thesis.

The average value of the two techniques was used for comparison. The calculations are shown below.

Absorber Case with Recycle

The reported value from literature (0.25 kWh/N m^3) was first multiplied by the volume flow of biogas found in Aspen Plus as shown in equation B.2.2.

$$0.25 \text{ kWh/N}m^3 \cdot 494.74 m^3/h = 123.69 \text{ kW} \tag{A.2.2}$$

H_2S absorbed: 0.3534879 kg/h = $9.819108611 \cdot 10^{-5}$ kg/s $\approx 9.82 \cdot 10^{-5}$ kg/s

CO_2 absorbed: 78.84 kg/h = 0.0219 kg/s $\approx$ 0.02 kg/s

Air Stripping

The same procedure was followed for the Air Stripping case.

$$0.25 \text{ kWh/N}m^3 \cdot 493.10 m^3/h = 123.28 kW \tag{A.2.3}$$

H_2S absorbed: 0.35288151 kg/h = $9.802264167 \cdot 10^{-5}$ kg/s $\approx 9.80 \cdot 10^{-5}$ kg/s

CO_2 absorbed: 173.73 kg/h = 0.04827027778 kg/s $\approx$ 0.05 kg/s

The average energy, mass flow of H_2S and mass flow of CO_2 for the absorber case with gas recycle and air stripping are calculated in equation A.2.4, A.2.5 and A.2.6.

$$\frac{123.69+123.28}{2} = 123.49kW \tag{A.2.4}$$

$$\frac{9.82 \cdot 10^{-5}+9.80 \cdot 10^{-5}}{2} = 9.81 \cdot 10^{-5} kg_{H_2S}/s \tag{A.2.5}$$

$$\frac{0.02+0.05}{2} = 0.035 kg_{CO_2}/s \tag{A.2.6}$$

The energy per amount of H_2S and CO_2 was found by dividing the net energy by the mass flow of H_2S and CO_2 respectively.

$$\frac{123.49}{9.81 \cdot 10^{-5}}=1258817.53kJ/kg_{H_2S}=1258.82MJ/kg_{H_2S} \tag{A.2.7}$$

$$\frac{123.49}{0.035}=3528.29kJ/kg_{CO_2}=3.53MJ/kg_{CO_2} \tag{A.2.8}$$

The amount of energy per kg H_2S and CO_2 was calculated in the same way, only with the combined mass flow.

$$\frac{123.49}{9.81 \cdot 10^{-5}+0.035}=3518.42kJ/kg_{H_2S+CO_2}=3.52MJ/kg_{H_2S+CO_2} \tag{A.2.9}$$

Martine Paulsen

Master's thesis

NTNU
Norwegian University of
Science and Technology